

The Drift Diffusion Simulation of Coupled Ionic-Electronic Devices

by

Cem Bonfil, B. Eng.

A thesis submitted to the Faculty of Graduate and Postdoctoral Affairs in
partial fulfillment of the requirements for the degree of

Master of Applied Science

in

Electrical and Computer Engineering

Ottawa-Carleton Institute for Electrical and Computer Engineering

Department of Electronics

Carleton University

Ottawa, Ontario, Canada

©2014, Cem Bonfil

Abstract

The purpose of the work presented in this thesis was to create a numerical simulation scheme for a coupled ionic electronic device and use it to simulate a memristor which is based on an organic conductor called poly(3,4 ethylenedioxothiophene):polystyrenesulfonate (PEDOT:PSS). The memristor that was modeled consists of a thin PEDOT:PSS strip with a metal contact on both sides and a drop of an electrolyte solution with lithium and perchlorate ions. The conductivity of the memristor changes when lithium ions in the electrolyte dedopes the PEDOT:PSS by bonding with PSS polymers. A numerical drift diffusion and a Poisson solver was implemented with special features to model the physical properties of the memristor. The developed simulation algorithm was tested using analytical solutions to the drift diffusion equations and Poisson's equation. 1-D and 2-D memristors were simulated using various applied potentials and the results were compared to each other. 1-D simulations were more computationally efficient but they require some parameter fitting in order to produce results similar to 2-D simulations which capture the physical effects more accurately. The comparison of 2-D simulations and experimental results showed that proposed model worked as expected and produced results that were similar to an actual memristor. The work presented in this thesis showed promising results for the simulation of a memristor which can be improved in

the future by additional modeling of the charge transport mechanisms.

Acknowledgements

Contents

Acknowledgements	iii
List of Figures	vi
List of Tables	viii
Abbreviations	ix
Physical Constants	x
Symbols	xi
1 Introduction	1
1.1 Thesis Objectives	1
1.2 Thesis Overview	1
1.3 Contributions	3
1.4 Background	3
2 Theory	7
2.1 Carrier Transport Equations	7
2.2 Analytic Solutions	13
2.2.1 Steady State Solution Over a Finite Domain	13
2.2.2 Transient Solution Over an Infinite Domain	16
2.2.3 PN Junction	20
3 Numerical Solution of Drift-Diffusion and Poisson's Equation	25
3.1 Finite Difference Method	25
3.2 Poisson Solver	29
3.3 Current Density Equations	31
3.3.1 Continuity Equation	32
3.4 Stability and Computational Efficiency	34
3.4.1 Physical Limitations	34
3.4.2 Numerical Limitations	35
3.4.3 Explicit vs. Implicit Solution	36
3.5 Simulation Procedure	37

4 Simulation of a Memristor as a Coupled Electronic Device	39
4.1 Memristor Structure and Initial Conditions	41
4.2 Boundary Conditions of the Memristor Model	42
4.2.1 Drift Diffusion Equations	42
4.2.2 Metal Contacts	46
4.2.3 Poisson's Equation	48
4.3 Simulation Requirements	50
5 Testing The Drift Diffusion Solver	53
5.1 Solution for Closed Boundary	53
5.2 Solutions for Open Boundary	57
5.3 PN Junction	58
5.4 Region Specific Particle Density Limit	61
6 1-D Memristor Simulation	67
6.1 1-D Memristor Approximation	67
6.2 1-D Memristor Simulations	70
6.2.1 1-D Memristor Simulation Using a Potential Pulse Train	70
6.2.2 1-D Memristor Simulation Using a Sinusoid	74
6.2.3 1-D Memristor Simulation With Increasing Charge Density (I got a few questions)	77
7 2-D Memristor Simulation	82
7.1 Effect of PEDOT:PSS Thickness	82
7.2 2-D Memristor Simulation Using a Potential Pulse Train	87
7.3 2-D Memristor Simulation Using a Sinusoid	91
7.4 Experiment vs. Simulation	94
8 Conclusion	99
Bibliography	101

List of Figures

2.1	Increased accumulation of particles due to increased electric field	15
2.2	A gaussian particle density distribution drifting and diffusing over time . .	19
2.3	A rectangular particle density distribution drifting and diffusing over time .	19
2.4	PN junction electron/hole density	20
2.5	Approximate Solution of a PN Junction	24
3.1	Finite Difference Drift-Diffusion Scheme Flowchart	38
4.1	Organic memristor with electrolyte and PEDOT:PSS (not to scale)	39
4.2	The structure of the memristor used for simulation (not to scale)	41
4.3	Boundary conditions for the holes	44
4.4	Boundary conditions for the lithium ions	44
4.5	Boundary conditions for the perchlorate ions	45
4.6	Boundary conditions for electric potential	49
4.7	Spatial and temporal requirements for simulation	52
5.1	Potential Distribution	54
5.2	Electric Field Distribution	54
5.3	Steady State Negative Particle Density	55
5.4	Finite Difference Drift and Diffusion Current Densities	56
5.5	Gaussian Carrier Distribution Evolving Over time	57
5.6	Electron/hole Concentration of a PN Junction	58
5.7	Potential Distribution of a PN Junction	59
5.8	Electric Field Distribution of a PN Junction	60
5.9	Total Charge Distribution of a PN Junction	60
5.10	Initial Particle Density	61
5.11	Limited Density Accumulation on the Right Side	62
5.12	Limited Concentration Density on the Left Side	62
5.13	Accumulation at the right wall over time	63
5.14	a) COMSOL Simulation for Particle Density Limit b)COMSOL and Finite Difference Simulation	64
5.15	a) COMSOL Simulation for Particle Density Limit b)COMSOL and Finite Difference Simulation	65
5.16	a) COMSOL Simulation for Particle Density Limit b)COMSOL and Finite Difference Simulation	66
5.17	a) COMSOL Simulation for Particle Density Limit b)COMSOL and Finite Difference Simulation	66
6.1	1-D Memristor Model	68

6.2	Change in current density over time due to applied potential	70
6.3	Potential and electric field at steady state	71
6.4	Lithium and hole density distribution over time	72
6.5	Normalized Current vs. applied potential at different frequencies	74
6.6	Normalized current over time	75
6.7	Hole density over time at different frequencies	76
6.8	Lithium density over time at different frequencies	76
6.9	Normalized hole densities at steady state	78
6.10	Normalized lithium densities at steady state	79
6.11	Normalized hole current densities	79
6.12	Average difference for hole, lithium and current densities for various initial hole densities	80
7.1	Normalized current over time or different PEDOT:PSS thicknesses	83
7.2	Hole distribution at steady state for different PEDOT:PSS thicknesses . .	84
7.3	Lithium distribution at steady state for different PEDOT:PSS thicknesses	85
7.4	Perchlorate distribution at steady state for different PEDOT:PSS thicknesses	85
7.5	Electric field strength at steady state for different PEDOT:PSS thicknesses	86
7.6	Applied potential and normalized current over time of a 2-D memristor .	87
7.7	Electric field and potential at steady state along PEDOT:PSS	88
7.8	Lithium and hole density distributions over time	89
7.9	Lithium current density over time	90
7.10	Normalized Current vs. applied potential at different frequencies	91
7.11	Hole distribution over time at different frequencies	92
7.12	Lithium distribution over time at different frequencies	93
7.13	Experimental results for various applied potentials at 0.1 Hz (Courtesy of Eduardo Barrera)[37]	94
7.14	Simulation results for various applied potentials at 0.1 Hz	94
7.15	Experimental results for various applied potentials at 1.0 Hz (Courtesy of Eduardo Barrera)[37]	95
7.16	Simulation results for various applied potentials at 1.0 Hz	95
7.17	Measured I-V curve at different frequencies (Courtesy of Eduardo Barrera)[37]	96
7.18	Simulated I-V curve at different frequencies	96
7.19	Experimental results for accumulation of lithium inside PEDOT:PSS (Courtesy of Eduardo Barrera)[37]	97
7.20	Simulation results for accumulation of lithium inside PEDOT:PSS	97

List of Tables

Abbreviations

BTE	Boltzmann Transport Equations
CFL	Courant-Friedrichs-Lowy
ClO_4^-	Perchlorate
DD	Drift Diffusion
FD	Finite Difference
Li^+	Lithium
PEDOT	Poly(3,4-ethylenedioxythiophene)
PSS	Poly(styrenesulfonate)

Physical Constants

Boltzmann Constant $k = 8.6173324 \cdot 10^{-5}$ eV/K

Elementary Charge $q = 1.6021765 \cdot 10^{-19}$ C

Vacuum Permittivity $\epsilon_0 = 8.8541878 \cdot 10^{-12}$ F/m

Symbols

D	Diffusivity	m^2/s
E	Electric Field	V/m
h	Unit Distance	m
I	Current	A
J	Current Density	A/m^2
L_D	Debye Length	m
l_f	Mean Free Path	m
M	Memristance	Ω
n	Electron Density	m^{-3}
N_A	Acceptor Density	m^{-3}
N_D	Donor Density	m^{-3}
n_i	Intrinsic Carrier Density	m^{-3}
T	Temperature	K
t	Time	s
t_{dr}	Dielectric Relaxation Time	s
U	Generation Recombination Rate	$m^{-3}s^{-1}$
V	Potential	V
V_{th}	Thermal Voltage	V
Δ	Unit Distance	m
ϵ_r	Relative Permittivity	unitless
μ	Mobility	$m^2/(Vs)$
φ	Flux Linkage	Wb
ρ	Charge Density	C/m^3
v	Drift Speed	m/s

Chapter 1

Introduction

1.1 Thesis Objectives

The purpose of this thesis is to create a numerical simulation which captures the physics behind the operation of a coupled ionic-electronic device.. The proposed model can be used for researching the physics behind the actual device through further modeling or as a tool for designing coupled ionic electronic devices for a specific purpose.

As an example of a coupled ionic-electronic device, a memristor model is created using only the essential components and physical effects. A numerical solver for the coupled drift diffusion and Poisson equations is developed and tested. A memristor simulation is created by modifying the drift diffusion solver to accommodate all the essential physical effects. Finally simulation results are compared with experimental results from a memristor fabricated at Carleton University.

1.2 Thesis Overview

After a brief introduction to coupled ionic electronic devices, the discovery of the memristor and challenges in memristor research is introduced in the first chapter. It emphasizes the need for better physical modeling for the memristor and the lack of simulation tools required for further analysis and research.

In chapter 2 , the Boltzmann Transport Equations (BTE) is introduced. This introduction is followed by the explanation of the charge transport mechanisms captured through the BTE. Additionally drift diffusion equations (a simplified form of BTE) which are used for the simulation of a coupled ionic-electronic device are discussed. Finally various analytic solutions to drift diffusion equations, such as charged particles moving over an infinite conductor and a PN junction, are derived and plotted.

A numerical solution to the drift diffusion equations is formed in chapter 3 in order to calculate the movement of all the charged particles in a coupled ionic-electronic device. First a finite difference method, which is the basis for all the simulations in this thesis is introduced. Then it is applied to the drift diffusion equations. Additionally, a Poisson solver to be used with the drift diffusion equations is developed in order to calculate the electric field generated by charged particles and metal contacts. Various schemes for solving these differential equations as well as numerical and physical limitations are discussed in detail.

The structure of the organic memristor and the physical model used for the simulation is discussed in detail in chapter 4. The set of equations and boundary conditions necessary for the solution of both the drift diffusion equations and the Poisson solver are introduced. A special mechanism that was developed to limit the ion density at a particular area is discussed in detail. All the equations, additional physical effects and boundary conditions combined generate a set of equations to be solved for the simulation of the memristor.

In chapter 5, the numerical solver developed in chapter 3 is tested against analytic solutions as well as numerical solutions generated by a commercially available simulator called (COMSOL Multiphysics)[23]. A mechanism to limit the maximum density of any particle, which is essential for memristor simulation, is developed and tested.

After the stability and the accuracy of the simulation scheme is tested in chapter 6 a 1-D approximation for a 2-D memristor simulation is proposed and simulated. Upon demonstrating that the simulations produced reasonable results, the validity of the approximations made for 1-D and 2-D simulations are investigated.

A full 2-D simulation is discussed in chapter 7. Memristors with various PEDOT:PSS thicknesses are simulated and compared to each other. The simulation with thinnest PEDOT is compared to 1-D simulations made in the previous chapter. Finally memristor simulations are compared against experimental data.

The concluding chapter summarizes the findings of the thesis, discusses the advantages and disadvantages of the proposed simulation methods and provides suggestions for improvements on the model and opportunities for further research.

1.3 Contributions

- Numerical modelling of an organic memristor, which is a charge dependent resistor, using drift diffusion equations.
- Development of a numerical method to model physical processes limiting the amount of lithium ions that can accumulate inside the PEDOT:PSS.
- Simulation of two different ionic electronic structures, a single strip and a notched PEDOT:PSS, for various applied potentials.
- Model verification through experimental results.

1.4 Background

A coupled electronic-ionic device's behavior is determined by the movement of mobile charged particles such as ions, holes and electrons inside a confined space. There are many examples of engineered and natural coupled electronic ionic devices. A good example of a natural ionic-electronic device is the ionic-channels in organic membranes which carry ions such as sodium, potassium, chlorine and calcium [1][2]. In electrical engineering coupled electronic-ionic devices are commonly proposed as an alternative to non-volatile memory devices due to ease of scalability and fabrication as well as low operation voltages [3][4]. They have also been proposed to be used as organic field effect transistors[5]. It is possible to find many physical models that are used simulate the

behavior of an ionic electronic device using the drift-diffusion (aka. Poisson-Nernst-Planck) equations [3][6][7].

As an example of a coupled ionic-electronic device, the modeling and the simulation of a memristor is studied in this thesis. The term memristor was first used by Leon Chua in 1971 in his paper called “Memristor The Missing Circuit Element” [8]. He theorized that there is a fourth passive circuit element yet to be discovered in addition to resistor, capacitor and inductor. He said that we already know and use five out of six possible combinations that can be made out of four fundamental circuit variables, current I , voltage V , charge q and flux linkage φ . Chua claimed that there is a missing circuit element which produces a relationship between flux linkage (time integral of the potential) and charge. He introduced a new variable named memristance which has units of resistance and it is a function of charge. The relationship between the current and the potential of a memristor is calculated by replacing the resistance by memristance in ohms law [9]:

$$v(t) = M(q(t))i(t) \quad (1.1)$$

Theoretically a memristor retains its resistance in the absence of any power source. When a potential is applied, the resistance can be influenced by the direction and the magnitude of the current. If the current flows in one direction the resistance increases and if it flows in the other direction the resistance decreases. This produces an I-V response which looks like a pinched hysteresis curve. This response is the main characteristic of a memristor.

This new element remained mostly a theory and it did not get a lot of academic attention until a group of researchers in Hewlett Packard developed a fully functioning memristor [10]. They successfully fabricated a nano scale memristor using TiO_2 (titanium dioxide). After the discovery in HP labs there was an increase of interest in different types of memristors due to their potential applications for data storage and the addition of learning capabilities into passive circuits [11] [12] [13].

Organic memristors are usually constructed on a larger scale than the TiO_2 fabricated at the HP labs. The memristor studied in this thesis is in the millimeter rather than nano meter scale and uses a conductor made out of a polymer called PEDOT:PSS. It is composed of two polymer chains, PEDOT and PSS attached together and conducts electricity via hole transport. Unfortunately the conduction mechanism is not perfectly understood and needs further research due to the complexity of the material [14].

Unlike an inorganic semiconductor like silicon, the structure of a polymer is quite irregular [14]. Polymers are formed of individual molecules with different chain lengths and a variable amount of defects. Additionally, they can be amorphous or partially crystalline and further differences occur through aging. The conduction and the electronic properties depend on the orientation of the polymer chains which are anisotropic and variable. These irregularities in the structure makes these conducting polymers resemble amorphous inorganic semiconductors. Following the concept of charge transport in amorphous inorganic semiconductors, the conduction mechanism of conducting polymers is commonly explained by variable range hopping. This mechanism was first introduced by Mott[15]. He proposed a model for charge transport in systems that are randomly disordered. In variable range hopping, charge transport occurs via jumps between available sites. Every charge carrier has a probability of jumping between two sites depending on its energy and the distance to the next available site. The conductivity is strongly effected by temperature as it changes the structure of the molecules and increases the energy of the charge carriers.

Apart from the temperature there are other methods to influence the conductivity of the PEDOT:PSS. It is possible to affect the conductivity by either doping or counter doping [16]. Depending on the method used, doping can be reversible or permanent. When reversible doping is employed, the resulting device behaves like a memristor since its resistance becomes dependent on charge. All these effects make physical modeling, experimentation and simulation very challenging.

Memristor modeling is in its infancy. A few compact models for inorganic memristors similar to the one produced in HP labs have been proposed [17][18][19]. There are also a number of modeling studies of organic memristors [6][20]. However, the work is slight

leaving room for further exploration. The physics behind the conduction mechanism and the changes in the conductivity due to doping requires further research and the development of a computer model can help in various ways. Theories that explain the movement of charged particles and their interactions with each other are difficult to formulate since it is hard to obtain required experimental data. A simulator can be a useful tool in testing various theories without having to set up and perform complicated experiments. Also once a solid understanding of the conduction mechanism is achieved and a reliable memristor model is developed, simulations can be very useful to test different device structures and optimize them before fabrication.

Chapter 2

Theory

The equations presented in this chapter as well as the derivation of drift diffusion equations form a basis for simulating coupled ionic-electronic devices. First, the Boltzmann transport equation which is the starting point for generating the drift diffusion equation is introduced. The introduction of the Boltzmann transport equation is followed by the derivation of the drift diffusion equation and the presentation of the set of equations that describe the behavior of a coupled ionic-electronic device. The last part of the chapter shows analytic solutions to the drift diffusion equations which are used to test the numerical methods derived in chapter 4.

2.1 Carrier Transport Equations

Drift diffusion equations, which are based on Boltzmann Transport Equations (BTE) [21], need to be solved in order to model the complex behaviour of an ionic electronic device. The drift diffusion equations used are derived by simplifying the BTE equation via approximations. These simplifications dictate the limits of the drift-diffusion model, therefore they need to be well understood.

The derivation of the Boltzmann transport equation starts by stating that a distribution of charged particles can be defined by their position in space \mathbf{r} and momentum \mathbf{k} in time t using a probability distribution function $f(k, r, t)$. This results in the most general form of the Boltzmann transport equation[22].

$$\frac{d}{dt}f(k, r, t) = 0 \quad (2.1)$$

This general form of BTE needs to be expanded and relevant physical equations need to be placed in to get an equation describing a specific problem or a device. Many different device simulators use some sort of approximation to the BTE. In commercial semiconductor simulators drift diffusion equations are commonly used to describe the movement of charge carriers such as holes (p) and electrons (n) in a material[23][24][25].

After this brief introduction to the BTE, rather than going through the mathematical derivation of the drift diffusion model, the approximations that are made along the process of derivation are discussed in order to get a better insight on the model. The approximations and equations presented in this chapter is based on C.M Snowden's book called "Semiconductor Device Modelling"[22]. It must be noted that the following derivation is only true for isotropic media but it can be extended to accommodate anisotropic media by using appropriate tensor equations for carrier /tjsrdrift and diffusionmobilities and diffusivities.

As a particle travels in a solid state device it collides with other particles as well as the atoms in the device. For the drift-diffusion equations individual lattice scattering events or collisions are averaged and all the particles have an average constant drift velocity under the effects of an electric field [22]. This means that all the particles respond instantaneously to the changes in the electric field. The movement of the particles due to the electric field is called the drift current. The relationship between the drift velocity and the electric field is given by the following equation:

$$v = \mu E \quad (2.2)$$

μ is called the mobility and it determines the average speed at which the particles move when subject to an electric field. Mobility of a particle can be a function of variables such as temperature or the electric field. Drift current density can be derived based on the drift velocity[22].

$$J_E = qn\mu E = qnv \quad (2.3)$$

Where q is the elementary charge and n is the electron density. In addition to the previous assumptions, it is assumed that the lattice is perfectly uniform, has a uniform temperature distribution and all the temperature of the particles are close to the temperature of the lattice. Based on this assumption it is possible say that all the particles move due to thermal effects with the same thermal velocity (v_{th}) and mean free path (l_f). These quantities can be combined into one single coefficient called the diffusion constant,

$$D = v_{th} l_f \quad (2.4)$$

The Drift and diffusion coefficients are related to each other via the Einstein relationship[22]:

$$D = \frac{\mu kT}{q} \quad (2.5)$$

Where k is the Boltzmann constant and T is the lattice temperature. The random thermally driven motion produces diffusion and results in a second term which contributes to the carrier movement and it is called the diffusion current density,

$$J_D = qD \frac{dn}{dx} \quad (2.6)$$

Unlike the drift current density, which is directly related to the carrier density, diffusion current density is related to the carrier density's first order derivative in space. Combining these two terms results in the following the current density equation for electrons in one dimension,

$$\vec{J}_n^x = q\mu_n n \vec{E}_x + qD_n \frac{dn}{dx} \quad (2.7)$$

This equation can be easily extended to other dimensions by simply using the appropriate terms:

$$\vec{J}_n^y = q\mu_n n \vec{E}_y + qD_n \frac{dn}{dy} \quad (2.8)$$

The current density equations can be used for both positively and negatively charged particles by changing the sign of the diffusion current density.

$$\vec{J}_p^x = q\mu_p p \vec{E}_x - qD_p \frac{dp}{dx} \quad (2.9)$$

Anisotropic drift and diffusion coefficients can be handled with ease by using different coefficients for different directions. Also the mobility and the diffusivity can be a function of any variable such as position or temperature.

Current density equations by themselves are not enough to solve this time dependent problem. It is necessary to account for the movement of charge over time which is captured in the continuity equation. It is a statement of conservation of particle density over time. The change in the amount of carriers over time in a particular area must be equal to the difference in current density over the same area. Additionally the amount of charge can change due to generation-recombination of charged particles. The continuity is captured by equations:

$$\frac{\partial n}{\partial t} = \frac{1}{q} \nabla \cdot \vec{J}_n + U_n \quad (2.10)$$

$$\frac{\partial p}{\partial t} = -\frac{1}{q} \nabla \cdot \vec{J}_p + U_p \quad (2.11)$$

U_n and U_p are net generation recombination rates.

Electric field can be generated in two different ways. One is through the distribution of net charge over the area and the other one is an externally applied potential. It is possible to calculate the potential distribution over an area by using Poisson's equation [21],

$$\nabla \cdot (\epsilon \nabla V) = -\rho \quad (2.12)$$

Where the variables ϵ , V , ρ are permittivity, electric potential and charge density respectively. Once the electric potential is known the electric field can be obtained by just calculating the negative gradient of the electric potential,

$$\vec{E} = -\nabla V \quad (2.13)$$

The electric field can be split into multiple components depending on the dimensions of the problem. In a 2-D case they are \vec{E}_x and \vec{E}_y .

$$\vec{E}_x = -\hat{x} \frac{\partial V}{\partial x} \quad (2.14)$$

$$\vec{E}_y = -\hat{y} \frac{\partial V}{\partial y} \quad (2.15)$$

Once the electric field and the current density is known, the current at any point in the device can be easily calculated by using the following integral [22],

$$I = \int_s \vec{J}_{tot} \cdot ds = \int_s (J_n + J_p + \varepsilon \frac{\partial E}{\partial t}) ds \quad (2.16)$$

Poisson's equation and drift-diffusion equations are coupled through the electric field and net charge distribution. The strength of this non-linear coupling depends on the size of the device and the charge density which determines the total amount of charge over an area. In a strongly coupled system of differential equations, small changes in either the charge density or the electric field can easily cause instabilities in the simulation. This is further discussed in the next chapter while developing a numerical scheme to solve the system of equations described in this chapter.

The main equations for the drift-diffusion model that are used for the coupled electronic-ionic simulation can be compactly written as:

$$\nabla \cdot (\varepsilon \nabla V) = -q(p - n + N_c - N_a + N_f) \quad (2.17)$$

$$\vec{J}_p = q\mu_p p \vec{E} - qD_p \nabla p \quad (2.18)$$

$$\vec{J}_n = q\mu_n n \vec{E} + qD_n \nabla n \quad (2.19)$$

$$\vec{J}_{N_a} = q\mu_{N_a} N_a \vec{E} + qD_{N_a} \nabla N_a \quad (2.20)$$

$$\vec{J}_{N_c} = q\mu_{N_c} N_c \vec{E} - qD_{N_c} \nabla N_c \quad (2.21)$$

$$\frac{\partial p}{\partial t} = -\frac{1}{q} \nabla \cdot \vec{J}_p + U_p \quad (2.22)$$

$$\frac{\partial n}{\partial t} = \frac{1}{q} \nabla \cdot \vec{J}_n + U_n \quad (2.23)$$

$$\frac{\partial N_a}{\partial t} = \frac{1}{q} \nabla \cdot \vec{J}_{N_a} + U_{N_a} \quad (2.24)$$

$$\frac{\partial N_c}{\partial t} = -\frac{1}{q} \nabla \cdot \vec{J}_{N_c} + U_{N_c} \quad (2.25)$$

This system of equations consist of 4 different mobile charged particles, holes (p), electrons (n), cations (N_c) and anions (N_a). N_f is used for fixed charge which can be positive or negative depending on the device. U is used for the generation recombination term of each mobile charge carrier. The particles are coupled to each other through Poisson's equation since they all carry electric charge. A drift diffusion model does not limit the number of mobile particles that can be simulated in a device. So this model can be easily modified to accommodate any number of mobile species based on what is physically present in a device. Even after many approximations to the BTE, the drift diffusion equations have analytical solutions for only few isolated cases. The analytical solutions developed in the rest of this chapter are used in the testing of the numerical method developed for simulating a memristor.

2.2 Analytic Solutions

Three different analytic solutions to drift diffusion equations are developed in this section. Initially a simple steady state problem with uniform electric field is solved. The second example, which is more complex than the first one, is a transient solution for a charge distribution moving under uniform electric field. Finally, a PN junction problem is solved which incorporates the drift diffusion equation with Poisson's equation and provides a steady state solution for electron/hole density distributions, electric potential and electric field.

2.2.1 Steady State Solution Over a Finite Domain

The problem that will be solved in this section consists of a finite amount of charge and a uniform electric field pushing this charge against a wall. It is assumed that the charge density is low enough not to affect the uniform electric field, therefore the solution of Poisson's equation is not necessary. To simplify the problem even further only a steady state solution is derived. Also it is important to note that the initial distribution of the charge density does not matter in this problem since all the charge will be redistributed in steady state. The only relevant information is the total amount of charge subject to the electric field. At steady state, drift and diffusion currents are in equilibrium and net current density is zero. Following equation shows the hole current density at equilibrium:

$$J_p(x) = q\mu_p pE - qD_p \frac{dp}{dx} = 0 \quad (2.26)$$

Total current density will only be zero when the drift current density generated by the electric field is completely balanced by the diffusion current density leading to:

$$q\mu_p pE = qD_p \frac{dp}{dx} \quad (2.27)$$

which can be rearranged to be,

$$\frac{\mu_p E}{D_p} p = \frac{dp}{dx} \quad (2.28)$$

This is a simple differential equation that can be solved by assuming that hole density has the following form:

$$p(x) = Ce^{ax} \quad (2.29)$$

C and **a** are arbitrary constants. Equation (2.29) can be placed into (2.28),

$$\frac{\mu_p E}{D_p} Ce^{ax} = aCe^{ax} \quad (2.30)$$

solving for *a* we have,

$$a = \frac{\mu_p E}{D_p} \quad (2.31)$$

A general form for the solution is generated by placing *a* back into equation (2.29) giving,

$$p(x) = Ce^{\frac{\mu_p E}{D_p} x} \quad (2.32)$$

It is possible to solve for **C** by observing that the total amount of charge at steady state must be equal to the initial amount of charges since all the holes remain inside the conductor. So the integral of the initial hole density distribution must be equal to the integral of the charge density at steady state,

$$\int_0^L Ce^{\frac{\mu_p E}{D_p} x} dx = \int_0^L p(t=0, x) dx$$

Which can be solved for *C*,

$$C = \frac{\int_0^L p(t=0, x) dx}{\int_0^L e^{\frac{\mu_p E}{D_p} x} dx} = \frac{\int_0^L p(t=0, x) dx}{\frac{D_p}{\mu_p E} [e^{\frac{\mu_p E}{D_p} L} - 1]} \quad (2.33)$$

Equation 2.32 combined with equation 2.33 gives a complete solution for this problem. This solution shows that increasing the electric field will increase the concentration of charge density at the edge of the conductor. Physically this behavior is reasonable, since the force that is pushing the particles against a wall is getting greater and it is making

the charges accumulate even more. The following plot demonstrates the affect of the electric field on the hole distribution.

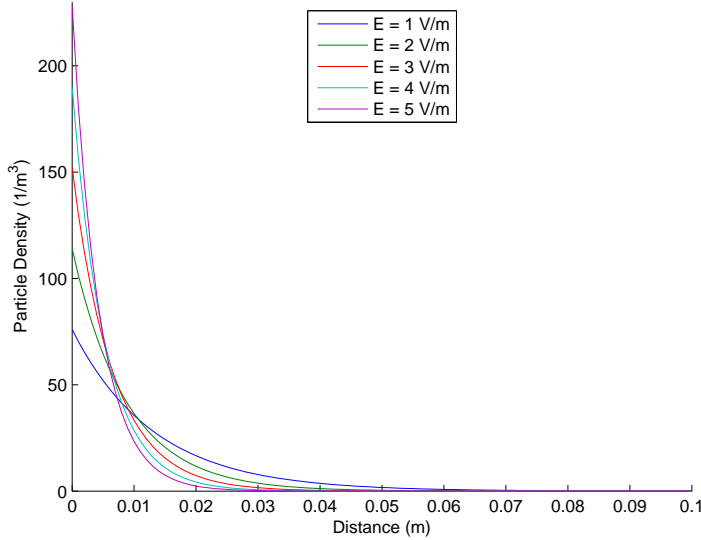


FIGURE 2.1: Increased accumulation of particles due to increased electric field

This phenomena is related to Debye screening which is characterized by the Debye length. The Debye length is the length over which mobile charge carriers screen out an external electric field and it determines how steeply charges will accumulate over a certain distance and it can be calculated using the following equation[21]:

$$L_D = \sqrt{\frac{\varepsilon V_{th}}{qn}} \quad (2.34)$$

Where the variables V_{th} , n and ε are thermal voltage, particle density and permittivity respectively. This example also illustrates the decrease in the debye length due to the increase in the charge density. Debye length is determined by the strength of the electric field created by the charge present in the material. The increase in the electric field in this example is analogous to the increase in charge density. Increased charge density creates a larger electric field. This creates a steeper accumulation of the charged particles and a decrease in the debye length.

2.2.2 Transient Solution Over an Infinite Domain

The problem that is solved in this section consists of an initial particle density distribution subject to a uniform electric field over an infinitely long conductor. The charge distribution drifts and diffuses over time. This requires a transient solution and therefore the continuity equation (2.10) needs to be solved. Again, it is assumed that charged particles do not affect the electric field since their density is low enough , therefore solution of Poisson's equation is not necessary.

The first step of the solution process is the insertion of (2.7) into (2.10).

$$\frac{\partial n}{\partial t} = \frac{1}{q} \nabla \cdot (\vec{J}_n) \quad (2.35)$$

Substituting in the drift-diffusion expression for J_n we obtain,

$$\frac{\partial n}{\partial t} = \frac{1}{q} \nabla \cdot (q\mu_n n \vec{E} + qD_n \frac{dn}{dx}) \quad (2.36)$$

For 1-D this can be simplified to:

$$\frac{\partial n}{\partial t} = \mu_n E \frac{dn}{dx} + D_n \frac{d^2 n}{dx^2} \quad (2.37)$$

Using separation of variables the solution can be separated into time and space dependent functions[26],

$$n(t, x) = n(t)n(x) = n_t n_x \quad (2.38)$$

Placing equation (2.38) into (2.37) and dividing by $n(t,x)$,

$$\frac{1}{n_t} \frac{dn_t}{dt} = \mu_n E \frac{1}{n_x} \frac{dn_x}{dx} + D \frac{1}{n_x} \frac{d^2 n_x}{dx^2} \quad (2.39)$$

Assuming both sides of the equation are equal to a constant $-k$, time dependent part of the problem becomes a simple first order differential equation.

$$\frac{1}{n_t} \frac{dn_t}{dt} = -k$$

$$\frac{dn_t}{dt} = -kn_t$$

Based on the above differential equation n_t can take the following form:

$$n_t = C_1 e^{-kt} \quad (2.40)$$

With for n_x assuming a solution of the form below,

$$n_x = C_2 e^{-j\omega x} \quad (2.41)$$

Placing (2.41) into (2.39) we obtain,

$$\omega^2 D C_2 e^{-j\omega x} - j\omega \mu_n E C_2 e^{-j\omega x} + k C_2 e^{-j\omega x} = 0 \quad (2.42)$$

Simplifying equation (2.42) and solving for k gives,

$$k = \omega^2 D + j\omega \mu_n E \quad (2.43)$$

Combining equation (2.40), (2.41) and (2.43) to get the initial form of the solution.

$(C = C_1 C_2)$

$$n = n_t n_x = C e^{(-\omega^2 D + j\omega \mu_n E)t} e^{-j\omega x} \quad (2.44)$$

The application of the superposition principle[27] leads to:

$$n = n_t n_x = \int_{-\infty}^{\infty} C(\omega) e^{(-\omega^2 D + j\omega \mu_n E)t} e^{-j\omega x} d\omega \quad (2.45)$$

The distribution of n_x is known at $t=0$.

$$n(x, t = 0) = \int_{-\infty}^{\infty} C(\omega) e^{-j\omega x} d\omega \quad (2.46)$$

$C(\omega)$ is the inverse Fourier transform of $n(x, 0)$,

$$C(\omega) = \int_{-\infty}^{\infty} n(x, 0) e^{j\omega x} dx \quad (2.47)$$

The final form of the solution is generated by placing equation (2.47) into (2.45):

$$n = \int_{-\infty}^{\infty} \int_{-\infty}^{\infty} n(z, 0) e^{j\omega z} dz e^{(\omega^2 D - j\omega \mu_n E)t} e^{j\omega x} d\omega \quad (2.48)$$

Rearranging equation (2.48),

$$n = \int_{-\infty}^{\infty} \int_{-\infty}^{\infty} n(z, 0) e^{(\omega^2 D - j\omega \mu_n E)t} e^{j\omega x} e^{j\omega z} dz d\omega \quad (2.49)$$

Using a gaussian initial distribution results in:

$$n(x, 0) = e^{-(\frac{x-x_o}{\sigma})^2} \quad (2.50)$$

$$n(x, t) = \frac{1}{\sqrt{4D_n t + \sigma^2}} e^{-\frac{(t\mu_n E - x + x_o)^2}{4D_n t + \sigma^2}} \quad (2.51)$$

If the initial distribution is a rectangular then the solution takes the following form:

$$n(x, 0) = \prod (w(x)) \quad (2.52)$$

which leads to,

$$n(x, t) = \frac{1}{2} \operatorname{erf}\left(\frac{w + 2t\mu_n E - 2x}{4\sqrt{D_n t}}\right) - \frac{1}{2} \operatorname{erf}\left(\frac{-w + 2t\mu_n E - 2x}{4\sqrt{D_n t}}\right) \quad (2.53)$$

Following plots show the evolution of two particle densities with the different initial distributions described above.

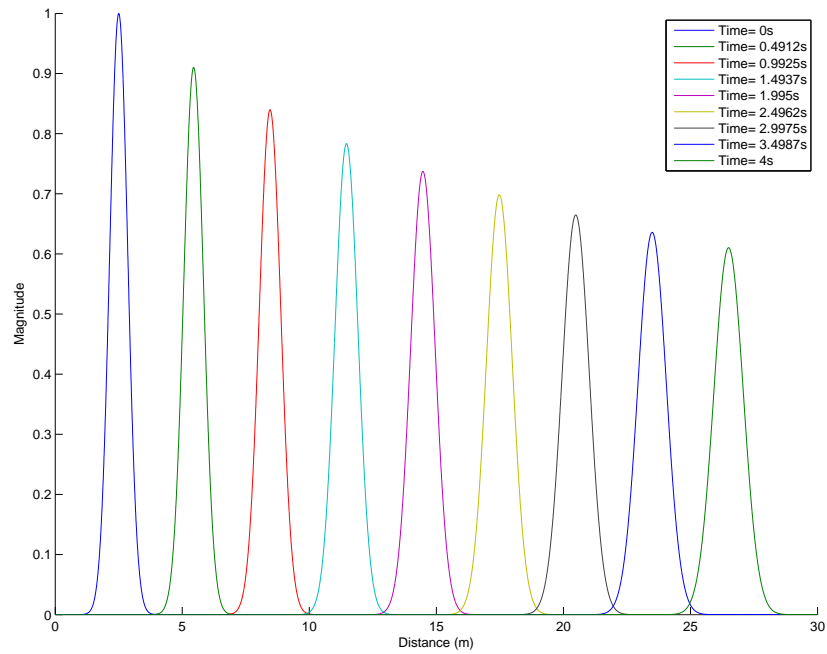


FIGURE 2.2: A gaussian particle density distribution drifting and diffusing over time

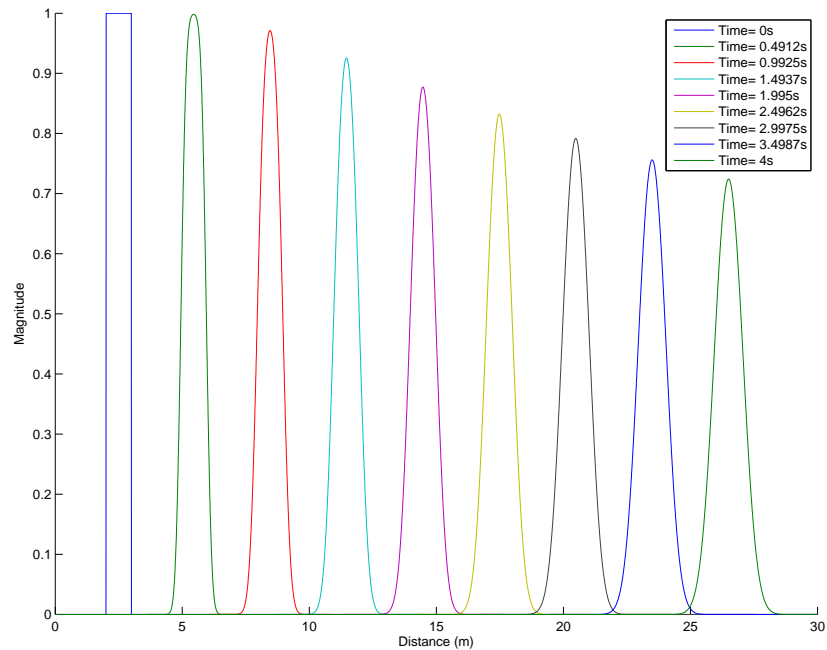


FIGURE 2.3: A rectangular particle density distribution drifting and diffusing over time

2.2.3 PN Junction

The previous analytical solutions involved the solution of Poisson's equation and the continuity equation which were assumed to be not coupled. An example where these equations are tightly coupled is examined in this section. There are usually no direct analytical solutions for coupled equations but it is possible to get a closed form solution by making use of certain approximations. One example of this situation is an abrupt p-n junction. The derivations for an abrupt junction presented in this section is mostly based on the book "Physics of Semiconductor Devices" written by Kwok K. Ng et al. [28].

An abrupt p-n junction is created when two materials of opposite doping, p-type and n-type, are brought together. For this example the p-type material has a net hole concentration of N_A and the n-type materials has a net electron concentration of N_D . The junction is defined at the interface where $N_A = N_D$ [28].

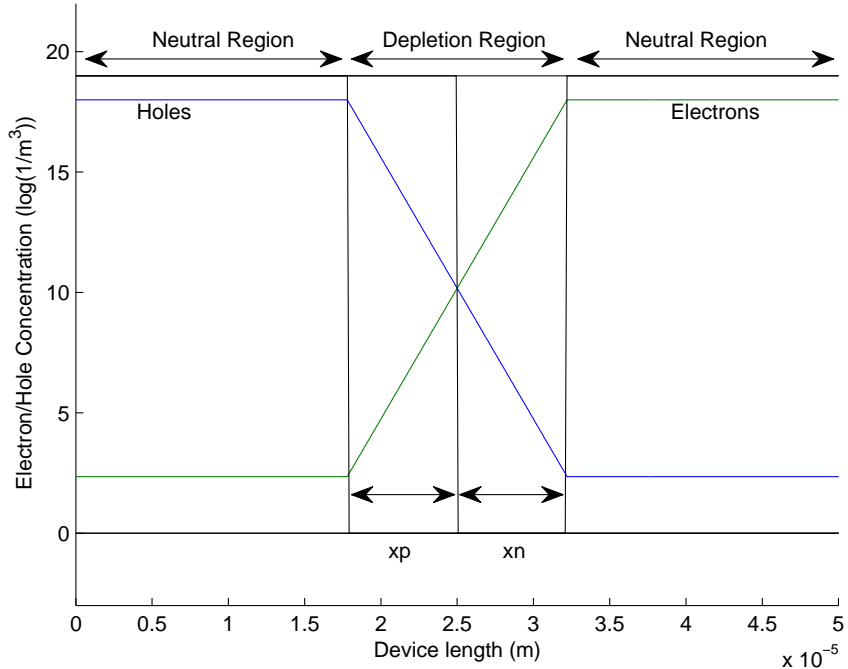


FIGURE 2.4: PN junction electron/hole density

In this example an analytical solution for an abrupt p-n junction is derived. To obtain a solution for this problem the depletion region approximation is used. This approximation starts by assuming that the charges are fully depleted around the junction[28]. All the

electric field is confined in the depletion region and regions far away from the junction are neutral. Based on this, the net charge density over the entire region is:

$$\frac{d\vec{E}}{dx} = \frac{\rho}{\epsilon} = \frac{q}{\epsilon}(-N_A + N_D) \quad (2.54)$$

with,

$$\rho = \begin{cases} 0 & \text{for } x < -x_p \\ -qN_A & \text{for } -x_p \leq x \leq 0 \\ qN_D & \text{for } 0 \leq x \leq x_n \\ 0 & \text{for } x > x_n \end{cases} \quad (2.55)$$

The electric field over the entire region can be calculated by integrating ρ ,

$$E = \begin{cases} \int \frac{-qN_A}{\epsilon} dx + C_1 & \text{for } -x_p \leq x \leq 0 \\ \int \frac{qN_D}{\epsilon} dx + C_2 & \text{for } 0 \leq x \leq x_n \end{cases} \quad (2.56)$$

It is possible to solve for C_1 and C_2 since electric field must go to zero at x_p and x_n ,

$$\begin{aligned} E(x = -x_p) &= 0 \Rightarrow C_1 = \frac{-qN_A}{\epsilon} x_p \\ E(x = x_n) &= 0 \Rightarrow C_2 = \frac{qN_D}{\epsilon} x_n \end{aligned} \quad (2.57)$$

Then $E(x)$ becomes:

$$E(x) = \begin{cases} \frac{-qN_A}{\epsilon}(x + x_p) & \text{for } -x_p \leq x \leq 0 \\ \frac{qN_D}{\epsilon}(x - x_n) & \text{for } 0 \leq x \leq x_n \end{cases} \quad (2.58)$$

Additionally, the electric field must be continuous across the interface therefore the electric field in the p-type side and the n-type side must equal each other at the interface or when $x = 0$ giving,

$$\frac{-qN_A}{\epsilon}(x_p) = \frac{qN_D}{\epsilon}(-x_n)$$

$$N_A x_p = N_D x_n \quad (2.59)$$

This equation states that the total charge on one side of the junction must be the same as the total charge on the other. In other words, the net charge on each side keeps the electric field confined to the depletion region.

To find the voltage as a function of distance, equation 2.13 can be integrated,

$$V(x) = \begin{cases} \int -E(x)dx = \int \frac{qN_A}{\varepsilon}(x + x_p)dx = \frac{qN_A}{\varepsilon}\left(\frac{x}{2} + x_p\right) + C_3 & \text{for } -x_p \leq x \leq 0 \\ \int -E(x)dx = \int \frac{qN_D}{\varepsilon}(x - x_n)dx = \frac{qN_D}{\varepsilon}\left(-\frac{x}{2} + x_n\right) + C_4 & \text{for } 0 \leq x \leq x_n \end{cases} \quad (2.60)$$

The potential at one side of the junction can be set to zero. Defining the voltage on the *p* type side as zero, such that at $x = x_p$, $V=0$ gives the constant C_3 as:

$$C_3 = \frac{qN_A}{2\varepsilon}x_p^2 \quad (2.61)$$

and we obtain for the potential distribution,

$$V(x) = \frac{qN_A}{2\varepsilon}(x + x_p)^2 \quad \text{for } -x_p \leq x \leq 0 \quad (2.62)$$

The constant C_4 can be found by using the fact that the potential on the n-type side and p-type side are equal at the interface, such that:

$$V_p(x = 0) = \frac{qN_A}{2\varepsilon}x_p^2 = V_n(x = 0) = \frac{qN_A}{2\varepsilon}(x_n - \frac{x}{2})x + C_4 \quad (2.63)$$

and we have,

$$C_4 = \frac{qN_A}{2\varepsilon}x_p^2 \quad (2.64)$$

Now an overall expression for $V(x)$ can be obtained,

$$V(x) = \begin{cases} \frac{qN_A}{\varepsilon}(x + x_p)^2 & \text{for } -x_p \leq x \leq 0 \\ \frac{qN_D}{\varepsilon}\left(-\frac{x}{2} + x_n\right)x & \text{for } 0 \leq x \leq x_n \end{cases} \quad (2.65)$$

The maximum voltage across the junction is at $x = x_n$, which is:

$$V_{bi} = \frac{q}{2\varepsilon} (N_D x_n^2 + N_A x_p^2) \quad (2.66)$$

Using (2.59) in the above equation and rearranging allows x_p and x_n to be determined.

They are:

$$x_n = \sqrt{\frac{2\varepsilon V_{bi}}{q} \frac{N_A}{N_D(N_D + N_A)}} \quad (2.67)$$

$$x_p = \sqrt{\frac{2\varepsilon V_{bi}}{q} \frac{N_D}{N_A(N_D + N_A)}} \quad (2.68)$$

The value of the built in potential can be calculated using the following equation[29]:

$$V_{bi} = \frac{kT}{q} \ln\left(\frac{N_A N_D}{n_i^2}\right) \quad (2.69)$$

The calculation of the built in potential completes all the necessary equations for the analytical solution of the pn junction without any external bias. The figure 2.5 shows the plots of approximate solutions for net charge, electric field and the junction potential.

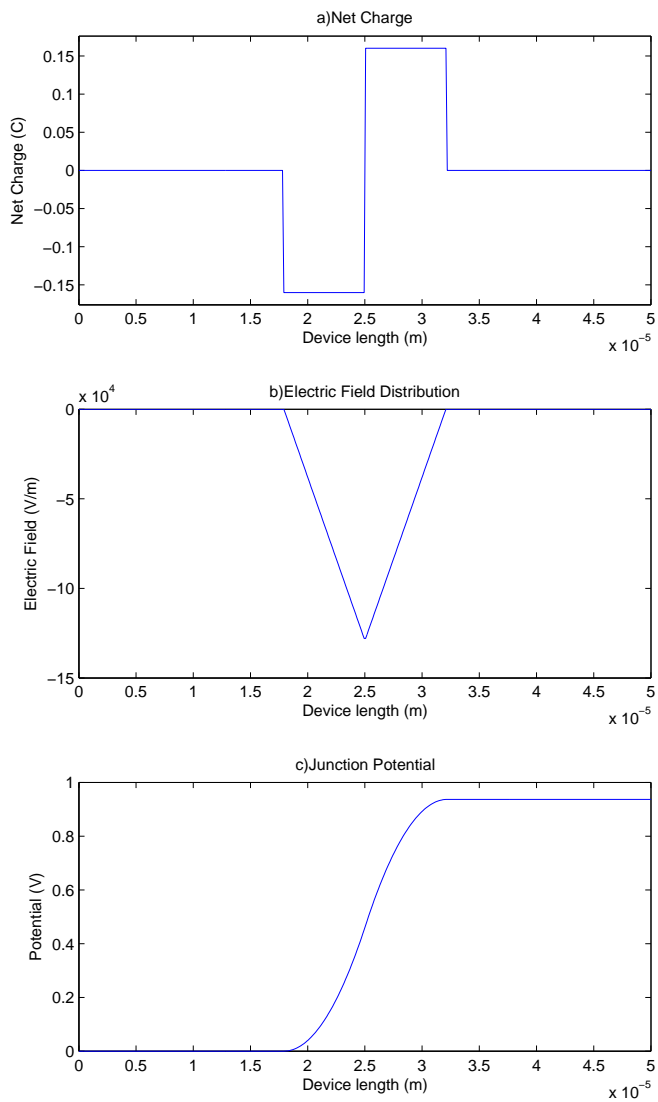


FIGURE 2.5: Approximate Solution of a PN Junction

Chapter 3

Numerical Solution of Drift-Diffusion and Poisson's Equation

The simulation method developed in this thesis to model charge transport in a region requires certain properties, such as the saturation of a particle density or a combination of 1-D and 2-D simulations, which are not available in most commercial simulators. In future extensions of this work it is anticipated that other unusual properties that are not studied in this thesis will be needed which are also not normally implemented in commercial solvers. For these reasons it was decided to write a Matlab based simulator and in this chapter a method for solving drift diffusion equations as well as Poisson's equation are developed based on finite difference method.

3.1 Finite Difference Method

There are many different methods that can be used to solve drift diffusion equations such as finite elements[30], finite difference[31] or meshless methods[32]. Finite difference was chosen as an appropriate method for this thesis due to its simplicity which allows straightforward implementation of unusual physical properties. Finite difference uses an approximation for the derivative of a function based on the mathematical definition of

the derivative[33],

$$\frac{df}{dx} = \lim_{h \rightarrow 0} \frac{f(x + h) - f(x)}{h} \quad (3.1)$$

It is possible to obtain a numerical approximation for the first derivative of a function by dropping the limit and assuming that h is small enough that the numerical derivative is reasonably close to the actual derivative. As h gets smaller the approximation becomes more and more accurate. The difference between the calculated value and the real value is called the truncation error and it is captured using $O(h^n)$ notation. n signifies the order of h which determines how fast the approximation is approaching the real solution as h decreases[33],

$$\frac{df}{dx} = \frac{f(x + h) - f(x)}{h} + O(h) \quad (3.2)$$

It is possible to uniformly discretize the entire region over which a function is defined in order to calculate its derivative. The first step is the division of the region over which the function is defined into $n-1$ segments. This creates n number of points. Then the length of each segment is defined using the following relationship:

$$h = \frac{L}{n} \quad (3.3)$$

A function is defined at the edge of every segment. All the points can be labeled consecutively, $x_0, x_1, x_2 \dots x_{n-1}$ where $x_i = ih$. The function is discretely defined on $f_i = f(x_i)$ where $i=0,1,2..n-1$. It is possible to use equation 3.2 to discretely calculate the first derivative of the function with respect to x ,

$$\frac{df(x_i)}{dx} = \frac{f(x_{i+1}) - f(x_i)}{h} + O(h) \quad (3.4)$$

Above equation is called forward difference because the derivative for point x_i was calculated using the point that is coming right after it, x_{i+1} ,

$$f'_i = \frac{f_{i+1} - f_i}{h} + O(h) \quad (3.5)$$

Forward difference is not the only way to calculate a numerical derivative. Here are a couple other ways calculate the same derivative by using different points.

$$f'_i = \frac{f_i - f_{i-1}}{h} + O(h) \quad (3.6)$$

$$f'_{i+\frac{1}{2}} = \frac{f_{i+1} - f_i}{h} + O(h^2) \quad (3.7)$$

Equation 3.6 is called backward difference and equation 3.7 is called central difference. One important aspect to note here is that in the central difference formula the derivative falls exactly in the middle of two points. It also gives more accurate results using the same number of points as forward and backward difference.

Using finite difference formulas it is possible to construct higher order derivatives. A formula for a second order derivative at point x_i using central difference can be calculated using a first order derivative on $x_{i-\frac{1}{2}}$, x_i and $x_{i+\frac{1}{2}}$

$$f'_{i+\frac{1}{2}} = \frac{f_{i+1} - f_i}{h} \quad (3.8)$$

$$f'_{i-\frac{1}{2}} = \frac{f_i - f_{i-1}}{h} \quad (3.9)$$

$$f'_i = \frac{f_{i+\frac{1}{2}} - f_{i-\frac{1}{2}}}{h} \quad (3.10)$$

The second order derivative is constructed by taking the second derivative of the last function. Then equations 3.8 and 3.9 are placed into 3.10,

$$f''_i = \frac{f'_{i+\frac{1}{2}} - f'_{i-\frac{1}{2}}}{h}$$

$$f''_i = \frac{\frac{f_{i+1}-f_i}{h} - \frac{f_i-f_{i-1}}{h}}{h}$$

$$f''_i = \frac{f_{i+1} - 2f_i + f_{i-1}}{h^2}$$

Second order derivative then takes the following form:

$$f''_i = \frac{f_{i+1} - 2f_i + f_{i-1}}{h^2} + O(h^2) \quad (3.11)$$

These finite difference equations are sufficient to solve drift diffusion equations. Even though all the derivations are done in 1-D it is trivial to extend them to other dimensions. This method can be used to solve Poisson's equation and drift diffusion equations.

3.2 Poisson Solver

Poisson's equation needs to be solved before drift diffusion equations in order find the potential distribution as well as the electric field inside the device. In order to solve for the electric field and the potential, Poisson's equation,

$$\nabla \cdot (\varepsilon \nabla V) = -\rho \quad (3.12)$$

is simplified through assumptions and then the finite difference method is used to solve this simplified equation[34]. The first step of simplification is assuming that the permittivity is isotropic which gives,

$$\nabla \cdot (\varepsilon \nabla V) = \varepsilon \nabla^2 V \quad (3.13)$$

Dividing both sides of (3.12) by the permittivity and expanding the left hand side we get,

$$\nabla^2 V = -\frac{\rho}{\varepsilon} \quad (3.14)$$

Where for two dimensions,

$$\nabla^2 V = \frac{\partial^2 V}{\partial x^2} + \frac{\partial^2 V}{\partial y^2} \quad (3.15)$$

After discretizing the electric potential over a uniform 2-D grid and using the second order central finite difference formula (3.11) the Laplacian of the electric potential can be calculated using[26]:

$$\nabla^2 V_{i,j} = \frac{V_{i+1,j} - 2V_{i,j} + V_{i-1,j}}{\Delta x^2} + \frac{V_{i,j+1} - 2V_{i,j} + V_{i,j-1}}{\Delta y^2} \quad (3.16)$$

Since the grid is uniform the distance between two nodes in x and y directions are equal only one variable is needed to represent the distance between two points.

$$\Delta = \Delta x = \Delta y \quad (3.17)$$

Net charge density and the permittivity is also discretized over the same uniform mesh and

a discretized form of Poisson's equation is generated by combining equations 3.14, 3.16 and 3.17,

$$\nabla^2 V_{i,j} = \frac{V_{i-1,j} + V_{i,j-1} - 4V_{i,j} + V_{i+1,j} + V_{i,j+1}}{\Delta^2} = -\frac{\rho_{i,j}}{\varepsilon_{i,j}} \quad (3.18)$$

This equation can be rearranged into the form below:

$$\varepsilon_{i,j}(V_{i-1,j} + V_{i,j-1} - 4V_{i,j} + V_{i+1,j} + V_{i,j+1}) = -\Delta^2 \rho_{i,j} \quad (3.19)$$

Combining the equations above (3.19, 4.16, 4.17 and 4.18) it is possible to turn Poisson's equation, which is a second order differential equation, into a linear set of coupled algebraic equation,

$$D_2 \vec{V} = -\Delta^2 \vec{\rho} - \vec{V}_b \quad (3.20)$$

The matrix D_2 is the Laplace operator converted into a matrix using the finite difference method. One can easily get the potential distribution by simply solving,

$$\vec{V} = D_2^{-1}(-\Delta^2 \vec{\rho}_{i,j} - \vec{V}_b) \quad (3.21)$$

Due to the nature of the problem the resulting matrix D_2 is quite sparse and using a sparse LU rather than a regular LU decomposition increases the computational efficiency. Additionally, the LU decomposition only needs to be performed once since the equation is static and the L and U matrices can be reused for all the solutions following the initial one.

After solving for the potential distribution it is straightforward to calculate the electric field distribution discretely by using the relationship between the electric field and the electric potential (2.13) and the central difference equation (3.7) using,

$$E_{i,j}^x = -\frac{V_{i+1,j} - V_{i-1,j}}{2\Delta} \quad (3.22)$$

$$E_{i,j}^y = -\frac{V_{i,j+1} - V_{i,j-1}}{2\Delta} \quad (3.23)$$

3.3 Current Density Equations

Both drift and diffusion currents can be calculated over the entire grid. Drift current does not involve any differentials but it is a function of the electric field and the diffusion current can be calculated using first order central difference[21]. The current density is calculated in such a way that it falls between two points which simplifies the application of the boundary conditions. We have for the current density in the x direction,

$$J_{i+\frac{1}{2},j,k}^x = q\mu_n n_{i+\frac{1}{2},j,k} E_{i+\frac{1}{2},j,k}^x + qD_n \frac{n_{i+1,j,k} - n_{i,j,k}}{\Delta} \quad (3.24)$$

The electric field is calculated exactly on the nodes and linear interpolation is used in order to get a value between the nodes. The same argument is also valid for particle densities p and n . They are defined at the nodes but they are linearly interpolated to be used in current density equations:

$$n_{i+\frac{1}{2},j,k} = \frac{n_{i+1,j,k} + n_{i,j,k}}{2}$$

$$E_{i+\frac{1}{2},j,k}^x = \frac{E_{i+1,j,k}^y + E_{i,j,k}^y}{2}$$

Current density in y direction is calculated by following the same method:

$$J_{i,j+\frac{1}{2},k}^y = q\mu_n n_{i,j+\frac{1}{2},k} E_{i,j+\frac{1}{2},k}^y + D_n \frac{n_{i,j+1,k} - n_{i,j,k}}{\Delta} \quad (3.25)$$

$$n_{i,j+\frac{1}{2},k} = \frac{n_{i,j+1,k} + n_{i,j,k}}{2}$$

$$E_{i,j+\frac{1}{2},k}^y = \frac{E_{i,j+1,k}^y + E_{i,j,k}^y}{2}$$

3.3.1 Continuity Equation

The continuity equation is needed to calculate a transient solution for the drift diffusion equations. The equation is simple to discretize using the finite difference method. There are two terms that need to be discretized, a first order derivative in time and a first order derivative in space. First the divergence term in the equation (2.10) needs to be evaluated:

$$\nabla \cdot J = \frac{dJ_x}{dx} + \frac{dJ_y}{dy} \quad (3.26)$$

It is possible to replace the derivative with central finite difference terms:

$$\frac{dJ_x}{dx} = \frac{J_{i+\frac{1}{2},j,k}^x - J_{i-\frac{1}{2},j,k}^x}{h} \quad (3.27)$$

$$\frac{dJ_y}{dy} = \frac{J_{i,j+\frac{1}{2},k}^y - J_{i,j-\frac{1}{2},k}^y}{h} \quad (3.28)$$

leading to,

$$\nabla \cdot J_{i,j,k} = \frac{J_{i+\frac{1}{2},j,k}^x - J_{i-\frac{1}{2},j,k}^x}{h} + \frac{J_{i,j+\frac{1}{2},k}^y - J_{i,j-\frac{1}{2},k}^y}{h} \quad (3.29)$$

This is the general form of the divergence of the current density at each node. These equations are a linear function of particle densities \vec{n} and can be formulated into a matrix equation at time t_k , where k indicates the current time step,

$$\nabla \cdot J_k = B\vec{n}_k \quad (3.30)$$

The time derivative can be replaced by a forward or a backward finite difference term respectively,

$$\frac{\partial \vec{n}_k}{\partial t} = \frac{\vec{n}_{k+1} - \vec{n}_k}{\Delta t} \quad (3.31)$$

$$\frac{\partial \vec{n}_k}{\partial t} = \frac{\vec{n}_k - \vec{n}_{k-1}}{\Delta t} \quad (3.32)$$

It is possible to find a numerical transient solution for the drift-diffusion problem by combining finite difference form of the time derivative ((3.31) or (3.32)) and the divergence of the current density equations (3.30).

Forward difference approximation can be used to get an explicit solution for the continuity equation[21].

$$\frac{\vec{n}_{k+1} - \vec{n}_k}{\Delta t} = B\vec{n}_k$$

$$\vec{n}_{k+1} = \vec{n}_k + \Delta t B\vec{n}_k \quad (3.33)$$

Both forward and backward difference formulas work sequentially in order to generate a transient solution. The solution from the previous time step is needed to calculate the solution for the next time step. The forward difference gives an explicit solution which has a few advantages. This solution can be implemented, without forming any matrices by directly calculating the divergence of the current density for each node and then marching through time using equation 3.33. Additionally, unlike backward difference, there is no matrix equation to be solved for every time step. These two properties ease the computational load of the problem and speed up the solution process. Unfortunately this scheme has stability conditions which have to be met in order to produce a solution[21].

Backward difference can be replaced by forward difference to get an implicit solution:

$$\frac{\vec{n}_k - \vec{n}_{k-1}}{\Delta t} = \frac{1}{q}(qB\vec{n}_k)$$

$$\vec{n}_k - \Delta t B\vec{n}_k = \vec{n}_{k-1}$$

$$\vec{n}_k = (I - \Delta t B)^{-1}\vec{n}_{k-1} \quad (3.34)$$

This solution needs a matrix inversion every time step but it is unconditionally stable[21] as long as it is not coupled with Poisson's equation. The decision to use an implicit or an explicit solution requires deliberate analysis and it will be discussed in detail in the section 3.4.

3.4 Stability and Computational Efficiency

Before discussing the numerical limitations of solving the drift diffusion equation via finite difference it is important to look into the physical limitations of the problem. These limitations persist no matter what kind of numerical scheme is employed to solve the drift diffusion equation.

3.4.1 Physical Limitations

The Debye length is the length over which mobile charge carriers screen out an external electric field and it determines how steeply charges will accumulate over a certain distance[21]:

$$L_D = \sqrt{\frac{\epsilon V_{th}}{qn}} \quad (3.35)$$

The Debye length limits how coarse the grid can be since the distribution of the charge density needs to be accurately captured. As it can be seen from the formula above the higher the charge density is the steeper the charge will accumulate. This behavior is also appears in the analytic solution provided in section 2.2.1 in chapter 2. The accumulation of the charged particle at the wall becomes steeper as the electric field strength increases. The Debye length can become a major problem for large devices with high charge densities since the mesh density needs to be extremely high.

The amount of time it takes for charge fluctuations to disappear is called Dielectric relaxation time. It limits the maximum time step of a simulation since the fluctuations that are not properly resolved over time will make the simulation unstable[21]:

$$t_{dr} = \frac{\epsilon}{qn\mu} \quad (3.36)$$

The dielectric relaxation time is only important when the electric potential is significantly affected by the redistribution of charge over time. Otherwise it has minimal impact on the stability of the problem.

3.4.2 Numerical Limitations

There are also numerical limits which can affect convergence and stability of a solution when using an explicit finite difference scheme. These are called Courant-Friedrichs-Lowy (CFL) conditions [26]. CFL conditions for diffusion and drift are shown in the following equations:

$$\frac{\Delta^2}{2D_n} > \Delta t \quad (3.37)$$

The above condition is for only diffusion and it restricts the maximum time step. The following condition is for drift dominated systems:

$$\frac{2\Delta}{\mu E} > \Delta t \quad (3.38)$$

This is the second numerical restriction on the simulation. The condition for drift depends on the electric field therefore needs to be satisfied at all times as the electric field changes over time during simulation.

Both physical and numerical constraints have to be evaluated and mesh density and the time step need to be selected in order to satisfy all these conditions discussed above. Particularly mesh density has a very strong impact on the accuracy, stability and the computational efficiency of the simulation. Increasing the mesh density increases the computational time needed to calculate every time step since there are more operations to be performed. Additionally because of the CFL condition for diffusion, the time step is related to the square of the mesh size. This means that maximum allowed step size decreases much quicker than the mesh density. Also, increasing charge density can decrease the maximum mesh size to a very small value. This can be improved by using a non-uniform mesh which can dramatically decrease the number points needed for the simulation. This is usually not very straightforward to implement in a finite difference scheme and a small mesh size requires small time steps. This cannot be avoided through non-uniform meshing. Both numerical and physical constraints for the memristor simulation are further discussed in chapter 4.

3.4.3 Explicit vs. Implicit Solution

Overall explicit and implicit solutions have their advantages and disadvantages. Choosing one over the other requires a careful analysis of the problem. Implicit solution by itself is unconditionally stable therefore it can support very large time steps without any stability issues. However, the accuracy of the transient solution decreases with a larger time step but the steady state solution is not affected. So for steady state solutions it is better to use an implicit method which can reach steady state very quickly. This advantage disappears when the particle densities are high enough to affect the electric field and Poisson's equation needs to be solved for every time step. In this scenario the maximum time step is determined by the dielectric relaxation time which can be around the same order as CFL conditions or even smaller. Since the time step is going to be around the same order for both implicit and explicit methods it is reasonable to use the explicit solution because it is computationally less expensive.

Usually an implicit solution is preferable when there is no coupling between Poisson's equation and the drift diffusion equations and the transient response is not very important. Explicit solution has an edge over the implicit solution due to its lower computational requirements when the equations are coupled and the time steps for both schemes are restricted to small values. For memristor simulation, the drift diffusion equations are strongly coupled with Poisson's equation. For this reason all the memristor simulations in this thesis use explicit time stepping.

3.5 Simulation Procedure

The different equations and schemes that were used to solve the drift diffusion and Poisson's equation have been presented over the past few sections. Using all this information it is possible create a general approach to solve a drift diffusion problem. The geometry and the physical properties of the problem as well as all the initial and the boundary conditions need to be defined at the beginning of the solution process. The initialization sets up the first time step of the problem at $t = 0$. Once this first step is done it is possible generate the required vectors and matrices and solve the problem for the next time steps, $t = t_i$.

The solution process starts by solving Poisson's equation using the charge distribution at the current time step. Once it is solved, the electric field distribution is calculated and used in the drift diffusion equations to calculate the current density distribution. Explicit time stepping is used to determine the carrier density in the next time step. Finally once the carrier distribution for the next step is calculated it is possible check for a stopping criterion. If this criterion is not met then the whole process will start all over again. If the charge concentration is so small that the equations are decoupled then it is possible to skip solving Poisson's equation for the rest of the simulation which speeds up the solution process.

There are two different criteria that can be used to decide whether to finalize the simulation process or not. The simulation can stop if it reaches a certain point in time. This is quite simple since the current time can be checked and if it is equal or greater than the required simulation time then the simulation can be stopped. It is also possible to simulate until the simulation reaches steady state. This can be determined by comparing the current carrier distributions with distribution at the previous time step. If the difference is very small then the time derivatives of the carrier densities are very close to zero and the simulation has reached steady state therefore the simulation process can be stopped. The flowchart in figure 3.1 summarizes the solution procedure.

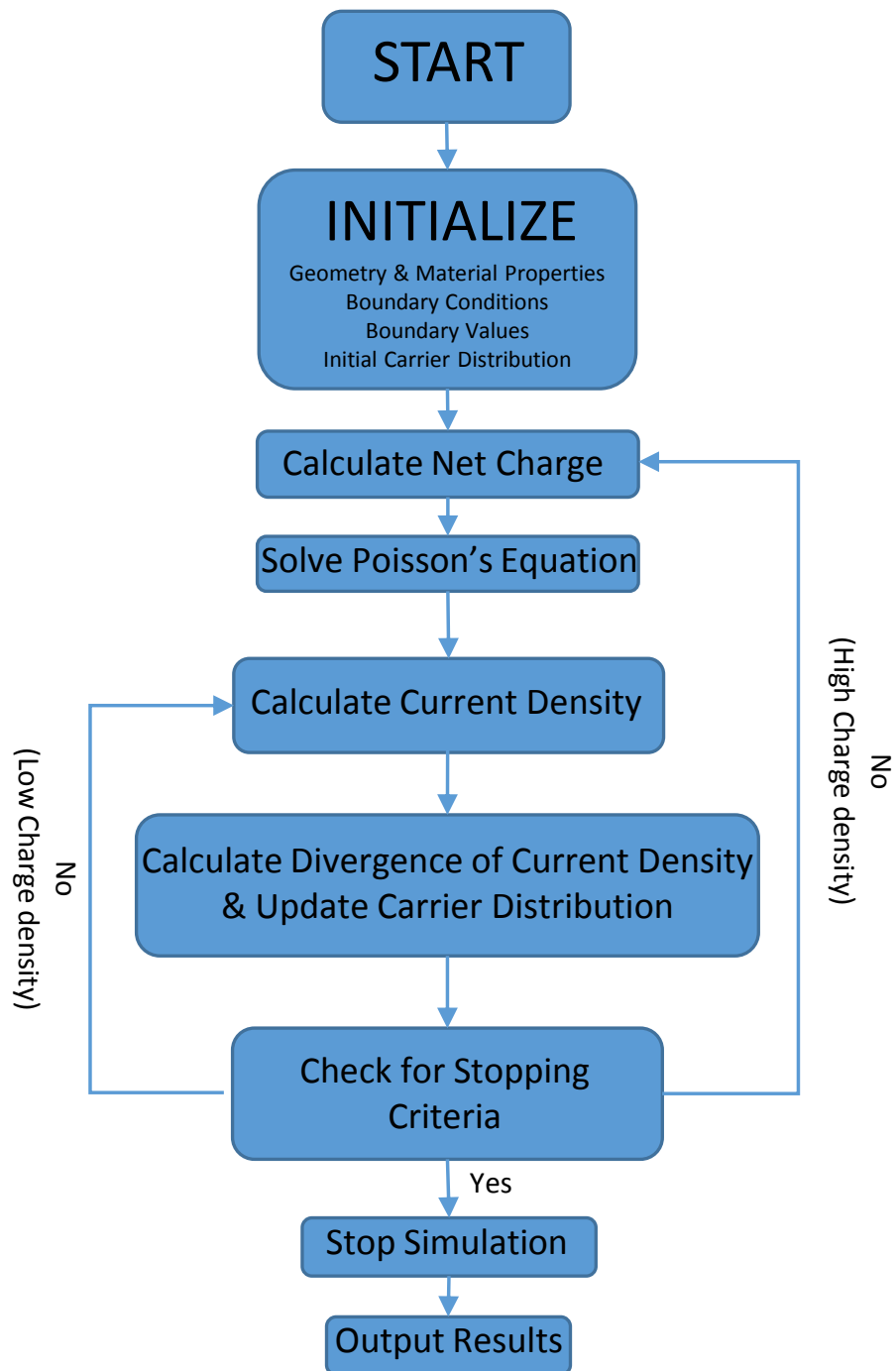


FIGURE 3.1: Finite Difference Drift-Diffusion Scheme Flowchart

Chapter 4

Simulation of a Memristor as a Coupled Electronic Device

An organic memristor, which is an example of a coupled ionic/electronic device, is simulated in this thesis. The memristor uses a strip of PEDOT:PSS as a conductor. A drop of an electrolytic solution which has lithium and perchlorate ions is placed on top of this conducting strip. When a potential is applied across the two ends of this conducting strip, lithium ions inside the electrolyte solution migrate into PEDOT:PSS and modify its conductivity. Figure 4.1 shows the memristor structure simulated in this thesis.

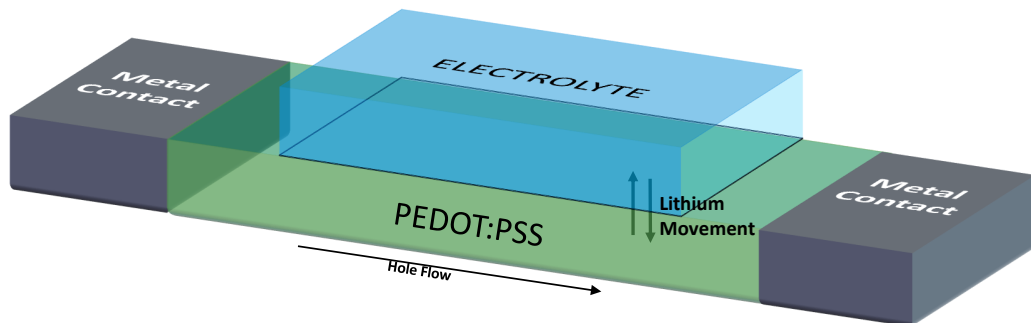


FIGURE 4.1: Organic memristor with electrolyte and PEDOT:PSS (not to scale)

One important characteristic of the simulated memristor is the movement of lithium ions inside PEDOT:PSS and how it limits the maximum resistivity of the device. As the lithium ions move into the PEDOT:PSS they bond with PSS polymer sites and replace holes. PEDOT:PSS can only absorb lithium as long as there are available PSS polymer sites to bond with therefore PEDOT:PSS has limited capacity to accept lithium ions. This physical property requires special treatment during simulation and the details are further discussed in section 4.2.1.

Hole transport inside PEDOT:PSS as well as lithium and perchlorate movement are modeled using basic drift diffusion equations which are derived in chapter 2. The following set of equations are used to simulate the ion and hole movement and the changes in electric field in an organic memristor using the finite difference method:

$$\nabla \cdot (\varepsilon \nabla V) = -q(p - N_{PSS} + N_{Li} - N_{ClO_4}) \quad (4.1)$$

$$\vec{J}_p = q\mu_p p \vec{E} - qD_p \nabla p \quad (4.2)$$

$$\vec{J}_{N_{ClO_4}} = q\mu_{N_{ClO_4}} N_{ClO_4} \vec{E} + qD_{N_{ClO_4}} \nabla N_{ClO_4} \quad (4.3)$$

$$\vec{J}_{N_{Li}} = q\mu_{N_{Li}} N_{Li} \vec{E} - qD_{N_{Li}} \nabla N_{Li} \quad (4.4)$$

$$\frac{\partial p}{\partial t} = -\frac{1}{q} \nabla \cdot \vec{J}_p \quad (4.5)$$

$$\frac{\partial N_A^-}{\partial t} = \frac{1}{q} \nabla \cdot \vec{J}_{N_{ClO_4}} \quad (4.6)$$

$$\frac{\partial N_{Li}}{\partial t} = -\frac{1}{q} \nabla \cdot \vec{J}_{N_{Li}} \quad (4.7)$$

The drift diffusion equations shown above hold for the ions in the electrolyte as long as fluid effects can be ignored. As it can be seen from the equations, there are three distinct types of mobile charged particles, holes (p), lithium (N_{Li}) and perchlorate(N_{ClO_4}) ions. In PEDOT:PSS there is also a finite amount of negatively charged particles which are immobile. They are only included in Poisson's equation.

The following sections define the boundary and the initial conditions that are used to solve drift diffusion equations for the memristor.

4.1 Memristor Structure and Initial Conditions

The following figure (4.2) shows the cross section of a simple memristor which is taken as a basis for all the memristor simulations presented in this thesis. It consists of 2 metal contacts, a polymer conductor strip (PEDOT:PSS) and an electrolyte solution which has lithium and perchlorate ions (perchlorate/lithium density $\approx 6.02 \cdot 10^{23} m^{-3}$). The memristor is about 1 cm long and 1 mm wide. The thickness of the conductive layer is around 1 μm . During the experiment, the electrolyte solution is deposited on PEDOT:PSS using a syringe so its thickness can vary drastically but as long as the amount of ions in the electrolyte solution is enough to saturate PEDOT:PSS this does not make a significant difference in the operation of the memristor.

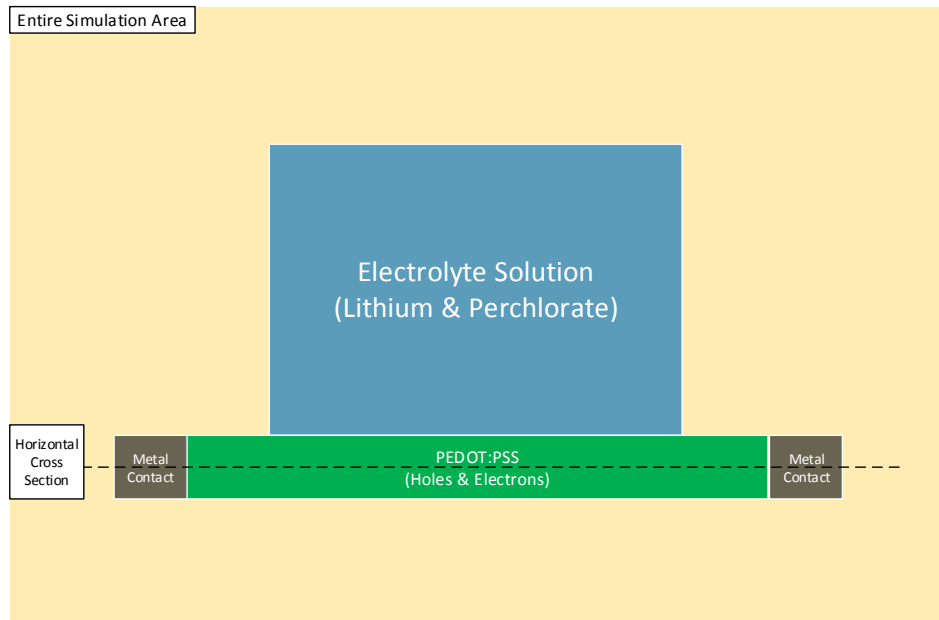


FIGURE 4.2: The structure of the memristor used for simulation (not to scale)

The initial conditions for all the charge carriers are the same. Negative and positive charges are balanced and uniformly distributed. Perchlorate ions are not allowed to move outside the electrolyte solution so a no flow boundary condition is used around the electrolyte. This results in the formation of an electric double layer. Lithium ions are free to move between PEDOT:PSS and the electrolyte solution but their maximum concentration is limited inside the PEDOT:PSS. The mobility of the lithium ions has further restrictions inside PEDOT:PSS. Lithium ions have higher mobility in PEDOT:PSS

under the electrolyte solution, referred as wet PEDOT:PSS, than the region without any contact with electrolyte, dry PEDOT:PSS. In fact due to this difference only a very little amount of lithium reaches the metal contacts. This decrease in the mobility was modeled by making the mobility of lithium a function of position in PEDOT:PSS. The mobility of lithium ions were assumed to be 100 times slower than the mobility of holes in the wet PEDOT:PSS and it is zero in the dry PEDOT:PSS($\mu_{hole} \approx 10^{-3} m^2/Vs$).

PEDOT:PSS is a regular polymer conductor with fixed negative charges and mobile holes. Holes can move in and out of the PEDOT:PSS through the metal contacts which preserve the charge neutrality of the initial condition throughout the simulation. The interface between PEDOT and electrolyte only allows the exchange of lithium ions. During the simulation, the movement of lithium ions changes the conductivity of the PEDOT:PSS by increasing or decreasing the amount of available holes. In the actual memristor lithium ions also change the conductivity through additional physical effects like changing the mobility of holes by modifying their hopping distance. Even though the mobility of the holes can simply be made a function of the lithium density, the shape of this function is not known. The physical details of the additional effects are beyond the scope of this thesis.

4.2 Boundary Conditions of the Memristor Model

For the simulation of the memristor there are two different types of equations which require boundary and initial conditions, drift diffusion and Poisson's equation. For the drift diffusion equations the boundary conditions are applied on particle and current densities. For Poisson's equation the boundary conditions are applied on the electric potential or the derivative of the electric potential.

4.2.1 Drift Diffusion Equations

For the drift diffusion problem solved in this thesis there are two different possibilities for boundary conditions on the three different mobile charged particles. For metal contacts the boundary condition is enforced by keeping the net charge at zero at all times. There

are two sub types of no flow boundary conditions used during simulation, a regular and a dependent no flow boundary condition. A regular no flow condition is used when the particles cannot go past a certain boundary. This is achieved by setting the particle flow at any boundary to zero ($J = 0$).

Dependent no flow boundary condition is a term that is used to describe a boundary condition which can be a function of any variable such as temperature, particle or charge density. For the lithium ions this condition is a function of lithium density and it is used not only for the boundaries but also for the points inside the PEDOT:PSS. The density limiting behavior is captured in the model by blocking the particle flow into an area if the density will go over a set limit. This can be achieved in various different ways.

A soft limit can be set by making the particle mobility and diffusivity a function of its density. This function can be defined in such a way that it switches from a high to a low value when the particle density approaches a defined limit. This implementation is straightforward and can be used in commercial simulators but it has some drawbacks. Once the maximum particle density is reached the mobility and the diffusivity of the lithium particles are stuck at very low values. If there is an outflux of particles from that particular area then the lithium density is stuck at the limit until the mobility and the diffusivity function goes back to a value which allows more particle flow. This can introduce a considerable artificial lag in the response of the model.

An alternative approach is pre-calculating the particle density of a density limited node at the next time step, setting any influx to zero if the density is going to go over the limit and finally recalculating the particle densities at the next time step using the updated current densities. This mechanism sets a hard limit on the density since there is a sudden break instead of a gradual slowdown in the current flow. This density limiting mechanism is more responsive than the previous one but it requires the calculation of the next time step twice for the species that has a limit. Also a large influx of particles caused by either a big time step or a high electric field can force the algorithm to cut the current flow into a node before the density reaches its limit.

To avoid adding any unwanted lag into the system the latter method is used for the memristor simulations in this thesis. This method is implemented in the finite difference

drift diffusion solver. Also a soft limit is implemented in the commercial simulator COMSOL[23] for comparison since it does not support the hard limit method.

Figures 4.3, 4.4 and 4.5 show the boundary conditions used for holes, lithium and perchlorate ions.

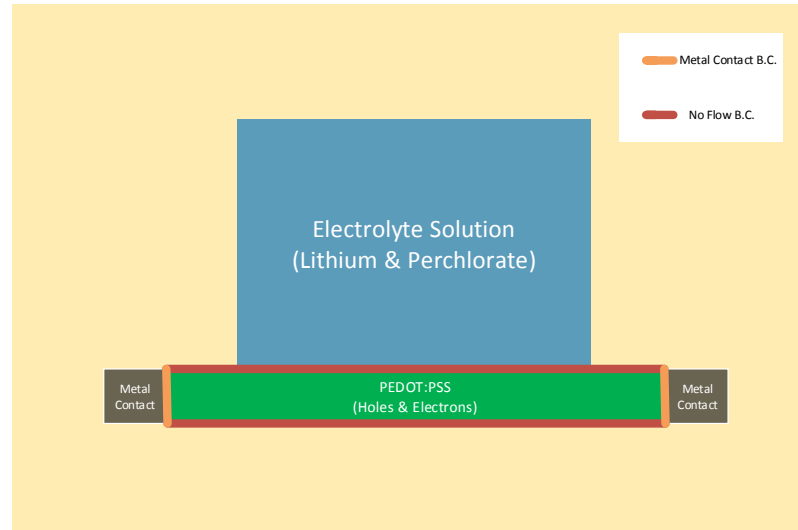


FIGURE 4.3: Boundary conditions for the holes



FIGURE 4.4: Boundary conditions for the lithium ions

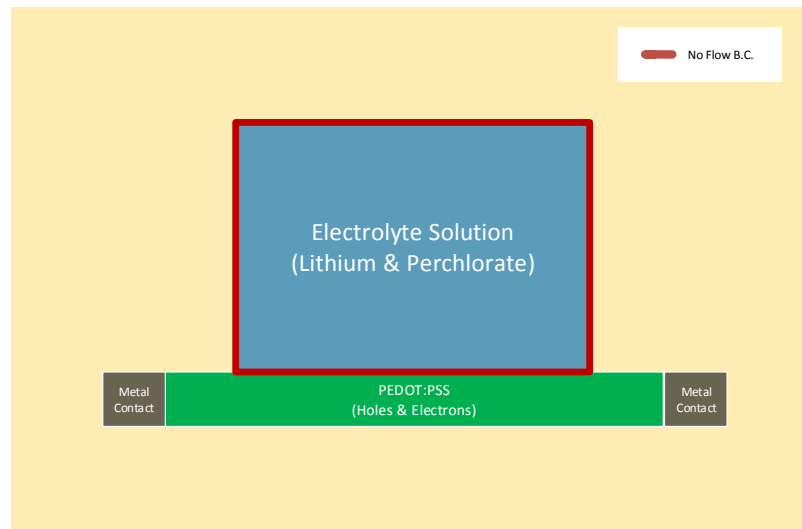


FIGURE 4.5: Boundary conditions for the perchlorate ions

4.2.2 Metal Contacts

To simulate the metal contacts it is assumed that they hold an unlimited amount of positive and negative charges and the boundary is always charge neutral. For example for holes, electrons, and positive and negative ions it is assumed that at the boundary positive charge concentration will be equal to the negative charge concentration:

$$N_{Li} + p = n + N_{ClO_4} \quad (4.8)$$

In semiconductor like devices holes and electrons have to obey the mass action law[28],

$$np = n_i^2 \quad (4.9)$$

where n_i is the concentration at equilibrium before any ions move into the PEDOT:PSS.

Solving (4.9) and (4.8) together results in the equation below:

$$p = \frac{1}{2}(N_{ClO_4} - N_{Li} + \sqrt{(N_{ClO_4} - N_{Li})^2 + 4n_i^2}) \quad (4.10)$$

Equation 4.10 can be further simplified to equation 4.11 by observing that lithium and perchlorate ions never reach the metal contact through PEDOT:PSS; therefore their density will always be zero for the setup shown in (4.1) and we have,

$$p = n_i \quad (4.11)$$

During simulation, the application of the metal contact boundary condition differs from the no flow boundary which is applied implicitly. All the boundaries are simulated using a no flow condition by default but for metal contacts boundary values for particle densities are set to the appropriate values at the end of every time step. The lack of charge is compensated and excess charge is taken off by the metal contact. The difference between the boundary value of the charge density and its actual value is used to calculate the derivative of the current density with respect to time. The current in and out of the

device is calculated by using the derivative of the charge density over time,

$$\frac{d\rho}{dt} = q \frac{n_{ex} - n_{eq}}{\Delta t} \quad (4.12)$$

where n_{ex} is the excess carrier density and n_{eq} is the equilibrium carrier density at the contact. Using these boundary conditions for holes and electrons and the following two equations it is possible to calculate incoming and outgoing currents[35]:

$$Q = Vqn \quad (4.13)$$

$$I = \frac{dQ}{dt} \quad (4.14)$$

Equation 4.13 is an approximate relationship between charge and charge density, calculated by using a first order approximation, where Q is total charge, V is the volume holding that charge. Equation 4.14 is simply the general definition of current. By combining these two equations it is possible to derive a formula for calculating the current leaving or entering the device at any metal contact,

$$I = Vq \frac{dn}{dt} \quad (4.15)$$

Since the main characteristic of a memristor is the change in current output due to change in resistivity over time it is important to develop a standard approach for measuring the change in the current output. Initially, simulations in chapters 6 and 7 are run until steady state without the movement of lithium/perchlorate ions. Ions in the electrolyte start to move after holes reach steady state. The movement of ions create another transient which involves changes in resistivity and current density. The current density (at steady state) obtained from the simulation without the movement of ions is used as a normalizing factor in order to determine the changes in current after the ion movement has started.

4.2.3 Poisson's Equation

Discretized form of Poisson's equation (3.19) is valid for almost all the nodes in the system except the boundary nodes. There are two different types of boundary conditions. The first one is the Dirichlet boundary condition which forces a particular value for the potential at the boundary[36],

$$V_{i,j} = V_b \quad (4.16)$$

Where V_b is the value of the potential at the boundary. The other possible boundary condition is called a Neumann boundary condition which states that the derivative of the potential at the boundary is zero[36]. This gives the following equation:

$$\frac{\partial V}{\partial x} = \frac{V_{i+1,j} - V_{i,j}}{\Delta} = 0 \quad (4.17)$$

So for a boundary in y direction:

$$V_{i+1,j} = V_{i,j} \quad (4.18)$$

A Neumann boundary condition in x direction is obtained by using the same procedure.

$$V_{i,j+1} = V_{i,j} \quad (4.19)$$

Neumann boundary condition is used to let the potential float at the edge of the simulation domain and Dirichlet boundary condition is used to set applied potentials at the metal contacts. These boundary conditions are shown in figure 4.6.



FIGURE 4.6: Boundary conditions for electric potential

4.3 Simulation Requirements

After setting all the initial and boundary conditions the last step before simulation is analyzing the computational requirements of a simulation in order to determine the required mesh size and asses the feasibility of the computational scheme. In this case, it is possible to determine the spacial and the temporal requirements using equations 3.35 and 3.38 which describe physical and numerical limitations of the simulation. The following graph 4.7 shows the requirements for a memristor of the scale discussed above and a typical semiconductor device size around $1 \mu\text{m}$. The mesh density has to be high enough in order to capture the exponential charge accumulation for charge shielding so the minimum step size was set to be 5 times smaller than the Debye length. The plots 4.7.a and 4.7.c show the amount of points required to simulate a semiconductor and a memristor based on minimum step size. It is important to note that these values are for 1-D simulation and they can be converted to 2-D and 3-D by taking the square or the cube of the values in y axis respectively. Plots 4.7.b and 4.7.d are created using CFL conditions for drift and diffusion and dielectric relaxation time. A typical simulation time is estimated using the mobility and the electric field. Based on the estimated simulation time the number of time steps are calculated using the minimum time step obtained from CFL conditions and dielectric relaxation time.

	Memristor	Semiconductor
Hole Mobility (m^2/Vs)	$1.0 \cdot 10^{-3}$	0.45
Hole Density ($1/\text{m}^3$)	$1.0 \cdot 10^{24}$	$1.0 \cdot 10^{21}$
Device Length (m)	0.01	$1.0 \cdot 10^{-4}$
Applied Voltage (V)	1	1
Electric Field (V/m)	100	$1.0 \cdot 10^4$
Hole Velocity (m/s)	0.1	$4.5 \cdot 10^3$
Debye Length (m)	$1.2 \cdot 10^{-9}$	$3.81 \cdot 10^{-8}$
Relaxation Time (s)	$5.52 \cdot 10^{-14}$	$1.23 \cdot 10^{-13}$
Simulation Time (s)	0.1	$1.0 \cdot 10^{-6}$
Number Time Steps (Unitless)	$9.05 \cdot 10^{13}$	$4.07 \cdot 10^8$
Number of Points in x (Unitless)	$4.15 \cdot 10^7$	$1.31 \cdot 10^5$

It can be seen from graphs 4.7.a and 4.7.c that memristor simulations require much higher mesh densities compared to a typical semiconductor simulation such as 1 μm long PN diode. This is due to the larger size and higher charge density of the memristor. Plots 4.7.a and 4.7.b show that a memristor with 10^{26} m^{-3} charge density requires close to 10^9 points and 10^{14} time steps to simulate in 1-D. These requirements make the simulation of the memristor extremely challenging. In order to investigate and find possible solutions to this issue, first a memristor with low charge density ($\approx 10^{15}$) is simulated in chapter 6 in order to ensure that the simulation functions as designed. Then memristors with different charge densities are simulated (section 6.2.3) and compared to each other to assess whether the behavior at low charge densities will be comparable to the behavior at high charge densities.

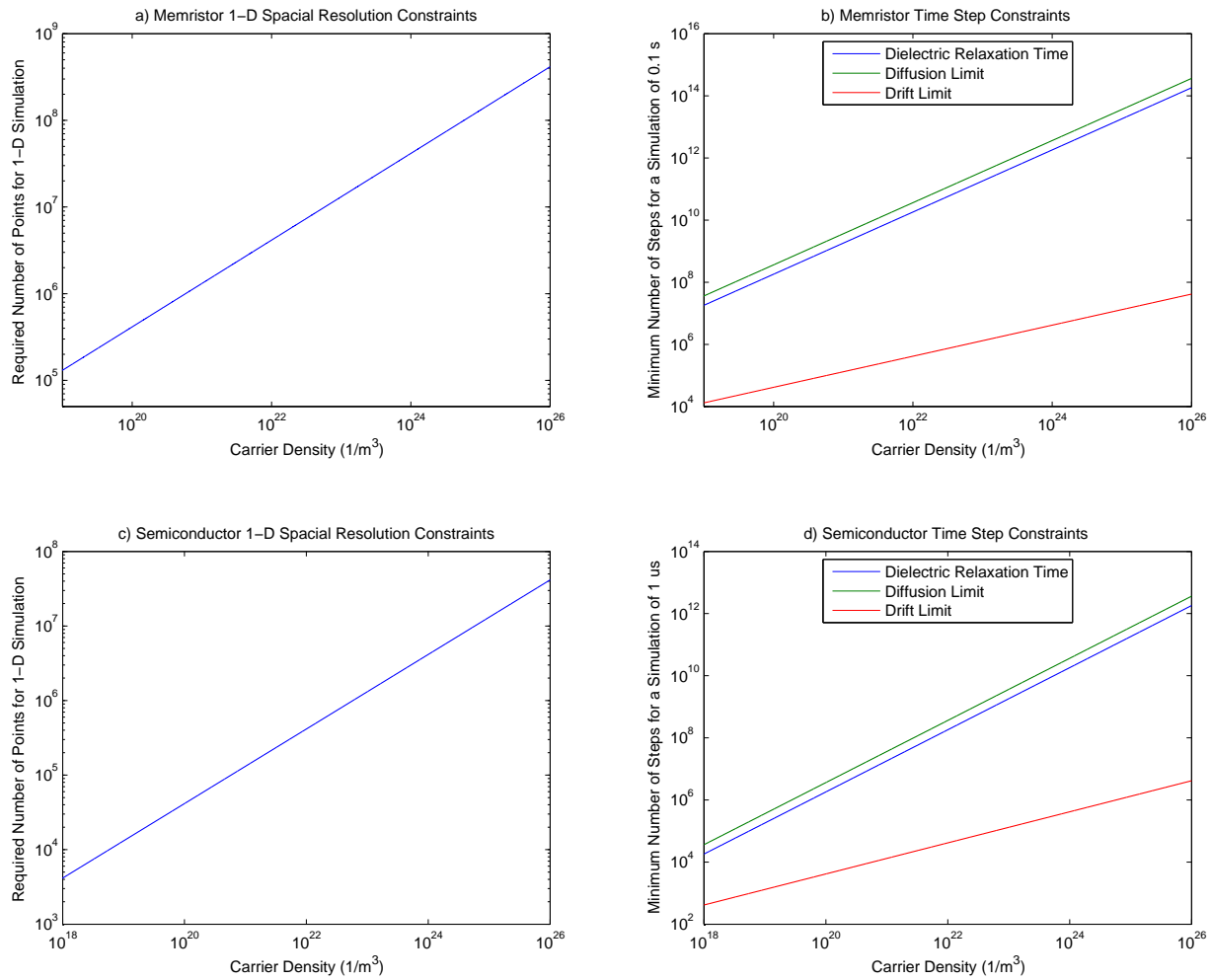


FIGURE 4.7: Spatial and temporal requirements for simulation

Chapter 5

Testing The Drift Diffusion Solver

The simulation scheme presented in chapter 3 needs to be tested thoroughly before attempting to simulate a memristor in order to ensure that it functions as expected and produces accurate results. In this chapter steady state and transient analysis for drift diffusion equations using finite difference is compared to analytical solutions as well as a commercially available simulator called “COMSOL Multiphysics” [23] which uses the finite element method instead of a finite difference approach.

5.1 Solution for Closed Boundary

In this section the accuracy of the finite difference solution in steady state is tested. In order to do this, a simple 1-D problem with a finite number of negatively charged particles distributed over a region subject to constant electric field is used. This is the same problem that is solved analytically in section 3.3.1. It is also assumed that the charge density is very low and does not affect the electric field. Both ends of the simulation domain have no flow boundary conditions for charged particles. The solution process requires an initial distribution for the charge density over the area. For this problem the density of the negative particles was initialized to be uniform over the entire region.

Since the differential equations are uncoupled solving Poisson’s equation only once is sufficient to determine the electric field over the course of the entire simulation. Figures

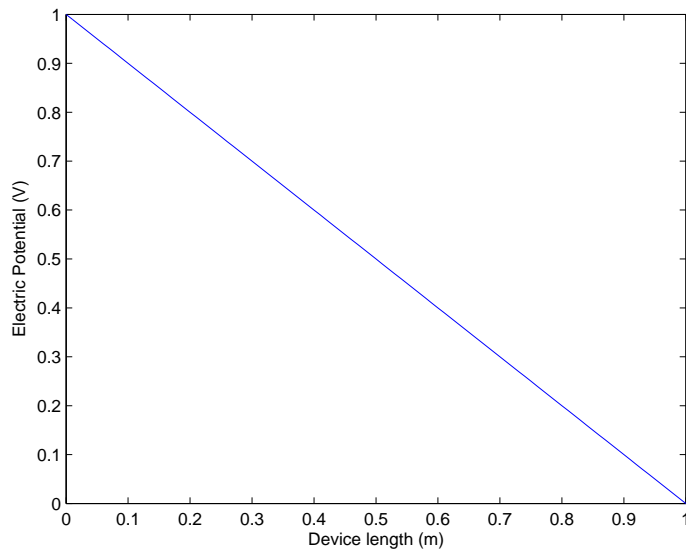


FIGURE 5.1: Potential Distribution

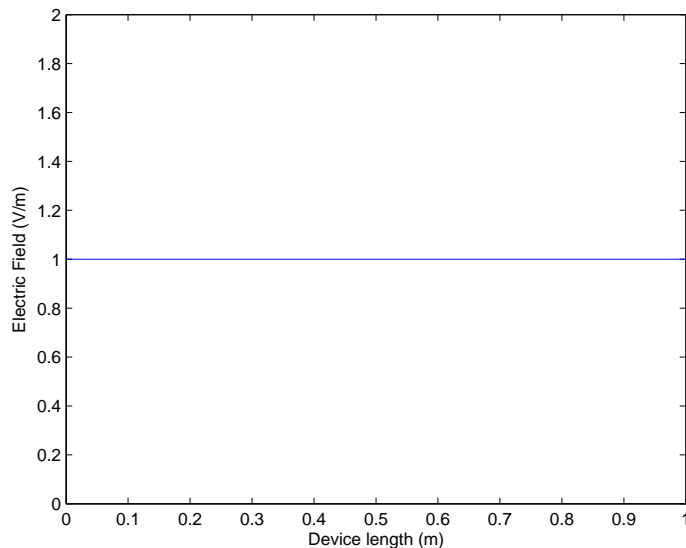


FIGURE 5.2: Electric Field Distribution

[5.2](#) and [5.1](#) show the potential and the electric field distribution over the entire simulation area calculated from Poisson's equation using finite difference.

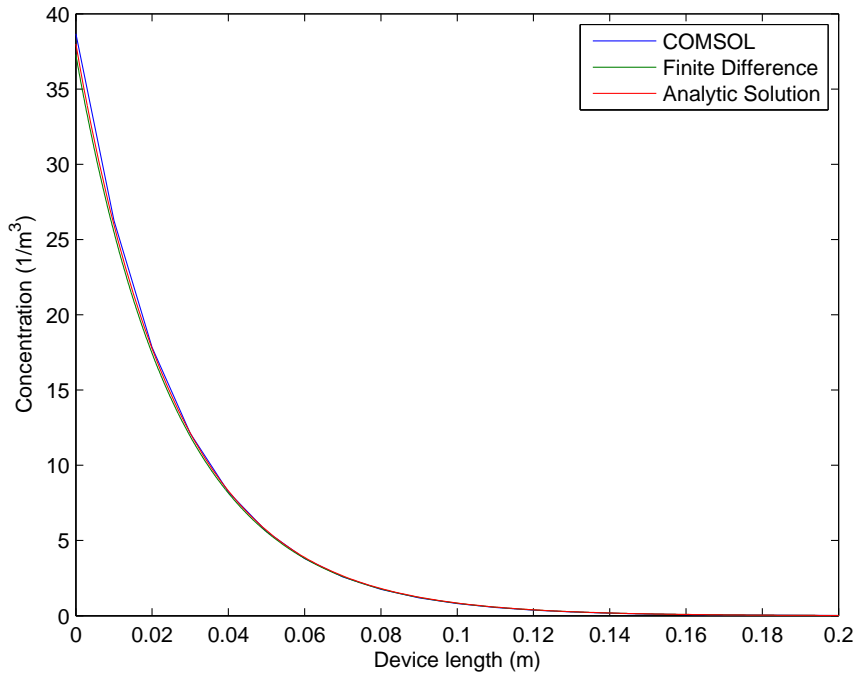


FIGURE 5.3: Steady State Negative Particle Density

Figure 5.3 has two simulation results as well as the exact solution of this problem. The green line represents the result given by the finite difference method at steady state. It can be seen from the graph that the steady state solution generated by both COMSOL and finite difference matched the analytical solution.

While deriving an analytical solution for this problem it was assumed that at steady state the drift current density must be equal and opposite in magnitude to the diffusion current density. In figure 5.4, drift and diffusion current densities are shown in log scale. Overall both currents match quite tightly.

Even though the simulation results are good for this example high electric fields due to either applied potential or high charge densities can introduce inaccuracies. If the electric field is very high then the accumulation of the charge can get very steep. The exponential accumulation requires higher mesh densities for accurate calculation.

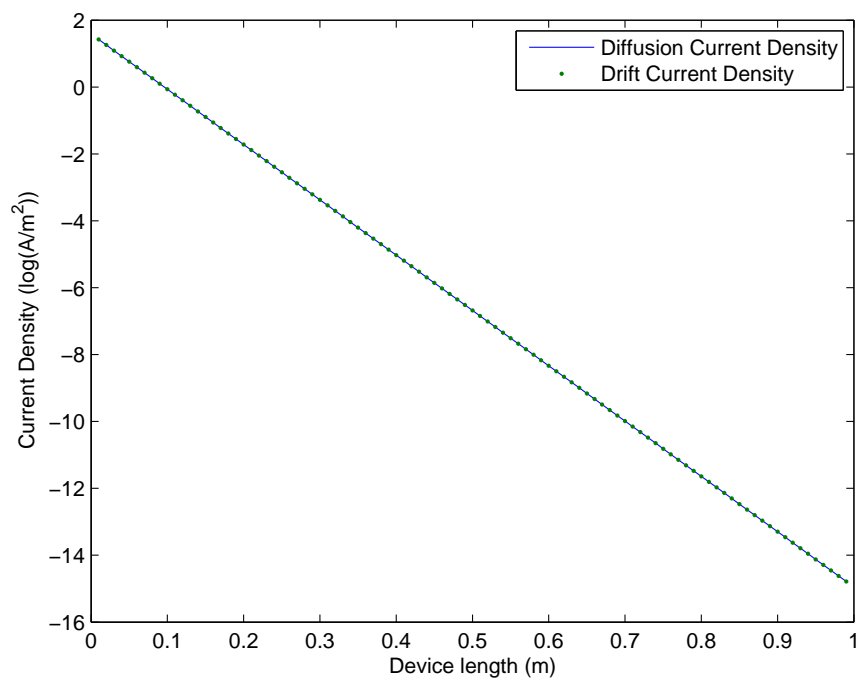


FIGURE 5.4: Finite Difference Drift and Diffusion Current Densities

5.2 Solutions for Open Boundary

Another crucial aspect of the drift-diffusion simulation is its transient response. Like the previous test case, the analytic solution can be used to test the accuracy of the transient response. Two different analytic solutions for a drift diffusion problem which involved infinite boundaries and a uniform electric field are shown in section 3.3.2. The only difference between two cases are their initial carrier distributions. One has a rectangular and the other one has a gaussian initial carrier distribution. The finite difference scheme does not allow simulation over an infinitely long conductor. For this test case, the simulation is performed until the carrier distribution gets close to a wall.

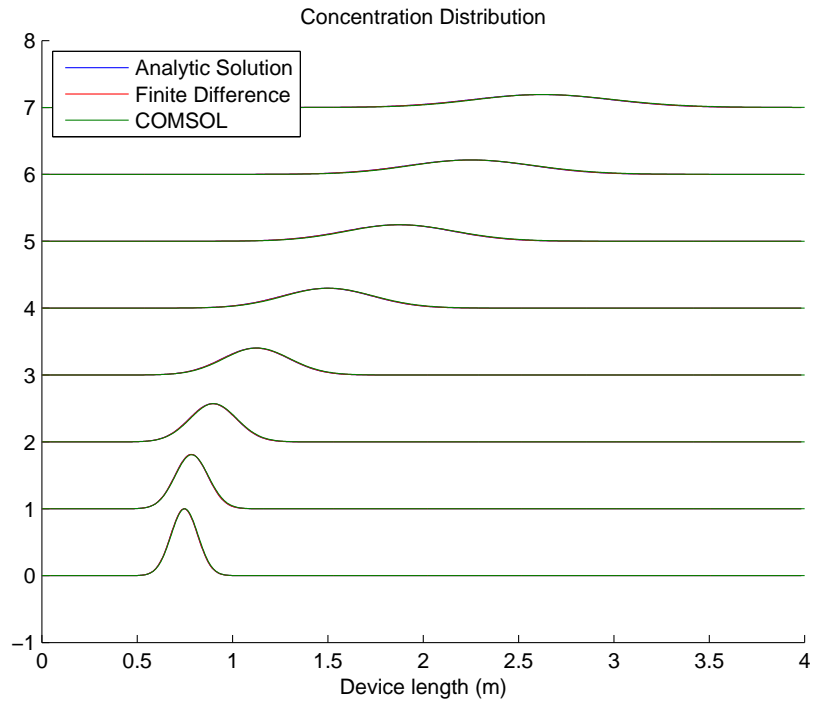


FIGURE 5.5: Gaussian Carrier Distribution Evolving Over time

Figure 5.5 has the transient responses from COMSOL, finite difference and analytical solution. Snapshots of the carrier distributions were taken for each method at different time steps and they were superposed on top of each other and are indistinguishable. Increasing levels on the y axis represent a carrier distributions at a different time starting from the bottom and moving forward in time towards the top. Figure 5.5 has a gaussian initial carrier distribution. It can be seen from that the transient solution generated by both COMSOL and finite difference are quite close to the analytical solution.

5.3 PN Junction

In previous test cases, Poisson's equation is not coupled with drift diffusion equations. In this example both drift diffusion and Poisson's equation are tested to investigate how well they work when they are coupled together. A simple pn junction is quite adequate for this task since it has analytical solutions (under certain assumptions) for electric potential, electric field and carrier distribution.

For the simulation, initial hole and electron distributions are determined using mass action law and they are assumed to be constant at the boundaries. Keeping carrier density constant creates a mechanism in which the charge can move in and out of the simulation domain. If the charge density at any time step is higher than the fixed density then the difference will move out of the system. If there is a lack of charge at the boundary then carriers will move in to fill in the gap. Following figure (5.6) shows the final result of bringing p and n type materials together.

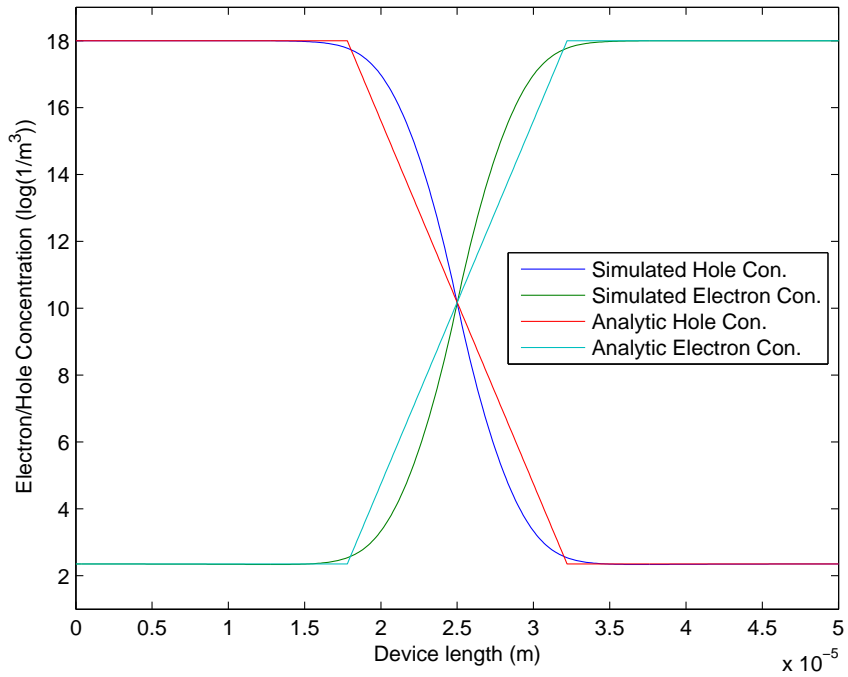


FIGURE 5.6: Electron/hole Concentration of a PN Junction

There is a little mismatch between simulated and analytic charge densities. The analytic solution has sharp edges and the simulated solution does not. This is due to all the

assumptions made in order to find an analytic solution. This mismatch can also be seen for electric field, electric potential and net charge .

Figure 5.7 shows the potential distribution for simulated and analytic solutions. A close match in electric potential distribution shows that coupled equations can generate accurate solutions.

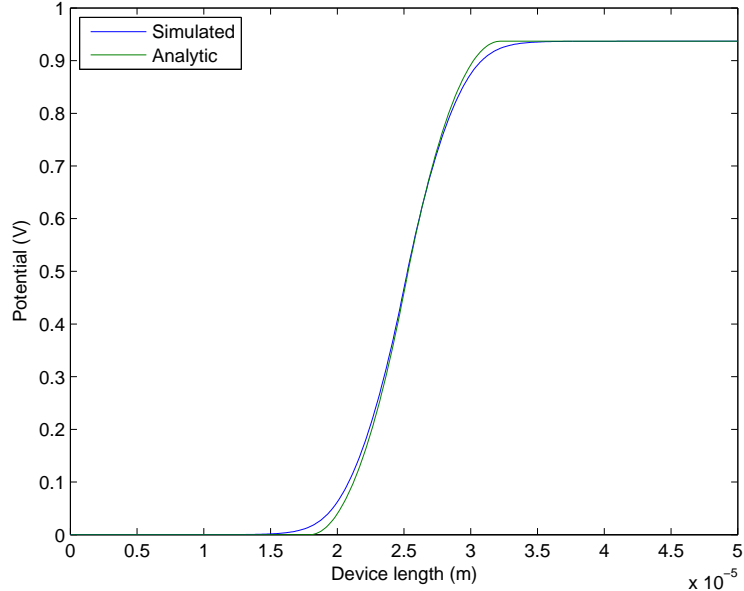


FIGURE 5.7: Potential Distribution of a PN Junction

Calculation of the electric field involves one basic derivative. Since the simulated potential matches the analytic solution quite nicely the electric field should follow a similar pattern. Figure 5.8 shows that this is indeed the case, as the simulated electric field matches the calculated electric field.

Figure 5.9 shows the total charge distribution at steady state. The simulated net charge density follows the analytic one except for the smoothing at the two ends where the assumption of full depletion made in the analytical solution breaks down.

This example showed that simulation of a system of coupled equations, drift diffusion and Poisson's equation, using finite difference can produce accurate results. This accuracy depends on the strength of the coupling. High charge densities can produce strongly coupled systems. This effect shows the importance of CFL conditions as well as the physical limitations of the simulation.

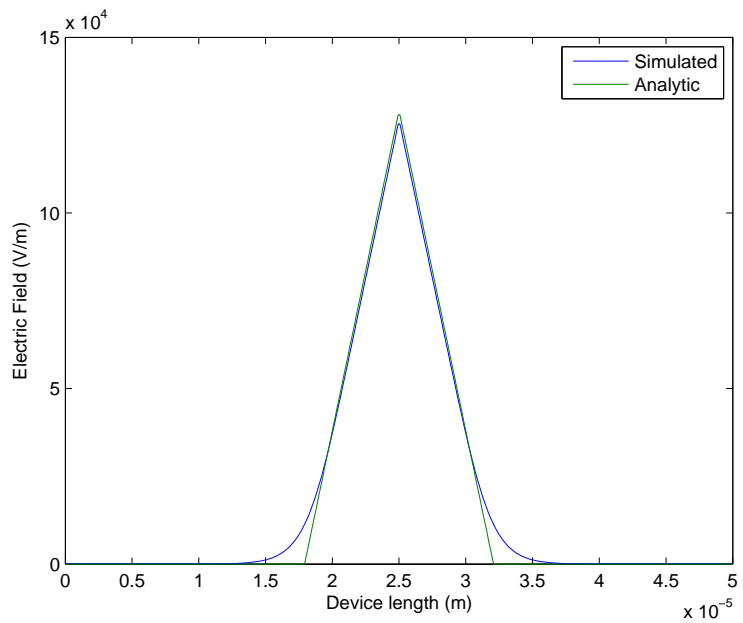


FIGURE 5.8: Electric Field Distribution of a PN Junction

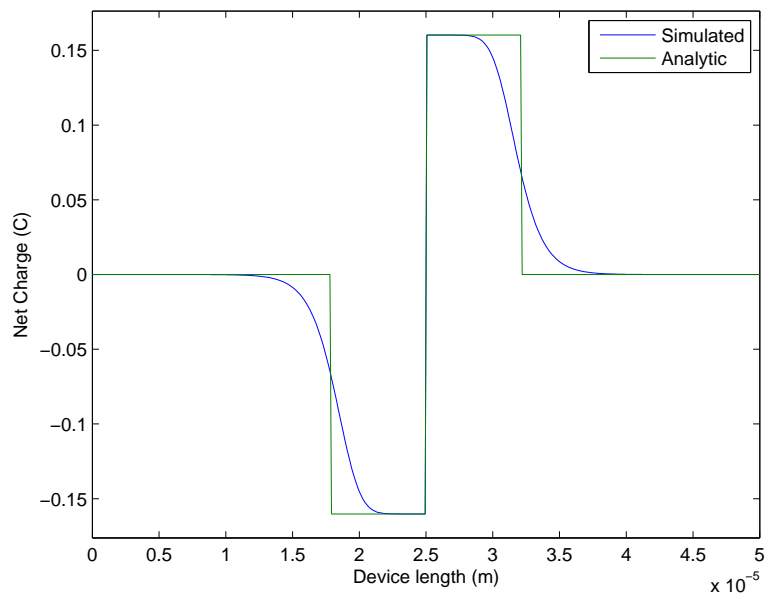


FIGURE 5.9: Total Charge Distribution of a PN Junction

5.4 Region Specific Particle Density Limit

The last property of the drift diffusion simulation scheme that is tested in this section concerns the movement of lithium ions. In order to test the density limiting method implemented for the memristor simulation a simple example is set up. Two simulations for the flow of positively charged particles are initialized as in the figure below (Fig. 5.10). In one simulation a density limit of 0.5 m^{-3} is placed on the right half of the simulation area and no limit on the left half. The other simulation has no restrictions present. The initial particle density on the left half of the simulation area is set to 1 m^{-3} for both simulations.

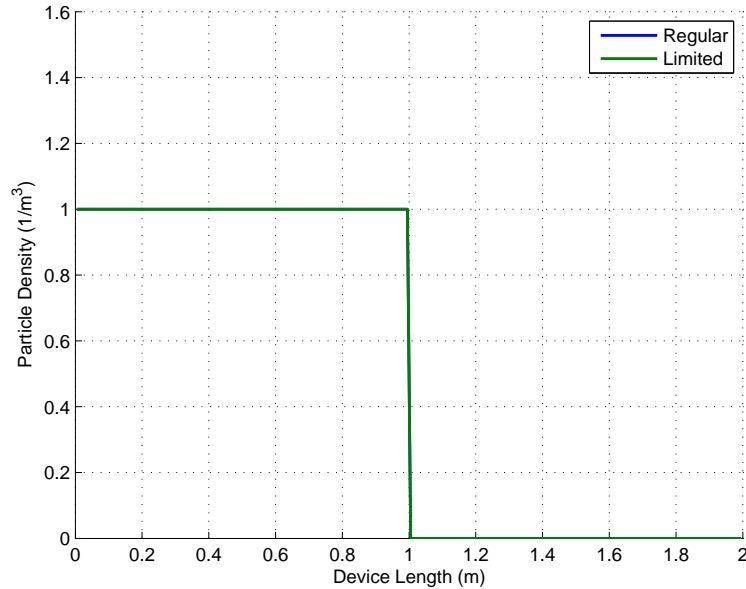


FIGURE 5.10: Initial Particle Density

This transient simulation uses a potential pulse train. The potential is applied at the left side of the device and the right side is always grounded. For the first 100 seconds of the transient simulation the applied potential is positive and for the rest of the simulation it is negative. Figure 5.11 shows how two simulations differ when the particles are pushed towards the right wall due to the electric field created by the positive potential. Particles with no limit on the right side move freely and accumulate on the right wall. For the other case the density limit present for the particles is effectively stopping them from

migrating and accumulating freely. Once the limit is reached at a certain node the density cannot increase any further and that node turns into a no flow wall.

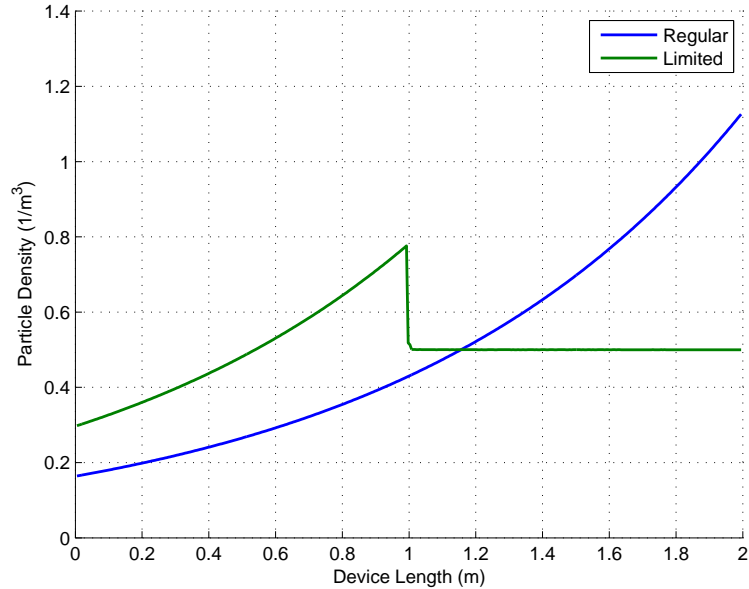


FIGURE 5.11: Limited Density Accumulation on the Right Side

When the potential is switched all the particles accumulate freely at the left side of the simulation domain since there are no restrictions on this side (figure 5.12).

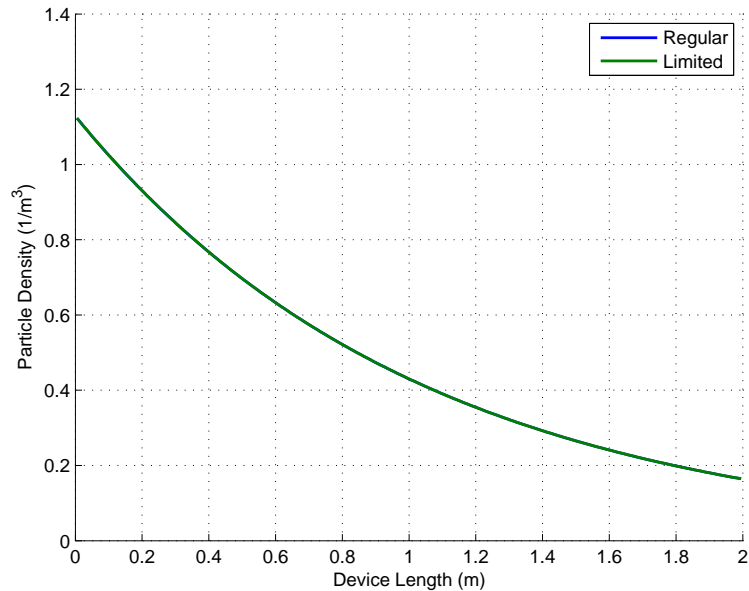


FIGURE 5.12: Limited Concentration Density on the Left Side

This last figure (5.13) shows the transient response over time of a single node on the right side. The potential is positive for the first 100 seconds and it is switched to negative for the rest of the simulation. The node without any limit keeps accepting charge until a steady state has been reached but the density limited node stops accepting charged particles once the limit is reached. After the potential is switched the density limited node has no problem releasing the particles.

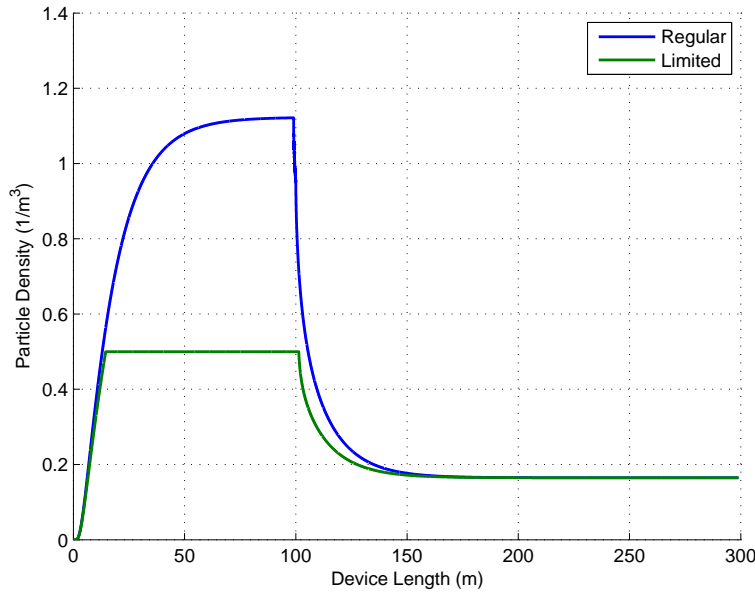


FIGURE 5.13: Accumulation at the right wall over time

In addition to the test that was run for the finite difference solver, COMSOL is used to test the soft limiting mechanism. COMSOL does not have a built in option that allows limiting the particle density. One possible solution to this is making particle mobility and diffusivity a function of particle density. It is possible to use a sigmoid function which switches from 1 to 0 very quickly when particle density is close to its limit. Here is the equation of the sigmoid function used to limit the particle flow:

$$\mu_v = \frac{\mu_0}{1 + e^{\sigma(n-n')}} \quad (5.1)$$

μ_0 is the original mobility of the charge carrier. σ controls the slope of the switch and n' determines the density at which the transition will be.

Another problem with COMSOL is the definition of mobility and diffusion coefficients.

When they are defined discontinuously and one of the mobilities is a function of the particle density like the example above COMSOL has convergence issues. To overcome the convergence problems, mobilities are set up to gradually switch from a constant value to a variable mobility using two more sigmoid functions which are dependent on position:

$$\mu = \frac{\mu_v}{1 + e^{\sigma_x(x-x')}} + \frac{\mu_c}{1 + e^{-\sigma_x(x-x')}} \quad (5.2)$$

In this problem μ_v is the same as equation 5.1 since the region on the right side has a variable mobility and μ_c is just a constant mobility defined for the left side. x' is the middle of the simulation area.

The initial carrier distribution for COMSOL is set to be exactly the same as finite difference simulation. Figures 5.14.a and 5.14.b show results for both COMSOL and finite difference simulations at steady state before the switch of the applied potential. The plot on the left side gives insight on how COMSOL simulation behaves for limited and limitless accumulation on the right wall. Due to the gradual change of mobility and diffusion constants between two areas, the density on the right side is higher than the limit which is 0.5 m^{-3} . Additionally, the particle density goes over its limit near the right wall. In figure 5.14.b the difference between COMSOL and finite difference becomes more visible. In FD simulation the accumulation is similarly shaped but unlike COMSOL it does not penetrate the right half of the simulation domain.

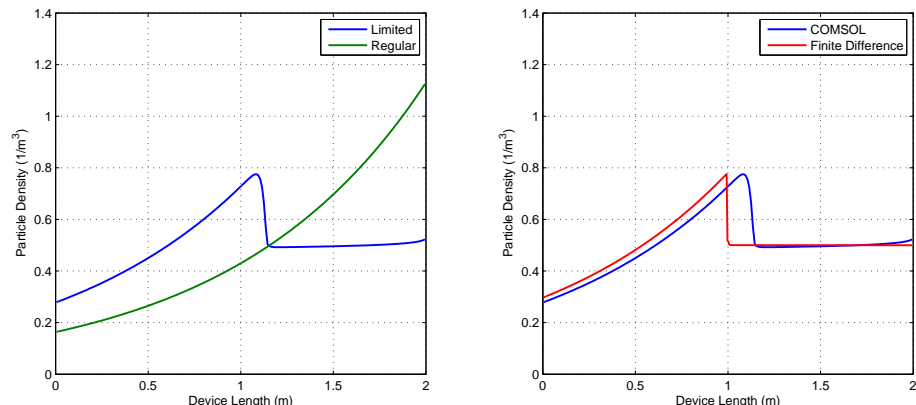


FIGURE 5.14: a) COMSOL Simulation for Particle Density Limit b) COMSOL and Finite Difference Simulation

In figure 5.15 it is possible to see a spike of charge in COMSOL simulation near the

middle section after the potential is switched. This is due to mobility being a function of distance and density. As the ions move from left to right they go from a low mobility region to a high mobility region and they slowly accumulate around the area where the change in mobility occurs. Figure 5.15.b comparing both COMSOL and finite difference shows that the accumulation does not happen in the case of finite difference due to the way density limiting mechanism is implemented.

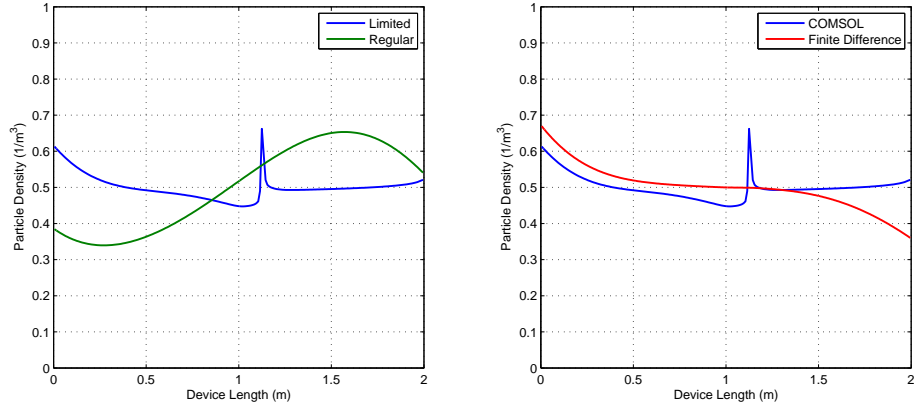


FIGURE 5.15: a) COMSOL Simulation for Particle Density Limit b) COMSOL and Finite Difference Simulation

With the decrease of ion density on the limited region the difference between low and high mobility regions diminish. Once the density on the limited side is low enough the whole system behaves as if there is no limit and ion mobility becomes equal for all regions and the ions freely accumulate on the left wall (figure 5.16). Both simulations behave the same way as they approach steady state. Figure 5.16.b shows densities at steady state.

This comparison can be finalized by looking the particle density transient response of the rightmost node (figure 5.17). For the first half of the simulation everything is the same as the finite difference case except COMSOL goes a little bit over the limit. When the potential is switched, node without the limit has no noticeable difference in behaviour. The node with density limit has a lag when it comes to releasing the particles. This is due to the sigmoid function used to achieve a limiting behaviour. Once the limit is reached mobility and diffusivity are stuck at a very low value until the particle density starts to go lower than the limit.

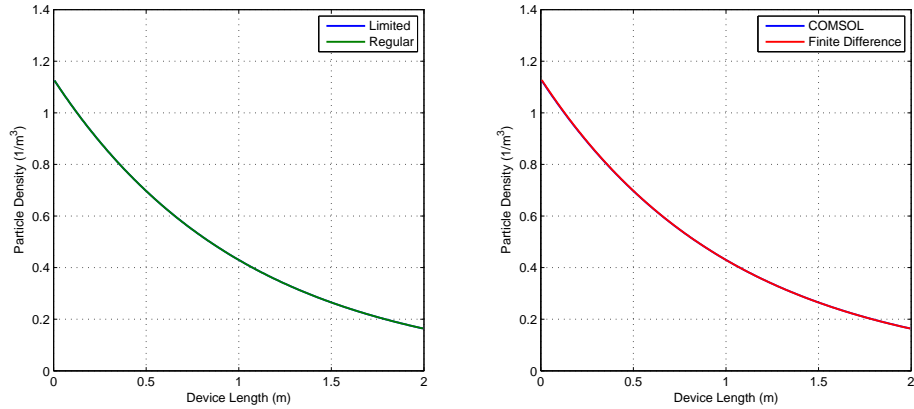


FIGURE 5.16: a) COMSOL Simulation for Particle Density Limit b) COMSOL and Finite Difference Simulation

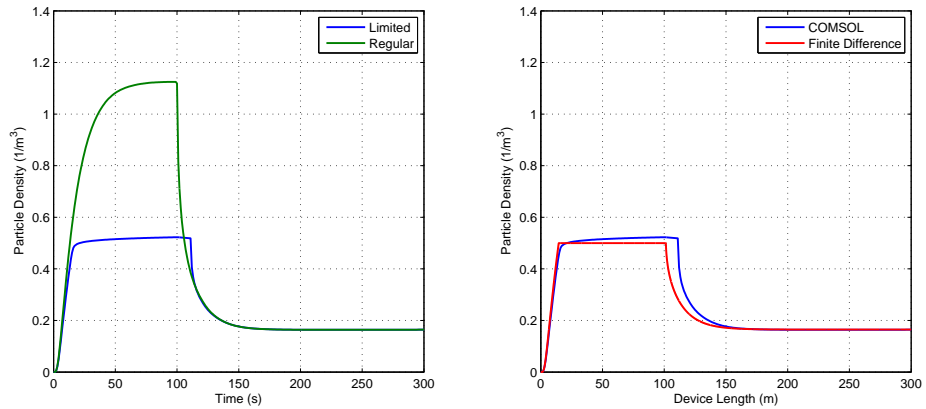


FIGURE 5.17: a) COMSOL Simulation for Particle Density Limit b) COMSOL and Finite Difference Simulation

The simulations above show that it is possible to impose a density limit over any area using a simple no flow boundary condition in a numerical simulation. For COMSOL some workarounds are implemented in order to simulate the same behavior without any convergence issues. However, the COMSOL implementation produces some undesirable effects and the finite difference model was found to be more useful.

Chapter 6

1-D Memristor Simulation

A numerical method for a coupled ionic-electronic device simulation was developed and tested in previous chapters based on drift-diffusion equations and finite difference. This chapter introduces a 1-D approximation for a 2-D cross section of the memristor. Then 1-D simulations of a memristor are shown under various conditions.

6.1 1-D Memristor Approximation

For the 1-D simulation it is assumed that there are always more than enough ions to saturate the PEDOT:PSS so the electrolyte is modeled as an infinite source/sink of ions. The top boundary of the electrolyte is assumed to be charge neutral at all times which provides a mechanism for moving ions in and out of the system. This way the movement of ions near the surface of the PEDOT can still be captured without having to simulate the ion movement for the entire electrolyte solution which is variable in size. This assumption is not used for 2-D simulations since the electrolyte is fully simulated.

The horizontal cross section from figure 4.2 has the most crucial elements of the memristor but its simulation in 1-D is not straightforward. This cross section through the PEDOT does not include the vertical movement of the lithium ions. Without this effect, PEDOT:PSS is just a regular conductor with a uniform current density. In order to overcome this problem a generation/recombination term for lithium ions (calculated at every time step) is added to capture the vertical movement in addition to the regular

drift diffusion equations which represents the horizontal movement. This generation/recombination term can be symbolized as a current source connected to all the nodes (figure 6.1). Perchlorate ions are not included in the simulation since they do not move into the PEDOT.

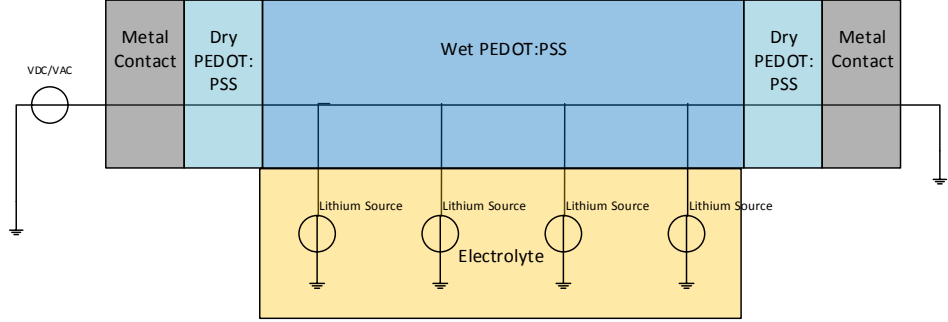


FIGURE 6.1: 1-D Memristor Model

The lithium source has two different terms, one for drift and another one for diffusion. It was assumed that the concentration of lithium is always constant in the electrolyte. This way the vertical diffusion current density can be calculated using the difference between the lithium density in PEDOT:PSS and electrolyte,

$$J_{diff} = K_1 q D \frac{n - n_c}{\Delta x} \quad (6.1)$$

n and n_c are lithium densities in the PEDOT:PSS and electrolyte respectively. K_1 is a fitting parameter that can be adjusted based on experimental results. For the drift term an electric field is estimated between the PEDOT:PSS and the electrolyte. First the potential of the electrolyte is assumed to be the average potential of both metal contacts,

$$V_{el} = \frac{V_L + V_R}{2} \quad (6.2)$$

Where V_L and V_R are the electric potentials of the left and right metal contacts. Then a vertical electric field is calculated using the electrolyte and the instantaneous potential of the PEDOT:PSS at different positions,

$$E_y = \frac{V_{el} - V}{\Delta x} \quad (6.3)$$

Finally a drift current for lithium ions is calculated using the estimated electric field,

$$J_{drift} = \begin{cases} K_2 q \mu n_c E_y & \text{for } E_y > 0 \\ K_2 q \mu n E_y & \text{for } E_y < 0 \end{cases} \quad (6.4)$$

K_2 is a fitting parameter for drift that can be adjusted based on experimental results. When the electric field is positive, lithium ions are being pulled into the PEDOT:PSS and when it is negative they are being absorbed by the electrolyte. Finally the drift and diffusion current densities can be added to calculate the net lithium current density for the lithium sources,

$$J_s = J_{drift} + J_{diff} \quad (6.5)$$

For both drift and diffusion the horizontal movement of lithium ions inside the electrolyte is not modeled. The 1D model therefore models the flow of Lithium in and out of the PEDOT as a strictly vertical 1D flow.

6.2 1-D Memristor Simulations

The following simulations are made based on the memristor approximations discussed above. The first two simulations are repeated in the next chapter using a 2-D drift diffusion and Poisson solver which captures a broader range of physical effects. Both approaches are compared in order to understand their advantages and disadvantages under different circumstances.

6.2.1 1-D Memristor Simulation Using a Potential Pulse Train

For the following simulation a potential pulse train, slow enough to let the memristor reach steady state between transitions, is applied at the left contact. Plot 6.2 shows the

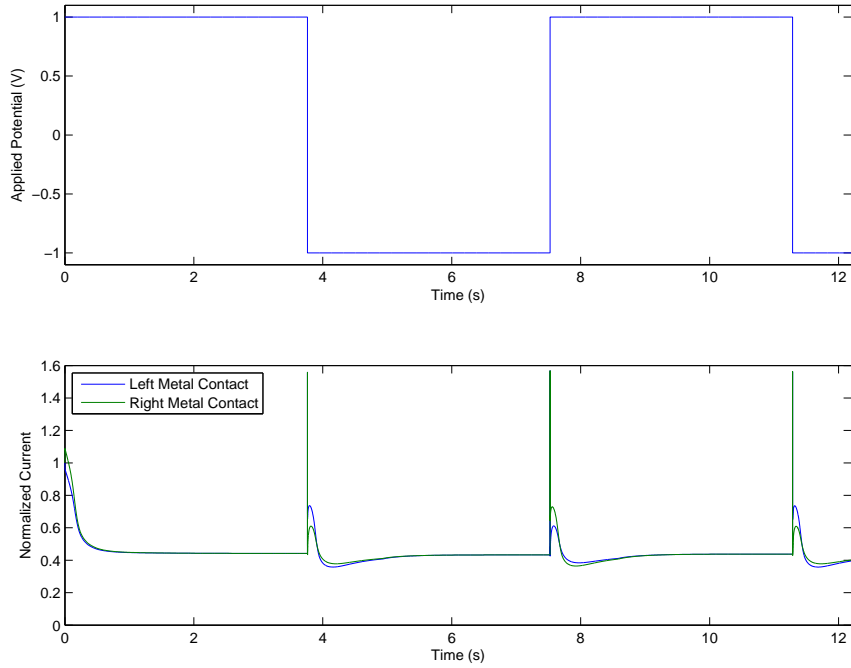


FIGURE 6.2: Change in current density over time due to applied potential

current density output for both contacts separately. As expected the current density of the device decreased as the lithium ions move in. Additionally, it can be seen from the graph 6.2 that the current density output from left and right contacts are not always the same over the duration of the simulation. This is due to the PEDOT:PSS layer losing

holes on one side and gaining holes on the other side which produces a difference in the measured current density between contacts. The scale of the difference depends on the rate of change in lithium movement on either side.

The current density in figure 6.2 shows a sudden increase when the potential is switched from 1 to 0 and vice versa. This sudden increase occurs because of the accumulation of lithium ions at the wet/dry interface which creates an opposing potential to the applied potential (see figure 6.3). When the electric potential changes suddenly, the previously opposing electric field now helps the movement of holes and lithium towards the other end of the device. This additional electric field momentarily increases the current density output of the device.

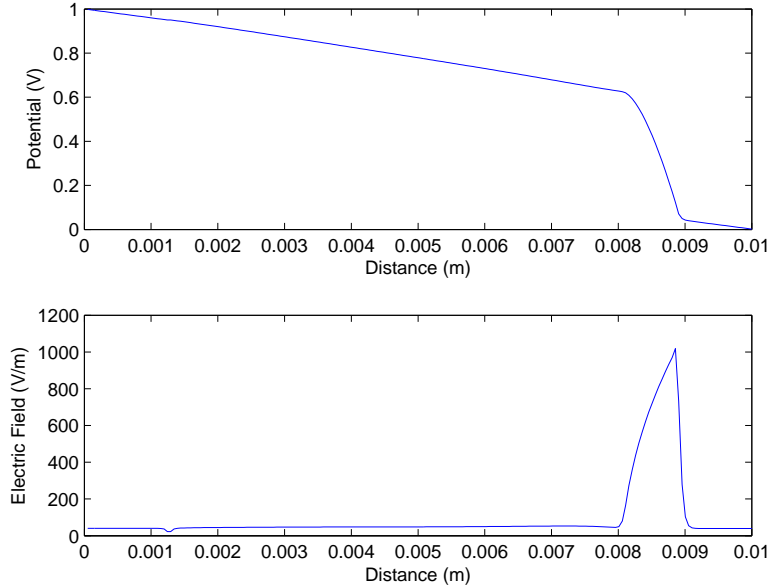


FIGURE 6.3: Potential and electric field at steady state

Figure 6.4 demonstrates the replacement of holes by lithium ions over time which directly effects current density. As lithium ions get pulled in from the electrolyte toward the contact they accumulate inside the PEDOT:PSS. Concurrently hole density decreases in areas where lithium accumulates. The decrease in the hole density in the PEDOT:PSS decreases the current density output of the memristor. This change in current density over time is illustrated in figure 6.2.

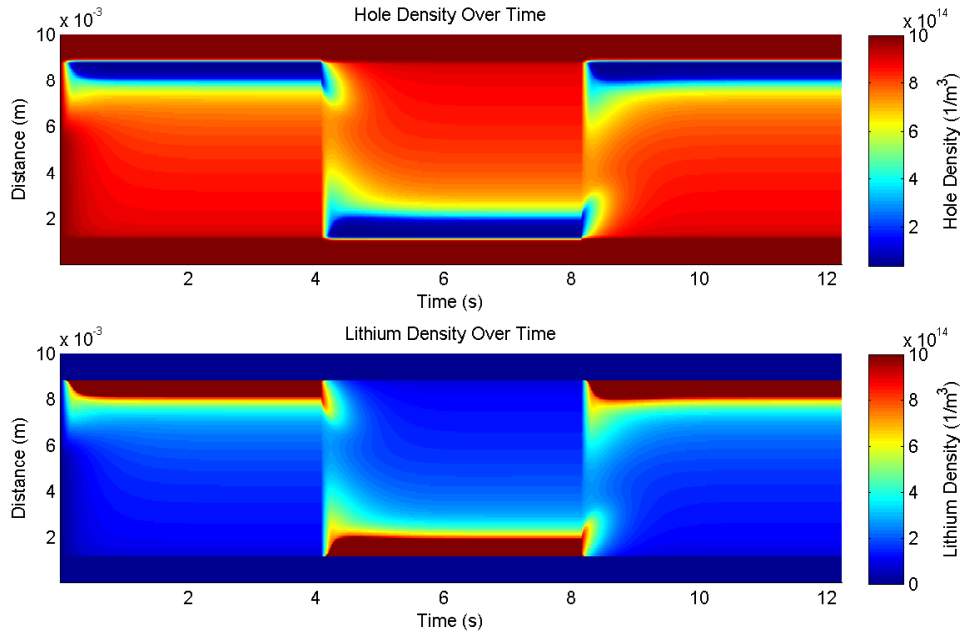


FIGURE 6.4: Lithium and hole density distribution over time

It is important to note that lithium ions are free to move in x and y directions. In figure 6.4 it can be seen that after the potential is switched as the lithium density moves from side to the other. Most of the lithium movement happens through the exchange of ions between PEDOT:PSS and the electrolyte since the distance between them is far less than the length of the PEDOT. So most of the lithium ions, traveling from the positive to the negative contact, are pulled into the electrolyte before they reach the other side. Near the negative contact lithium ions are quickly pulled into the PEDOT:PSS and accumulate at the wet/dry interface.

By examining the hole/lithium density plots of the PEDOT:PSS it is possible to conclude that it is composed of 3 distinct regions. 2 dry regions, where there is no contact with the electrolyte, have constant uniform resistance. Between these two resistances there is a variable non uniformly distributed resistance controlled by hole/lithium density and hole mobility. So this model captures the main characteristic of the memristor which is a variable charge dependent resistance where the resistance at any time depends on the past of the device. Following equation gives the total resistance/memristance for the memristor model developed for this thesis:

$$M(q(t))_{tot} = 2R_{dry} + R(Li, p, \mu_{hole}) \quad (6.6)$$

The minimum resistance of this device is just the total resistance of the PEDOT:PSS without the lithium ions. The maximum resistance depends on different factors such as applied potential and the distribution and density of lithium ions inside the PEDOT:PSS.

6.2.2 1-D Memristor Simulation Using a Sinusoid

The memristor with a pulse train simulation shows the change in the current density over time due to an applied potential but it does not clearly demonstrate the memory effects. The memory effect of the memristor can be clearly demonstrated in an I-V curve using a sinusoidal potential. Following four graphs (figure 6.5) are created using an AC potential with different frequencies at the contacts. All the plots show that current density can have more than one value for the same potential at different times. This means that simulated memristor's past state affects its present output, therefore the device has memory. There is an asymmetry in the current curve because it is measured from one contact which has relatively low change in resistance for a period of time during transient simulation.

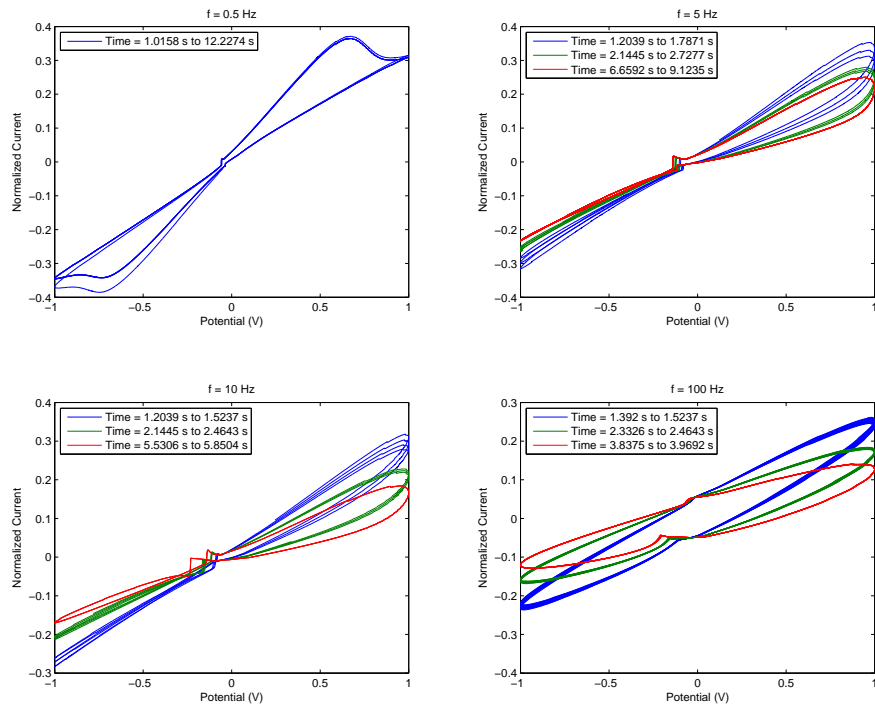


FIGURE 6.5: Normalized Current vs. applied potential at different frequencies

The sudden changes in current around 0 V can be attributed to the density limiting mechanism for lithium. Instead of a slowdown in the movement of lithium ions near maximum density, the current flow into that region is completely blocked. Even though this makes the lithium density more responsive to changes, a sharp block in the flow

combined with large time steps can result in fast changes which can be directly seen as abrupt changes in the hole/lithium current density during transient simulations.

The following plots (6.6) show that, at first, there is a drop in the average current for all frequencies as the lithium initially flows into the PEDOT:PSS. This transient effect disappears once enough lithium settles into the PEDOT:PSS to establish a stable distribution of lithium.

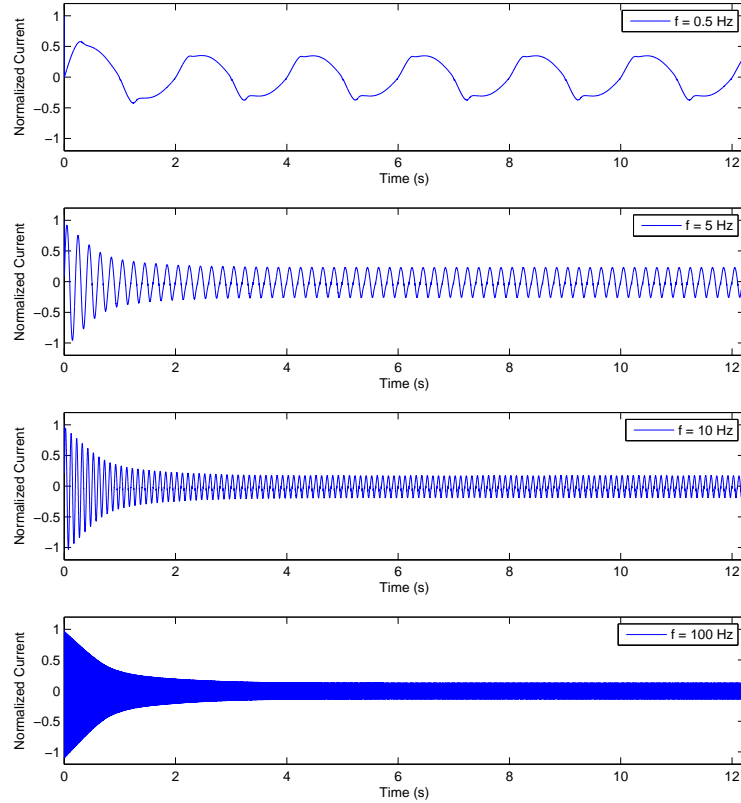


FIGURE 6.6: Normalized current over time

Figures 6.7 and 6.8 show the changes in the hole and lithium density in PEDOT:PSS over time. A visual comparison of the plots show that changes in the lithium density are tied to the changes in the hole density. As the frequency increases lithium diffusion becomes more dominant than lithium drift. At 100 Hz lithium drift due to the applied potential is barely present. Since the ions do not create a visible impact on the hole density, the resistivity of the device remains constant over time. This means that the memristor model behaves like a regular resistor at high frequencies.

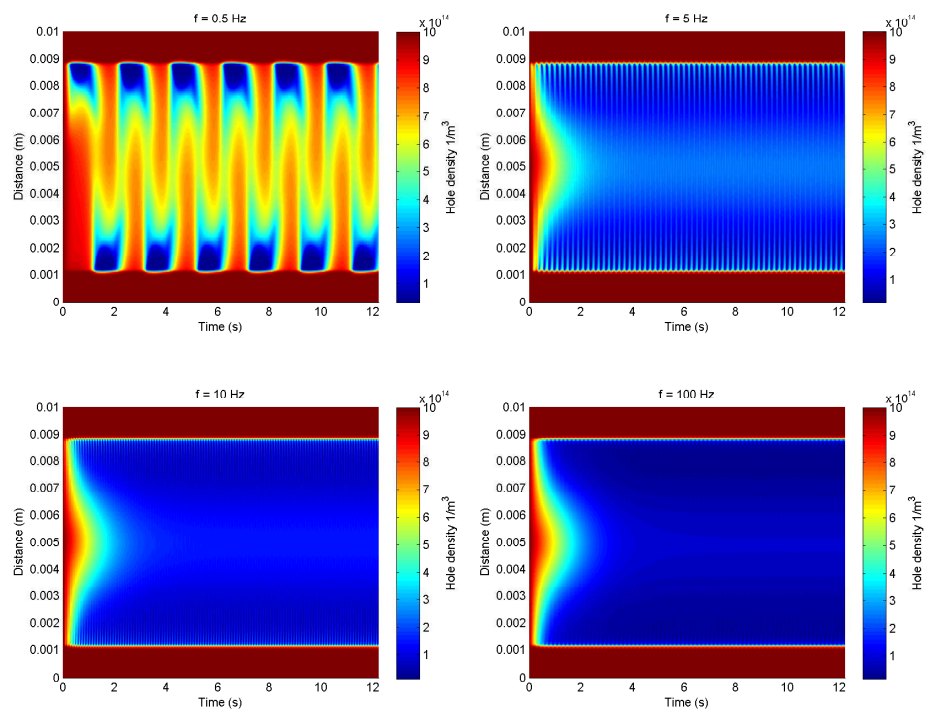


FIGURE 6.7: Hole density over time at different frequencies

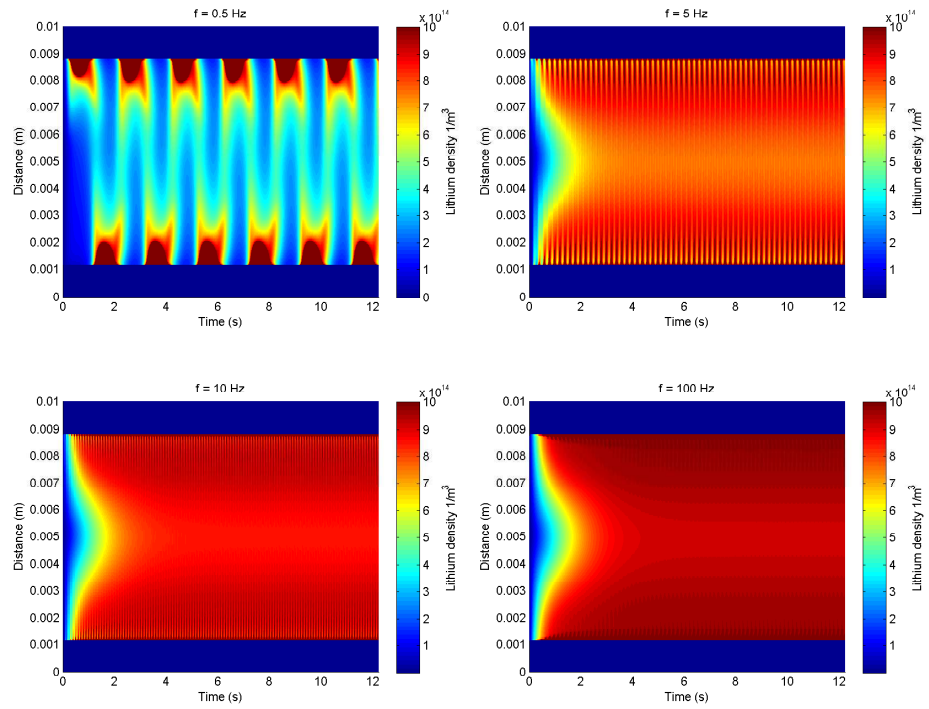


FIGURE 6.8: Lithium density over time at different frequencies

6.2.3 1-D Memristor Simulation With Increasing Charge Density (I got a few questions)

After establishing that the simulation behaves as expected it is important to investigate how charge density effects this model since the size of the device limits the maximum charge density that can be simulated. The actual device has a hole density in the range of $\approx 10^{26} \text{ m}^{-3}$ but the simulation is restricted to $\approx 10^{17} \text{ m}^{-3}$. In theory, if the densities used for the simulation have a limited affect on the behavior of the memristor then the simulations with low particle densities can be used as a proxy for the actual device which operates in much higher particle densities.

The following 3 graphs (6.9, 6.10 and 6.11) show the hole and the lithium densities at steady state as well as the current density over time at the right metal contact for various charge densities. The simulations are run using high mesh densities to allow stable simulation up to 10^{17} m^{-3} . 20 different simulations were made using densities ranging from $5 \times 10^{15} \text{ m}^{-3}$ to $1 \times 10^{17} \text{ m}^{-3}$ but only 5 of them are plotted for illustration purposes. All the values are normalized using respective hole/lithium density ratios. Following equations are used for the normalization procedure.

$$n_i(x, t)' = \frac{n_i(x, t)}{r_i} \quad (6.7)$$

$$J_i(t)' = \frac{J_i(t)}{r_i} \quad (6.8)$$

$$r_i = \frac{n_i(x, t=0)}{n_1(x, t=0)} \quad (6.9)$$

Where $n_i(x, t)'$ and $J_i(t)'$ are the particle and the current densities normalized by the coefficient r_i . This normalization coefficient is calculated by using the particle densities at $t = 0$.

$n_1(x, t=0)$ is the particle density of the plot with lowest initial hole or lithium density which is $5 \times 10^{15} \text{ 1/m}^3$ in this case. For example for a hole distribution with initial hole density at $65 \times 10^{15} \text{ 1/m}^3$ the normalization constant is,

$$r_i = \frac{n_i(x, t = 0)}{n_1(x, t = 0)} = \frac{65 \cdot 10^{15}}{5 \cdot 10^{15}} = 13 \quad (6.10)$$

Once the transient simulation is complete the hole distribution is normalized using the normalization constant calculated above(6.10). Different normalization constants are calculated for various hole and lithium densities and they are used to normalize the particle and current density distributions once the simulations are complete. The results are shown in figures 6.10, 6.9 and 6.11.

Plots for lithium ions (figure 6.10) and holes (figure 6.9) are nearly identical to each other in terms of the plot shapes. They both get sharper around the area where there is a substantial accumulation of lithium. This is not unexpected since the debye length gets smaller with increasing carrier density. So with increased density it is expected that the density accumulation at the wet/dry PEDOT interface will be more narrow. This affect is not as strong for lithium ions since there is a maximum density limit on them. Lithium and hole plots only show the difference carrier density makes at steady state. The effect of debye length on the device operation can be further explored by looking at the current density over time.

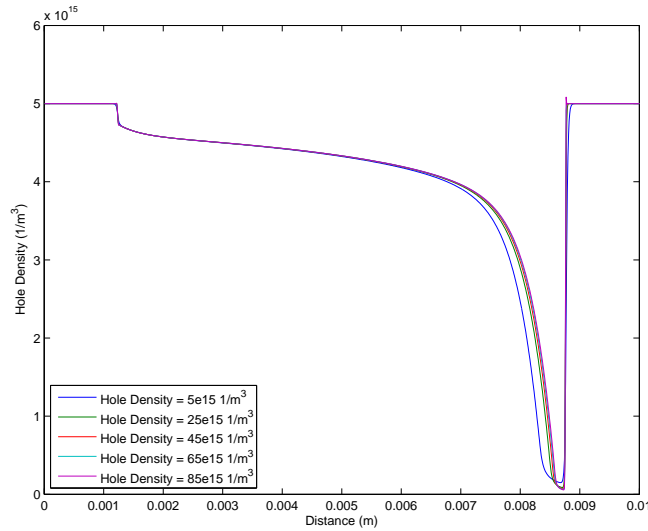


FIGURE 6.9: Normalized hole densities at steady state

To investigate this the first few milliseconds of a simulation is run without allowing the movement of lithium ions. At this stage normalized currents are identical to each other

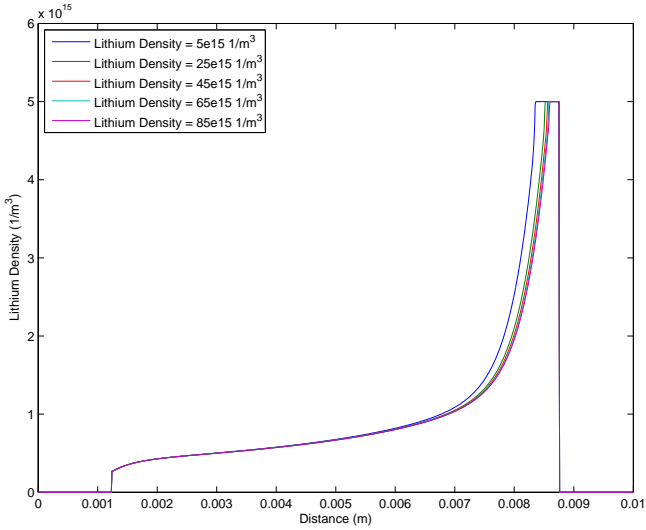


FIGURE 6.10: Normalized lithium densities at steady state

which means that a simulation with low density can be scaled up without introducing any errors. The introduction of lithium ions slowly deviates the current plots from each other over time but the overall behavior of the memristor remains unchanged. The current density decreases over time and reaches a steady state value. After the first plot which has the lowest hole density, consecutive plots get closer and they are almost impossible to distinguish from each other at steady state.

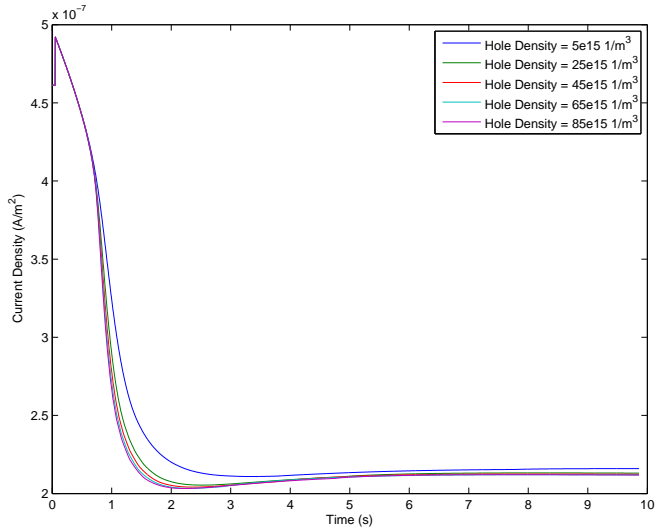


FIGURE 6.11: Normalized hole current densities

The impact of increasing charge density can be numerically explored using normalized plots. The following formula is used to calculate a percentage difference between different

normalized carrier densities as well as normalized current densities.

$$P_i^n = \frac{100}{K} \sum_{k=1}^K \left| \frac{n_i(x_k)' - n_1(x_k)}{n_1(x_k)} \right| \quad (6.11)$$

$$P_i^J = \frac{100}{T} \sum_{k=1}^T \left| \frac{J_i(t_k)' - J_1(t_k)}{J_1(t_k)} \right| \quad (6.12)$$

K is the total number of points along x axis and T is the total number of time steps taken by the simulator. x_k and t_k are used to describe a point in x axis and a point in time respectively. For various hole and lithium distributions at steady state, equation 6.11 is used to calculate the average percentage difference between the distribution which has the lowest initial particle density distribution ($n_1(x_k)$) and other normalized particle density distributions ($n_i(x_k)'$). The equation 6.12 is used to perform the same operation as equation 6.11 on current density outputs over time for various particle densities.

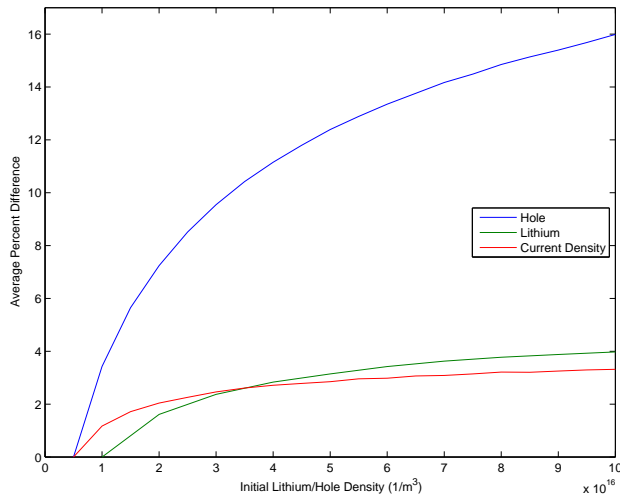


FIGURE 6.12: Average difference for hole, lithium and current densities for various initial hole densities

Figure 6.12 shows the impact of increasing hole/lithium density on the simulation results. In all 3 cases, there is an increase in average difference for increasing carrier density. Hole density shows the most difference between plots. Since holes are free to move inside the PEDOT:PSS they get directly affected by the change in the Debye length due to the increase in hole density. This is not the case for lithium ions because their movement is

restricted by the limit on lithium density. In contrast, current density is not as sensitive to density changes as lithium and hole distributions.

The difference in the hole distribution seems very large but the overall shape of the plot is always preserved since the highest amount change occurs around the wet/dry PEDOT interface where lithium accumulates. Based on the plots above it can be concluded that the behavior of the memristor simulated using a low charge density is very similar to the simulation at a high charge density

We need something like this – An approximate error estimation can be made for current density if a low hole/lithium density is used for simulation and then scaled up to match the actual memristor. Figure 6.12 shows a 3.3 % difference for 2 orders of magnitude increase in the hole density. Assuming the error scales linearly after that point a total of 6 orders of magnitude will result in 9.9 % error introduced in order to linearly scale from 10^{15} to 10^{21} . The actual error is likely to be less since the error progresses sub linearly. Following the same procedure 6 orders of magnitude difference produces a 12 % error for lithium distribution and 48 % error for hole distribution. The difference in the hole distribution seems very large but the overall shape of the plot is always preserved since the highest amount change occurs around the wet/dry PEDOT interface where lithium accumulates. Based on these error margins and previous plots it can be concluded that the behavior of the memristor simulated using a low charge density is very similar to the simulation at a high charge density.

Chapter 7

2-D Memristor Simulation

Even though 1-D simulation is able to capture the main characteristics of the memristor it is still lacking certain physical effects that can be captured in a 2-D simulation such as the movement of ions inside the electrolytic solution which cancels some of the applied electric field. This chapter shows the simulation of a memristor in 2-D and compares the results with 1-D simulations. It starts with the simulation of a memristor with different PEDOT:PSS layer thicknesses and shows the changes in particle density distributions, electric field and current density. Transient simulations with a potential pulse train and a sinusoidal potential are presented and compared to 1-D simulations. Finally current vs time and I-V curves for an actual memristor are used to show the accuracy of 2-D simulations in capturing the behavior of the actual device .

7.1 Effect of PEDOT:PSS Thickness

The physical dimensions of the memristor are presented in chapter 4. The thickness of the PEDOT:PSS layer is very small compared to the other dimensions of the device such as the thickness of the electrolyte and length of the conductive material. This complicates the simulation of the PEDOT:PSS strip using a uniform mesh. Although non uniform meshing seems like an appropriate solution for this problem, a close examination of the numerical limitations show that this is not the case. Decreasing the mesh

size in one dimension severely reduces the maximum time step for the entire simulation therefore non uniform meshing is not feasible for this problem.

An alternative solution to the meshing problem is embedding an infinitesimally thin PEDOT:PSS layer in a 2-D simulation. This method is used for the memristor simulations in this chapter. For PEDOT:PSS, the effects in 2-D are ignored since the layer thickness is 10000 times smaller than other dimensions such as the thickness of the electrolyte. For the holes in the conductive layer only the horizontal component of the electric field is used and all the current densities are calculated in 1-D. Following plots compare two simulations with PEDOT:PSS thicknesses higher than the actual device thickness and a 2-D simulation with a 1-D PEDOT:PSS layer.

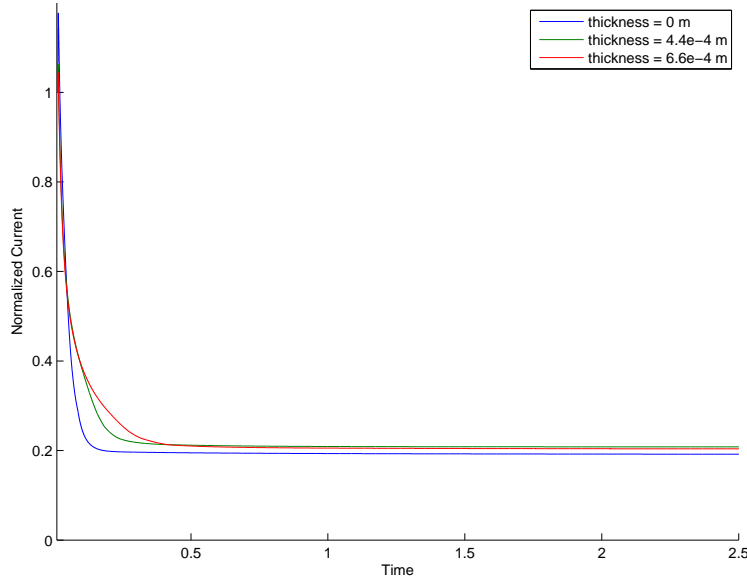


FIGURE 7.1: Normalized current over time for different PEDOT:PSS thicknesses

The memristor is simulated using a constant potential at the contacts. The left metal contact is at 1 V and the right metal contact is grounded. The current density measured at the right contact for different PEDOT:PSS thicknesses is shown in figure 7.1. These plots show that as the PEDOT:PSS thickness gets smaller the device responds faster. This is due to the decrease in volume of the PEDOT:PSS. Another change in the behavior of the memristor is its resistivity at steady state. The increase in resistivity for different PEDOT:PSS thicknesses at steady state can be attributed to the ion/hole interaction at

the interface between the PEDOT:PSS and the electrolyte solution which is illustrated in the following figures 7.2, 7.3 and 7.4.

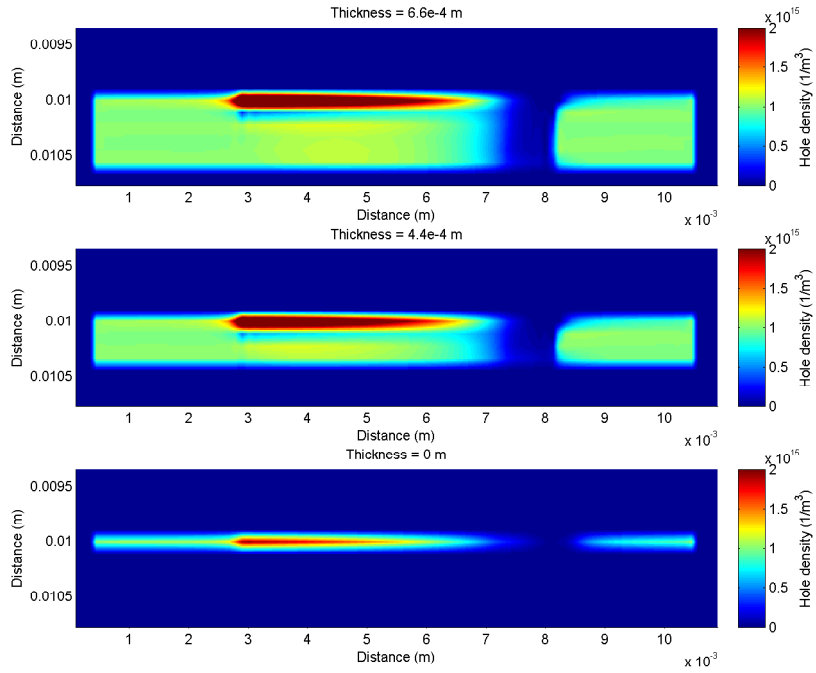


FIGURE 7.2: Hole distribution at steady state for different PEDOT:PSS thicknesses

Figure 7.2 shows the hole distribution in PEDOT:PSS at steady state for different thicknesses. The electrolyte is on top of PEDOT:PSS but it is not visible in these plots since its hole density is zero at all times. As lithium ions move into the PEDOT:PSS they move towards the metal contact and accumulate at the wet/dry interface. There is a lack of holes around the region where lithium ions accumulate. This effect can be seen in figures 7.2 and 7.3. For all the plots, there is a section of the hole distribution which is missing due to high concentration of lithium ions.

The accumulation of holes at the surface of the PEDOT:PSS is due to the perchlorate accumulation near the positive contact in the electrolyte (figure 7.4). As perchlorate ions accumulate on the surface of the PEDOT:PSS they also attract holes towards the surface.

As shown in the previous chapter, the electric field has the highest value where the lithium ions accumulate. The figure 7.5 shows the change in the shape of the electric

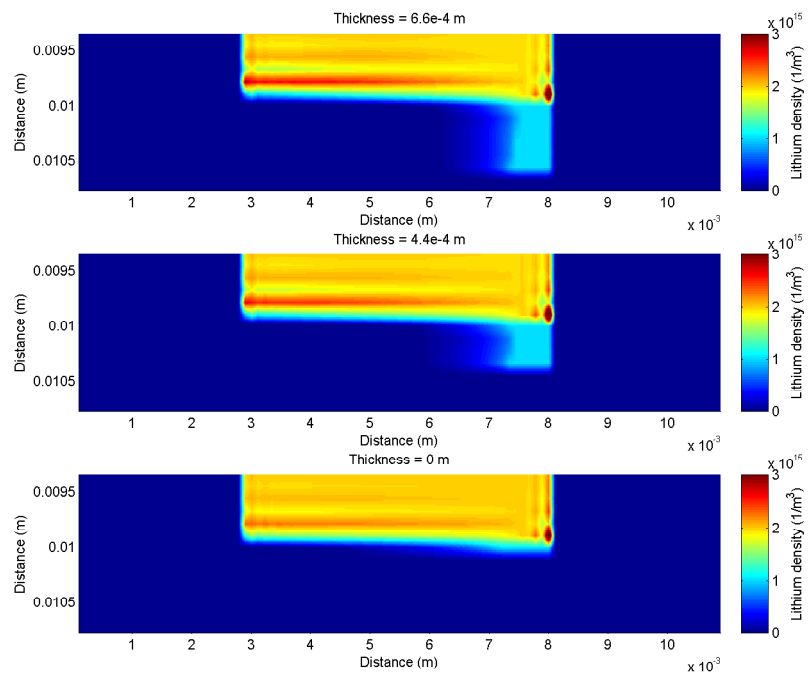


FIGURE 7.3: Lithium distribution at steady state for different PEDOT:PSS thicknesses

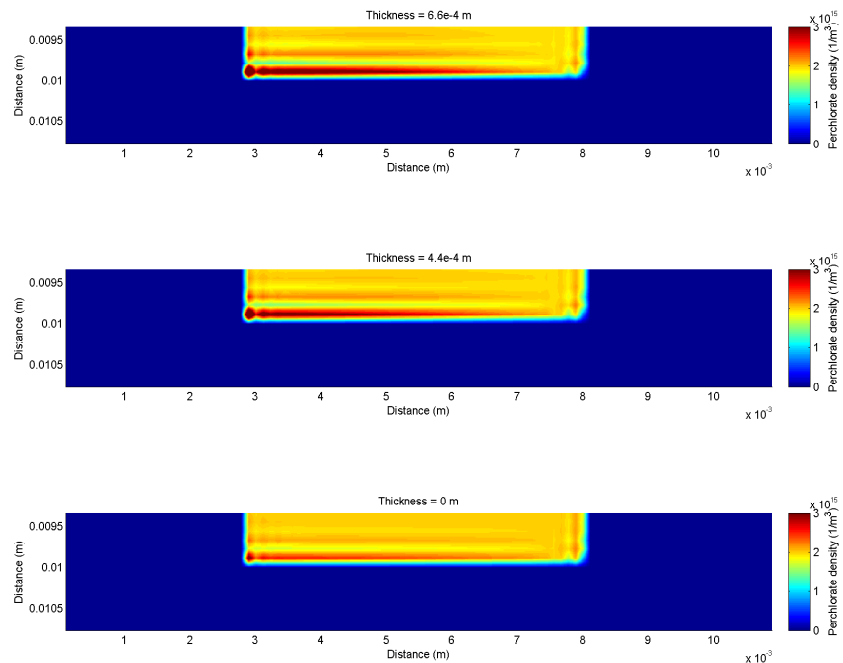


FIGURE 7.4: Perchlorate distribution at steady state for different PEDOT:PSS thicknesses

field as PEDOT:PSS gets thinner. For all the plots most of the potential drop occurs where lithium ions accumulate and it is concentrated at the surface of the PEDOT:PSS.

The above plots show that changing the thickness of the PEDOT:PSS does not have a drastic effect in the operation of the memristor since most of the changes occur at the interface between electrolyte and PEDOT:PSS. A 1-D approximation of the polymer conductor contains all the necessary physics for the simulation of the memristor described in chapter 5.

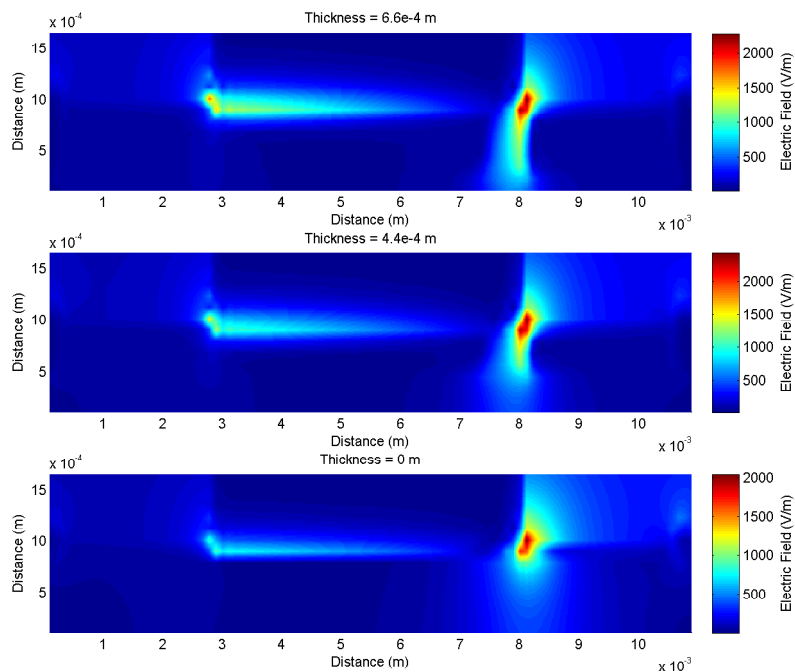


FIGURE 7.5: Electric field strength at steady state for different PEDOT:PSS thicknesses

7.2 2-D Memristor Simulation Using a Potential Pulse Train

The following results are generated using the same boundary and initial conditions as the simulations in the previous section in order to show the differences between 1-D and 2-D memristor models.

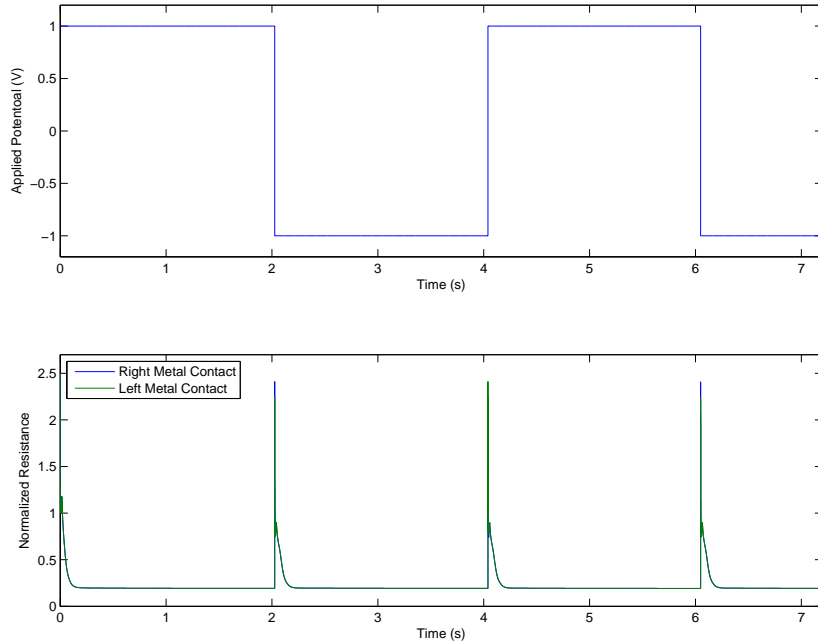


FIGURE 7.6: Applied potential and normalized current over time of a 2-D memristor

Even though the general trend of the current densities are similar for the plots (6.2 and 7.6), there are some essential differences between 1-D and 2-D simulations. The movement of the lithium ions controls the change in the resistivity over time therefore the response of the device is dependent on the velocity of the lithium ions which is a function of mobility and the electric field. In 1-D simulations the vertical mobility of the lithium needs to be adjusted in order to account for the thickness of the electrolyte since it is collapsed into a single layer for 1-D simulations. Because of this the mobility of the lithium has different values in different directions. Additionally the strength of the electric field is not constant over the entire PEDOT:PSS strip. The speed of the lithium ions vary depending on their position and direction due to the changes in the mobility and the electric field.

The amount of charge that can accumulate inside the PEDOT:PSS is dependent on the drift and the diffusion of the lithium ions. Due to the electric field, the lithium ions are forced to accumulate on one side of the PEDOT:PSS layer instead of being evenly distributed. The ratio of vertical to horizontal drift of the lithium near the metal contact determines the maximum amount of charge that can accumulate which determines the maximum resistivity of the material. The results of both simulations show that the relative strength of the lithium drift current from the electrolyte to the PEDOT:PSS compared to the drift from one contact to the other is greater in 1-D simulation. This explains why the current density at steady state is lower in 2-D memristor simulations.

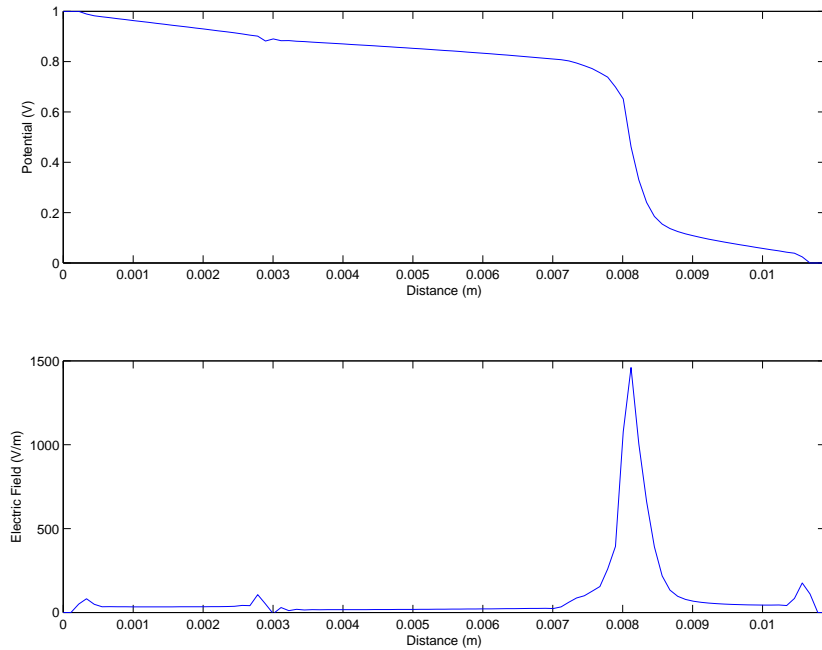


FIGURE 7.7: Electric field and potential at steady state along PEDOT:PSS

Electric field and potential distributions (figure 7.7) for 1-D and 2-D simulations are almost identical at steady state. In both cases most of the potential drop and electric field occurs where lithium ions accumulate.

The lithium and hole density plots shown in figure 7.8 are also similar to the plots (6.4) shown in section 6.4.1. For both of the simulations the lithium ions move into the PEDOT:PSS until the end of the wet region. At the same time holes move out of the wet/dry interface and create a high resistance region.

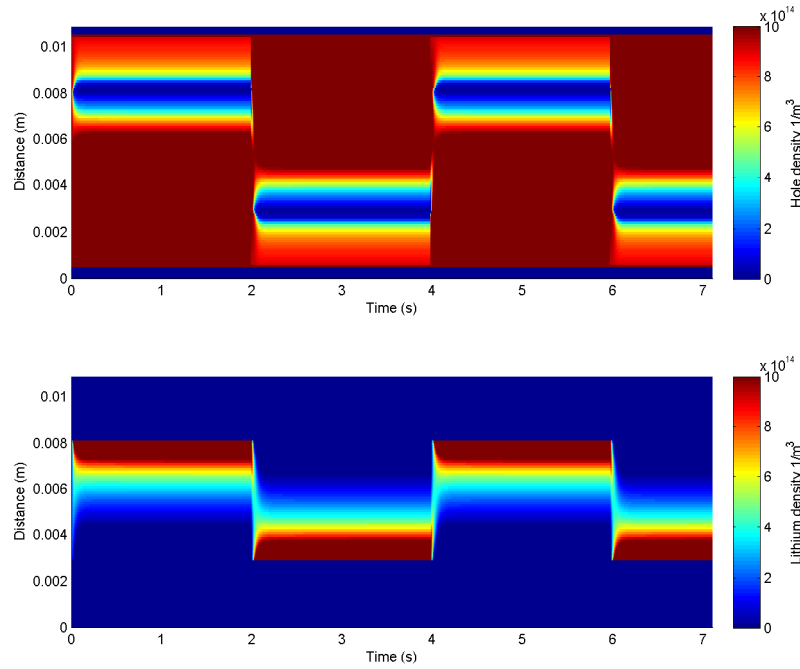


FIGURE 7.8: Lithium and hole density distributions over time

This final plot (figure 7.9) shows the magnitude of the lithium current density over time. Almost all of the lithium ion movement occurs at the wet/dry interface of PEDOT:PSS since most of the electric field concentrates around that region. So when the potential is flipped from one side to the other, most of the lithium ions drift and diffuse back into the electrolyte instead of going through the PEDOT:PSS. This effect is also demonstrated in section 7.4 (figures 7.19 and 7.20).

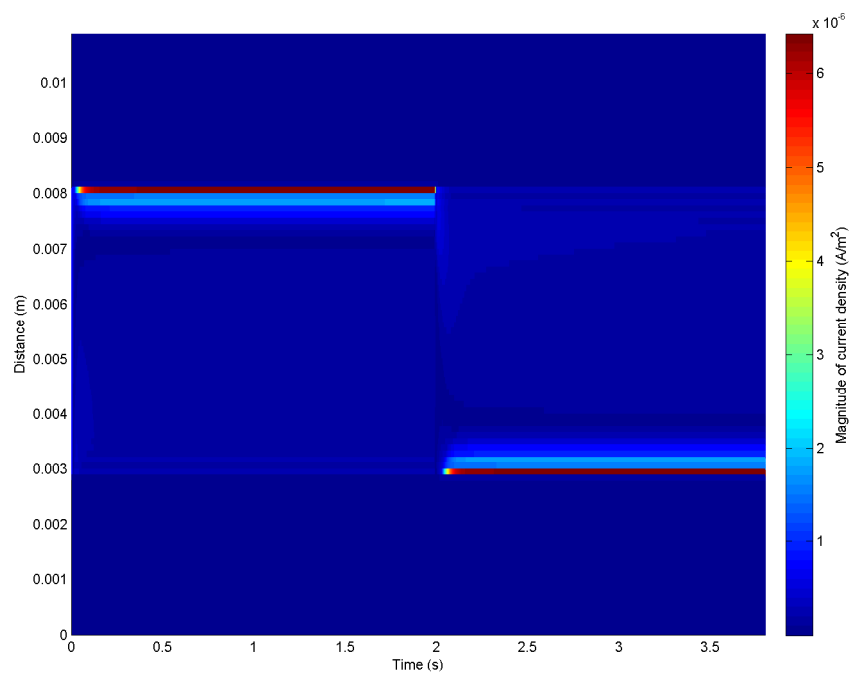


FIGURE 7.9: Lithium current density over time

7.3 2-D Memristor Simulation Using a Sinusoid

A memristor with an AC potential with different frequencies is simulated in this section. Following 4 plots (figure 7.10) show the I-V curves of the memristor for 0.5, 5, 10 and 100 Hz. In these simulations there are two effects working against each other, the increase in the applied potential which increases the current output and the lithium ions working against the increase of the current by migrating into the PEDOT:PSS and increasing resistivity. Both of these effects can be clearly seen in the I-V curve for 0.5 Hz. Initially as the potential increases from 0 to 0.5 V, there is an increase in the current which means that there are not enough lithium ions in PEDOT:PSS to increase the resistivity of the device. As the potential reaches 0.5 V the accumulation of the lithium ions overtake the increase in potential such that the output current starts to decrease even though the potential is increasing. This effect disappears at higher frequencies since the lithium ions are too slow to catch up with the change in the potential.

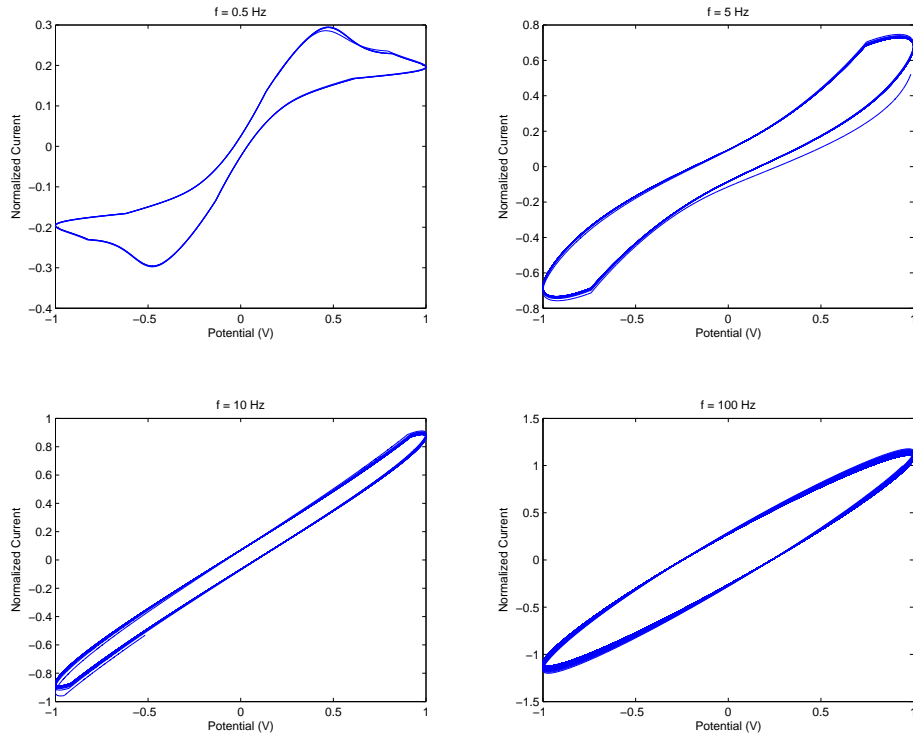


FIGURE 7.10: Normalized Current vs. applied potential at different frequencies

There are a few differences between 1-D and 2-D simulations using AC potential which can be explained by using observations from the previous section. In 2-D simulations the resistivity measured from the left and the right contacts match each other quite closely. So the device current is symmetrical for both negative and positive potentials.

During simulation, even though there is no applied potential, the current never goes to zero because of the stored electric field inside the PEDOT:PSS due to the accumulated charge. This capacitive effect prevents the current from going to zero when there is no applied potential. In 1-D simulations the amount of charge stored in the PEDOT:PSS is lower therefore the value of the current can get closer to zero compared to 2-D simulations.

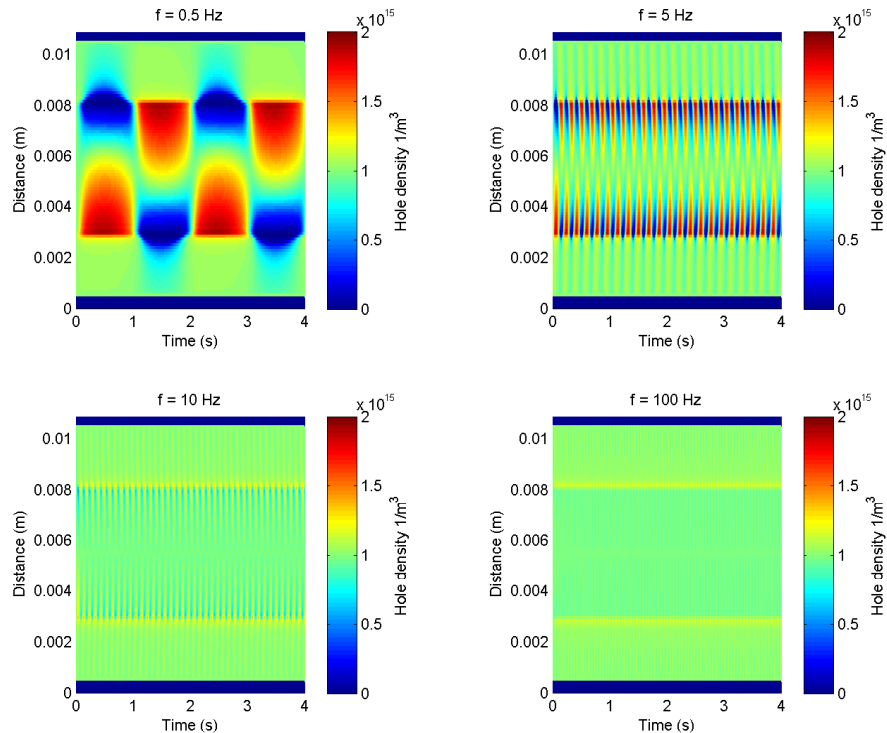


FIGURE 7.11: Hole distribution over time at different frequencies

Figures 7.11 and 7.12 show hole and lithium densities over time inside the PEDOT:PSS. At low frequencies the lack of holes due to the lithium ions as well as excess holes due to the perchlorate accumulation inside the electrolyte is clearly visible. At high frequencies, since the potential is changing rapidly, there is not enough time for the ions to accumulate on either side. So the hole distribution remains mostly undisturbed. For

in this case the lithium ions move into the PEDOT:PSS only through diffusion and they do not affect the hole distribution. Based on these plots, it is possible to conclude that both 1-D and 2-D memristor models behave like a regular resistor at high frequencies.

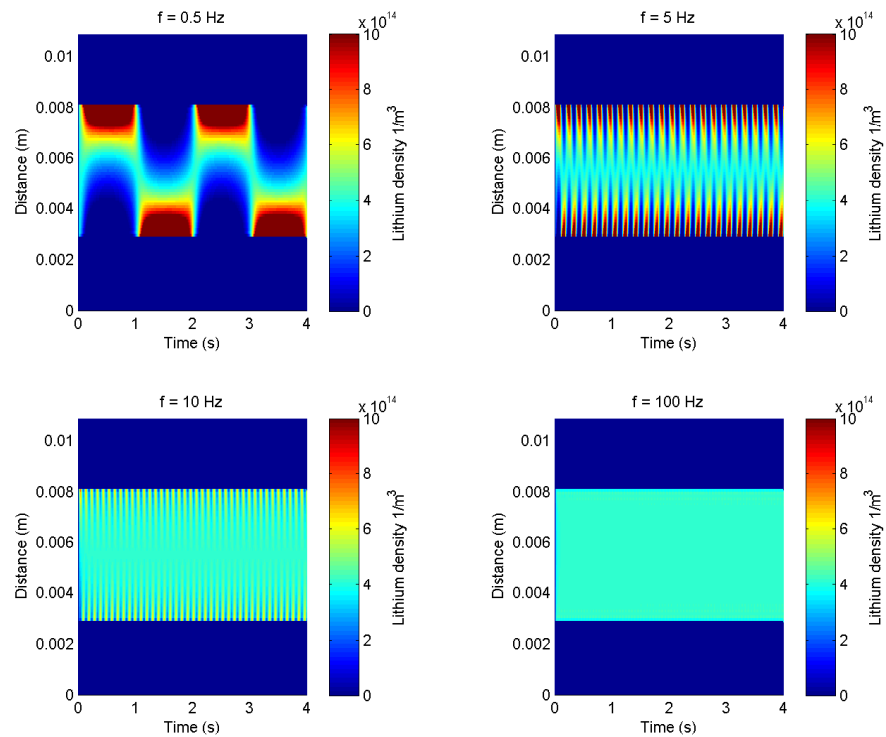


FIGURE 7.12: Lithium distribution over time at different frequencies

7.4 Experiment vs. Simulation

The memristor model presented in this thesis has many approximations and it is far from complete but the preliminary simulations show promising results. In this section 2-D memristor simulations are compared with the experimental results in order to validate the model developed in this thesis. Due to the approximations and difficulties in the simulation mentioned in the previous chapters the current values obtained from the simulation are much lower than the actual device therefore the memristor model is only behaviorally compared to the experimental results.

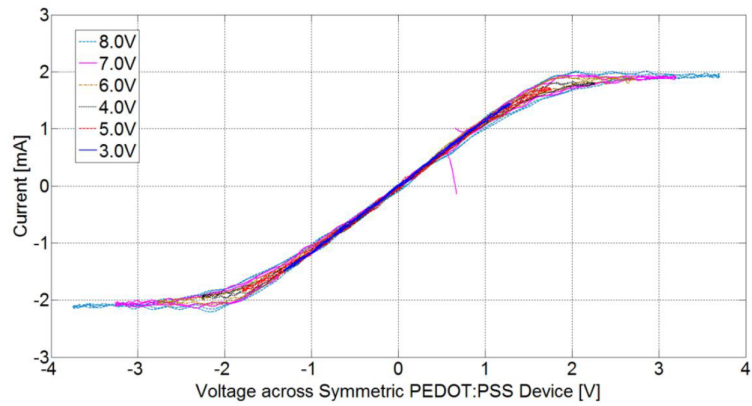


FIGURE 7.13: Experimental results for various applied potentials at 0.1 Hz (Courtesy of Eduardo Barrera)[37]

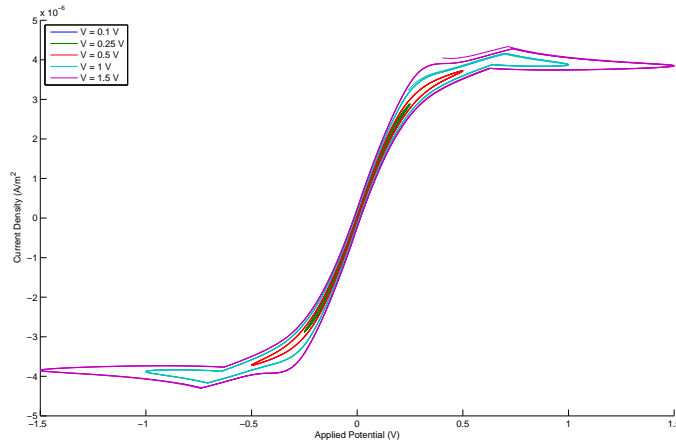


FIGURE 7.14: Simulation results for various applied potentials at 0.1 Hz

Figures 7.13 and 7.14 show the I-V curve of the memristor using various potentials. At low potentials the current voltage relationship is linear for both simulation and experimental results which means that the resistance is constant over time. At low

voltages lithium ions do not move very fast therefore the change in the resistivity of the PEDOT:PSS is minimal. At higher potentials the resistivity starts to increase due to the accumulation of the lithium ions and over time it completely cancels out the increase in the potential.

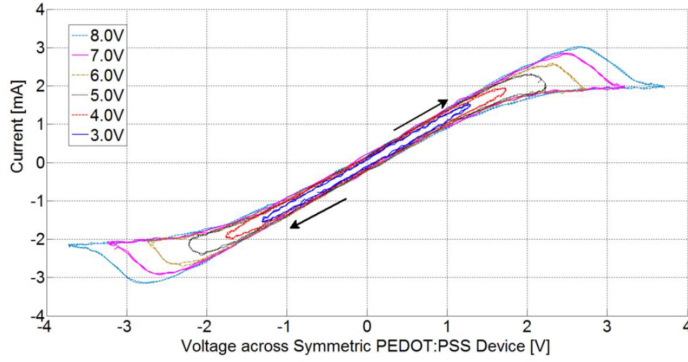


FIGURE 7.15: Experimental results for various applied potentials at 1.0 Hz (Courtesy of Eduardo Barrera)[37]

For the plots 7.15 and 7.16 the same experiment is repeated using a frequency of 1.0 Hz. This time the linear region is longer since the change in potential is faster and lithium ions cannot keep up with it. Once the movement of the lithium ions speeds up due to the applied potential and there is enough accumulation inside the PEDOT:PSS then the resistivity increases much faster than the increase in the potential.

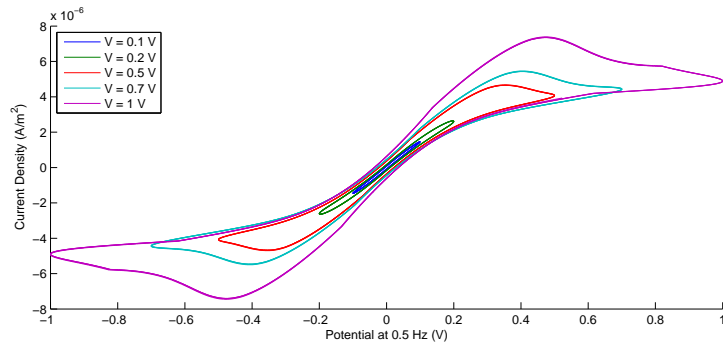


FIGURE 7.16: Simulation results for various applied potentials at 1.0 Hz

The pinched area towards the end of the outermost loop shows that the change in resistivity slows down as it starts to reach its maximum value. This is also apparent in the transient simulations with a potential pulse train. The increase in resistance is fast up to a certain value and then it slows down as PEDOT:PSS is saturated by lithium ions.

The following plots (7.17 and 7.18) are created using a variable frequency instead of a variable potential. For the simulation and the experiment, the memristor behaves more like a resistor as frequency increases. This is due to lithium ions not having enough time to drift into the PEDOT:PSS to make a change in the resistance. Even though the frequencies used for simulation are different than the ones used in the experiment, both plots show similar behavior. A better match can likely be achieved by improving the mobility models used for lithium ions and holes.

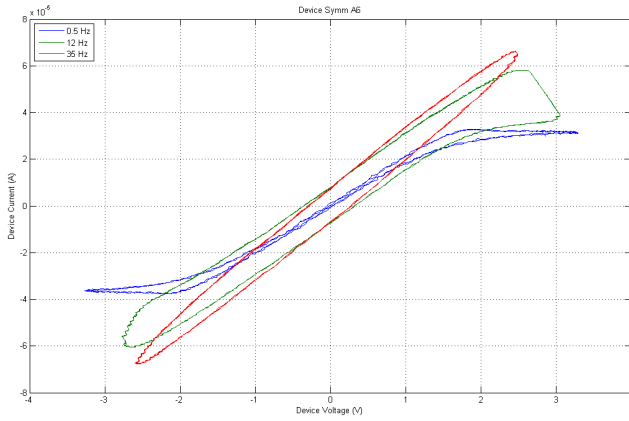


FIGURE 7.17: Measured I-V curve at different frequencies (Courtesy of Eduardo Barrera)[37]

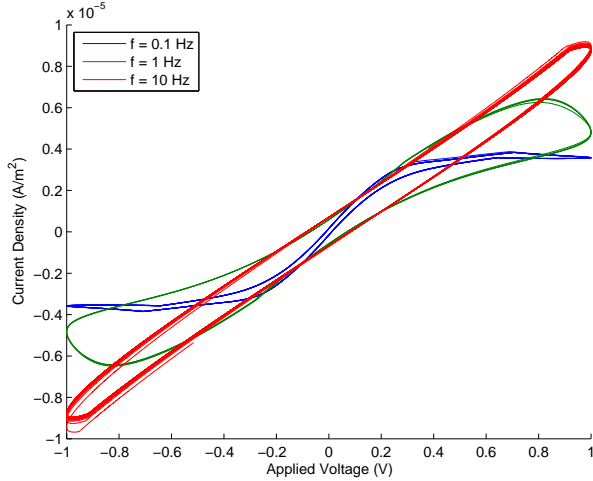


FIGURE 7.18: Simulated I-V curve at different frequencies

This last example consists of a coupled ionic-electronic device where PEDOT:PSS strip is separated into two pieces with a notch which prohibits the hole flow trough the device. Figure 7.19 shows the measured movement of lithium from the right strip to the left strip. Red color represents the lack of charge and blue color shows the presence of charge. For the simulation results (figure 7.20) red color represents a high charge density and blue color represents a low charge density.

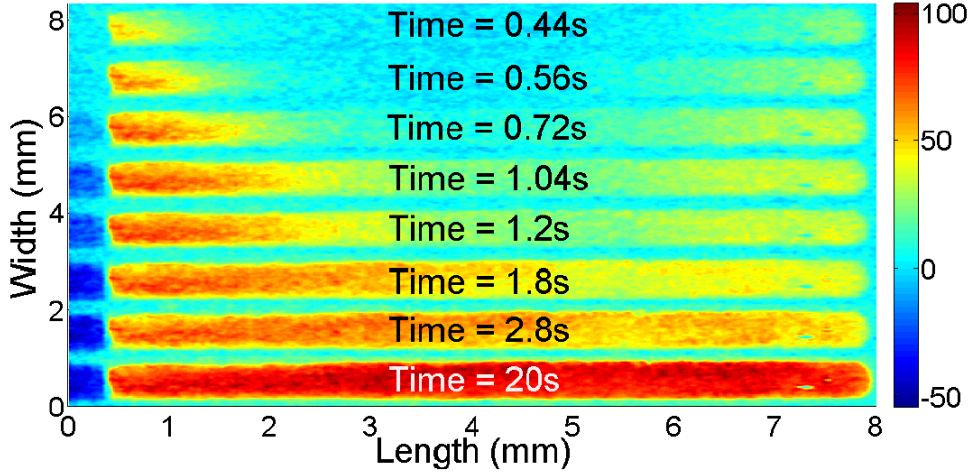


FIGURE 7.19: Experimental results for accumulation of lithium inside PEDOT:PSS
(Courtesy of Eduardo Barrera)[37]

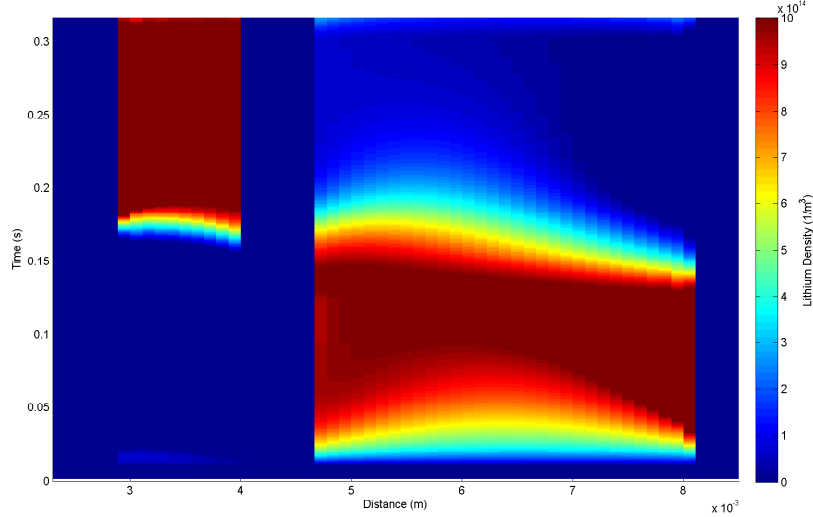


FIGURE 7.20: Simulation results for accumulation of lithium inside PEDOT:PSS

When a potential is applied, one side of the PEDOT:PSS strip is filled with lithium ions. It can be seen from both the simulation and the experimental results that the lithium ions start migrate out of the PEDOT:PSS near the notch and the wet/dry

PEDOT:PSS interface which are the areas with highest electric field. Both plots show that lithium ions uniformly distribute themselves inside PEDOT:PSS at steady state. This uniform distribution of lithium ions supports the assumption that there is a limit on how many lithium ions PEDOT:PSS can accept per unit area. If this was not the case the lithium ions would have accumulated on one side of the device instead of being uniformly distributed.

Chapter 8

Conclusion

The purpose of this thesis was to create a numerical scheme to simulate ionic-electronic devices. A developed numerical model was used to simulate the behavior of mobile charged particles inside a memristor. By looking at the experimental results versus the simulation it is possible to conclude that the memristor model captures a variety of physical effects that are present in the memristor and produces satisfactory results. The change in the conductivity is captured through the exchange of lithium ions between the electrolyte and the PEDOT:PSS and the dedoping of PEDOT:PSS. The transient simulation results match the experimental results behaviorally for both single strip and notched memristor. Although the simulation captures the essence of the experimental results, this model requires more work and can be improved through better numerical schemes, physical models and thorough experimentation. There are also a few limitations of this model due to the device's size and physical features.

Both 1-D and 2-D simulations are effective in capturing the essential physical effects such as the movement of ions and the change in conductivity over time. 1-D simulations have an advantage over 2-D simulations when it comes to computational speed. 1-D simulations take between 10 to 30 min on average (on a quad core Intel i7 CPU) where 2-D simulations take a minimum of 2 hours to complete. Even though 1-D simulations run faster than 2-D simulations, they also require fine tuning of the lithium mobility in order to get a comparable accuracy. Since the electrolyte is never fully simulated in 1-D, it cannot match the accuracy of 2-D simulations.

Even though the model that is used for the simulation of the memristor is very basic, the computational load to generate a transient response is very high in both 1-D and 2-D and simulation in 3-D is not feasible using a regular desktop computer. Modeling of additional physical effects can slow down the simulation even further. However, the model is still suitable for any structure that can be simulated in 2-D.

Another drawback of this model is the inability to simulate using high charge densities due to the Debye length. Mesh density can only be increased up to a certain value before the memory requirements of the simulation becomes unmanageable for a regular computer. Fortunately using a low charge density does not render the model useless since simulations in section 5.4.3 showed that it does not drastically alter the behaviour of the problem. Simulations using low charge densities can be scaled up using appropriate fitting parameters.

The model that is developed in this thesis is open for improvements on carrier transport models. A constant bulk mobility is used for holes in this model which is not an entirely accurate representation of the actual transport behavior of the holes which move from site to site via variable range hopping. Addition of the lithium ions into the PEDOT:PSS not only reduces the number of available holes but also decreases the amount of available sites through holes can move. A variable range hopping mechanism and some thermal effects can be added into this model for a more complete simulation. Also PEDOT:PSS is a disordered material and the way it was deposited on a substrate can make a big difference on the hole transport. Anisotropic hole mobility can be implemented in order to account for this issue.

The results showed that it is possible to simulate a memristor using a simple finite difference method. This model can be a very useful tool in understanding the way the ions and the holes move in PEDOT:PSS. The model developed in this thesis is a promising start for vast research and development opportunities for organic memristors and more generally polymer conductors.

Bibliography

- [1] CarlL. Gardner, Wolfgang Nonner, and RobertS. Eisenberg. Electrodiffusion model simulation of ionic channels: 1d simulations. *Journal of Computational Electronics*, 3(1):25–31, 2004. ISSN 1569-8025. doi: 10.1023/B:JCEL.0000029453.09980.fb. URL <http://dx.doi.org/10.1023/B:JCEL.0000029453.09980.fb>.
- [2] Maria G. Kurnikova, Rob D. Coalson, Peter Graf, and Abraham Nitzan. A lattice relaxation algorithm for three-dimensional poisson-nernst-planck theory with application to ion transport through the gramicidin a channel. *Biophysical Journal*, 76(2):642 – 656, 1999. ISSN 0006-3495. doi: [http://dx.doi.org/10.1016/S0006-3495\(99\)77232-2](http://dx.doi.org/10.1016/S0006-3495(99)77232-2). URL <http://www.sciencedirect.com/science/article/pii/S0006349599772322>.
- [3] Hyuck In Kwon and Umberto Ravaioli. Simulation of electronic/ionic mixed conduction in solid ionic memory devices. *Microelectronics Journal*, 37(10):1047 – 1051, 2006. ISSN 0026-2692. doi: <http://dx.doi.org/10.1016/j.mejo.2006.04.009>. URL <http://www.sciencedirect.com/science/article/pii/S0026269206000747>.
- [4] M.N. Kozicki, Mira Park, and M. Mitkova. Nanoscale memory elements based on solid-state electrolytes. *Nanotechnology, IEEE Transactions on*, 4(3):331–338, May 2005. ISSN 1536-125X. doi: 10.1109/TNANO.2005.846936.
- [5] Matthew J. Panzer and C. Daniel Frisbie. Exploiting ionic coupling in electronic devices: Electrolyte-gated organic field-effect transistors. *Advanced Materials*, 20(16):3177–3180, 2008. ISSN 1521-4095. doi: 10.1002/adma.200800617. URL <http://dx.doi.org/10.1002/adma.200800617>.
- [6] M.S. Islam, C. Johns, Long Do, D. A A Ohlberg, Shih-Yuan Wang, and R. Stanley Williams. Memristors based on an organic monolayer of molecules and a thin film of solid electrolytes. In *Electrical and Computer Engineering (ICECE), 2010 International Conference on*, pages 761–764, Dec 2010. doi: 10.1109/ICECE.2010.5700804.

- [7] Timothy R. Brumleve and Richard P. Buck. Numerical solution of the nernst-planck and poisson equation system with applications to membrane electrochemistry and solid state physics. *Journal of Electroanalytical Chemistry and Interfacial Electrochemistry*, 90(1):1 – 31, 1978. ISSN 0022-0728. doi: [http://dx.doi.org/10.1016/S0022-0728\(78\)80137-5](http://dx.doi.org/10.1016/S0022-0728(78)80137-5). URL <http://www.sciencedirect.com/science/article/pii/S0022072878801375>.
- [8] L.O. Chua. Memristor-the missing circuit element. *Circuit Theory, IEEE Transactions on*, 18(5):507–519, 1971. ISSN 0018-9324.
- [9] M. Di Ventra, Y.V. Pershin, and L.O. Chua. Circuit elements with memory: Memristors, memcapacitors, and meminductors. *Proceedings of the IEEE*, 97(10):1717–1724, 2009. ISSN 0018-9219. doi: 10.1109/JPROC.2009.2021077.
- [10] Duncan R. Stewart R. Stanley Williams Dmitri B. Strukov, Gregory S. Snider. Missing memristor found. *Nature*, 453:80–83, 2008. ISSN 0028-0836.
- [11] T. Berzina, Anteo Smerieri, Marco Bernabo, Andrea Pucci, Giacomo Ruggeri, V. Erokhin, and M.P. Fontana. Optimization of an organic memristor as an adaptive memory element. *Journal of Applied Physics*, 105(12):124515–124515–5, 2009. ISSN 0021-8979.
- [12] W. Alan Doolittle, W.L. Calley, and W. Henderson. Complementary oxide memristor technology facilitating both inhibitory and excitatory synapses for potential neuromorphic computing applications. In *Semiconductor Device Research Symposium, 2009. ISDRS '09. International*, pages 1–2, 2009.
- [13] Yuhao Wang, Wei Fei, and Hao Yu. Spice simulator for hybrid cmos memristor circuit and system. In *Cellular Nanoscale Networks and Their Applications (CNNA), 2012 13th International Workshop on*, pages 1–6, 2012.
- [14] W. Lvenich U. Merker K. Reuter A. Elschner, S. Kirchmeyer. *PEDOT*. Taylor and Francis Group,, Florida, United States, 2011. ISBN 978-1-4200-6911-2.
- [15] N.F. Mott. Charge transport in non-crystalline semiconductors. In O. Madelung, editor, *Festkrper Probleme {IX}*, pages 22 – 45. Pergamon, 1969. ISBN 978-0-08-015543-2.
- [16] Shawn Sapp, Silvia Luebben, Ya. B. Losovyj, P. Jeppson, D. L. Schulz, and A. N. Caruso. Work function and implications of doped poly(3,4-ethylenedioxythiophene)-co-poly(ethylene glycol). *Applied Physics Letters*, 88(15):152107, 2006.

- [17] Hyongsuk Kim, M.P. Sah, Changju Yang, Seongik Cho, and L.O. Chua. Memristor emulator for memristor circuit applications. *Circuits and Systems I: Regular Papers, IEEE Transactions on*, 59(10):2422–2431, 2012. ISSN 1549-8328.
- [18] A.F. Adzmi, A. Nasrudin, W.F.H. Abdullah, and S.H. Herman. Memristor spice model for designing analog circuit. In *Research and Development (SCOReD), 2012 IEEE Student Conference on*, pages 78–83, 2012.
- [19] Lu Zhang, Zhijie Chen, J. Joshua Yang, Bryant Wysocki, Nathan McDonald, and Yiran Chen. A compact modeling of tio₂-tio₂ memristor. *Applied Physics Letters*, 102(15):153503–153503–4, Apr 2013. ISSN 0003-6951. doi: 10.1063/1.4802206.
- [20] V. Erokhin. Organic memristors : Basic principles. In *Circuits and Systems (ISCAS), Proceedings of 2010 IEEE International Symposium on*, pages 5–8, 2010.
- [21] D. Vasileska and Stephen M. Goodnick. *Computational Electronics*. Morgan and Claypool, Arizona, United States, 2006.
- [22] Snowden C.M. *Semiconductor Device Modelling*. Peter Peregrinus Ltd., London, United Kingdom, 1988.
- [23] COMSOL Inc. Comsol multiphysics,semiconductor module, 2014. URL <http://www.comsol.com/semiconductor-module>.
- [24] SILVACO Inc. S-pisces, 2d silicon device simulator, 2014. URL http://www.silvaco.com/products/vwf/atlas/spisces/spisces_br.html.
- [25] Lumerical Solutions Inc. Device 3.1, 2014. URL <https://www.lumerical.com/tcad-products/device/>.
- [26] Mark H. Holmes. *Introduction to Numerical Methods in Differential Equations*. Springer Science,Business Media,, New York, United States, 2007. ISBN 978-0387-30891-3.
- [27] S.J. Farlow. *An Introduction to Differential Equations And Their Applications*. Dover Books on Mathematics Series. Dover Publications, 1994. ISBN 9780486445953.
- [28] S.M. Sze and K.K. Ng. *Physics of Semiconductor Devices*. Wiley, 2006. ISBN 9780470068304.
- [29] R.F. Wallis. *Semiconductor Physics and Applications*. Series on Semiconductor Science and Technology. OUP Oxford, 2000. ISBN 9780198517412.
- [30] G. Dhatt, E. Lefrançois, and G. Touzot. *Finite Element Method*. ISTE. Wiley, 2012. ISBN 9781118569702.

- [31] R.J. LeVeque. Finite Difference Methods for Ordinary and Partial Differential Equations: Steady-State and Time-Dependent Problems. Society for Industrial and Applied Mathematics, 2007. ISBN 9780898716290.
- [32] H. Li and S.S. Mulay. Meshless Methods and Their Numerical Properties. Taylor & Francis, 2013. ISBN 9781466517462.
- [33] G. Lindfield and J. Penny. Numerical Methods: Using MATLAB. Elsevier Science, 2012. ISBN 9780123869883.
- [34] G.D. Smith. Numerical Solution of Partial Differential Equations: Finite Difference Methods. Oxford applied mathematics and computing science series. Clarendon Press, 1985. ISBN 9780198596509.
- [35] H. Schmidt-Walter and R. Kories. Electrical Engineering: A Pocket Reference. Artech House, 2007. ISBN 9781596932449.
- [36] R.P. Agarwal and D. O'Regan. Ordinary and Partial Differential Equations: With Special Functions, Fourier Series, and Boundary Value Problems. Universitext. Springer, 2008. ISBN 9780387791463.
- [37] Eduardo Barrera Ramirez. Missing memristor found. Master's thesis, 2008.